Resonant Nanocantilever Chemical Vapor Sensors

Thesis by

Heather Catherine McCaig

In Partial Fulfillment of the Requirements

for the Degree of

Doctor of Philosophy

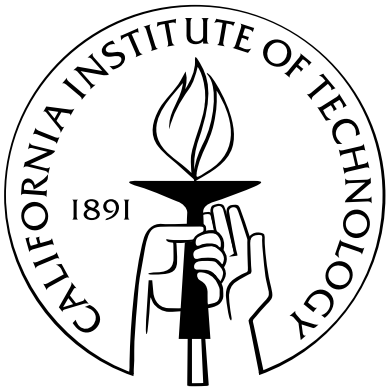

California Institute of Technology

Pasadena, California

2013

(Defended December 10, 2012)

To my family.

Acknowledgements

Firstly, I would like to thank my advisor, Professor Nate Lewis, for giving me the opportunity to join his lab and providing me with the freedom to learn how to conduct independent scientific research. Professor Michael Roukes, my unofficial co-advisor, enabled an exciting collaboration to combine his group's expertise in resonant nanoelectromechanical systems (NEMS) with the Lewis group's experience with chemical vapor sensors, which formed the foundation of my thesis work. I would also thank Professors Julie Kornfield and Jackie Barton for their time and support as members of my committee. The members of "team nose" were instrumental in my success, with Edgardo Garcia, Anna Folinsky, Marc Woodka, and Vince Martin being excellent colleagues to work with. Additionally, this work would have been impossible without "team nanocantilever." In particular, I'd like to thank Mo Li for his help in my preliminary nanocantilever vapor sensing work, and Ed Myers for his help in everything from tracking down bad wires to his modeling of the nanocantilever response behavior. Both Ed and Derrick Chi fabricated beautiful sensors for me to functionalize and break, and Xinchang Zhang built the electronics that enabled me to run more than one sensor at a time (which greatly increased my rate of data collection!). Craig Wiggenhorn has been a great officemate, computer-fixer, and caffeine-provider, who, among other things, helped me save essential data from a dying, clicking hard drive. I have had insightful discussions with members of both the Lewis group and Roukes group that led me to think more deeply about the sometimes-confusing data that I've collected. I would also like to thank Chi Ma for maintaining the GPS SEM,

where I spent the wee hours of the morning collecting images on multiple occasions, and Bruce Brunschwig for heading up the MMRC, which was essential for my surface and film characterization experiments. Barbara Miralles, Elyse Garlock, Su Naing, Agnes Tong, and Kathy Bubash have helped me navigate numerous administrative hurdles. Felicia Hunt has been extraordinarily supportive in all matters, and the Caltech Center for Diversity has offered a number of programs, such as the graduate women's lunch, which provided a great opportunity for meeting interesting folk outside of my lab. I must also thank all of the staff at the Caltech Health Center and Counseling Center for their dedication to student welfare and for keeping me functional during the rough patches. The Graduate Office graciously provided funding that allowed me to attend conferences to present my graduate work. A number of campus organizations such as the Caltech Ballet Club, the Caltech Dance Show, the Prufrock House (which gave me a real gardening space!), and the Caltech Folk Music Society enriched my time at Caltech and gave me many good memories. The "girly group" of Heather Hunt, Arwen Brown, Shelby Hutchens, and Lisa Hochrin kept my spirits up with lunches and cookie decorating. Additionally, Artemis Ailianou, Zuli Kurji, and Aileen Hui have made sure I ate well with potlucks. Pasadena Dance Theatre and Pasadena Civic Ballet gave me a dance home in Pasadena and many performance opportunities, enabling me to grow as an artist while I was learning to be a scientist. Diane De Franco Browne, Cynthia Young, Preston Li, Helga de Kansky, and Laurence Blake have all given me a deeper understanding of the art of dance. Kathy Braidhill has kept me dancing through her expertise in pilates, and has taught me a great deal about the anatomical basis of movement, which is something that I will always cherish. Brian Miller for helping me stay grounded, and for taking me on a (more-or-less) post-props, whirlwind tour of Europe. And lastly I thank my family, who has cheered me on throughout this adventure, encouraging me to take the path less traveled, even if it has been rather long and winding.

Abstract

Chemical vapor sensors are used in a wide variety of fields such as security, environmental monitoring, the food and beverage industry, and healthcare to detect disease biomarkers on exhaled breath. An electronic nose is composed of an array of cross-responsive chemical vapor sensors, in which every sensor responds to a varying degree to each chemical vapor, creating a "fingerprint" for that vapor. Incorporating an electronic nose into a highly-miniaturized vapor detection system, capable of bringing near laboratory-quality analysis into the field, requires the use of extremely small, fast, and sensitive sensors. One option is resonant nanocantilevers, which respond to changes in mass and stiffness by shifts in resonant frequency, and are capable of detecting mass-loading at the attogram (10^{-18} g) level in ambient conditions.

To determine whether nanocantilevers can be used in an electronic nose, an array of five nanocantilevers, wherein each sensor was coated with a different dropcast polymer film (2–10 nm thick), were exposed to seven chemical vapors with a range of functional groups. The array successfully discriminated between all vapors, indicating that sensor responses were dominated by vapor absorption into polymer films, and not by non-specific physisorption. The thinness of the polymer film, combined with the small vapor capture area of the nanocantilevers, resulted in lower sensitivity than desired, limiting their effectiveness. To overcome this challenge, surface initiated atom transfer radical polymerization (SI-ATRP) was used to grow a 100 nm thick, uniform films of poly(methylmethacrylate) (PMMA), poly(methyl acrylate) (PMA), and poly(n-butyl methacrylate)

(PBMA) on nanocantilevers. The thick polymer films absorbed more vapor, significantly increasing nanocantilever sensitivity. To determine the relative roles of mass loading and stiffness change on nanocantilever sensor response, SI-ATRP was combined with chromium masking, enabling polymer film growth to be localized to either the clamped end (sensitive to stiffness) or the free end (sensitive to mass-loading) of the nanocantilevers. These experiments revealed that changes in stiffness, induced by vapor absorption into the polymer films, dominated the sensor responses, and not mass-loading as was initially assumed. This work demonstrated that an array resonant nanocantilevers can be successfully used a sensitive, nanoscale electronic nose.

Contents

List of Figures

List of Tables

Chapter 1

Introduction

1.1 Chemical Vapor Sensors

Sensors are an integral part of modern life, from light switches and thermometers to touch screens in tablets and smartphones, providing information and enabling us to affect our environment. Chemical gas and vapor sensors encountered every day include smoke and carbon monoxide detectors, which are essential for public safety. Also familiar is the breathalyzer test used to detect the presence of ethanol on exhaled breath. Beyond those more commonly encountered examples, chemical vapor sensors are useful in a wide variety of fields such as in security to detect explosives and chemical warfare agents, in the food and beverage industry for quality control, and in healthcare to detect disease biomarkers on the exhaled breath of patients. Simply put, a chemical vapor sensor is composed of two elements: a selective material which interacts with the vapor, and a physical transducer, which translates that interaction into a measured signal, as shown in Figure 1.1, such as a change in color, film thickness, resonant frequency, or electrical resistance. This introductory chapter provides an overview of important concepts relevant to this thesis and lays out the framework that guided the work.

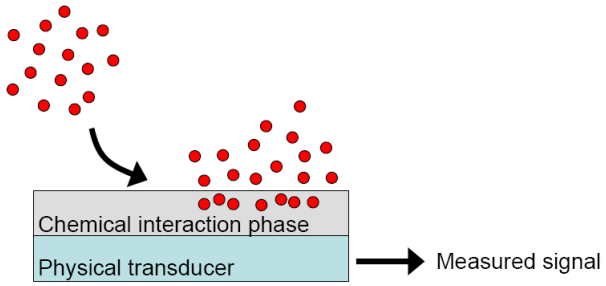

Figure 1.1: A chemical vapor sensor is composed of a phase that interacts with the vapor, and a physical transducer which converts the chemical interaction into a readable signal.

1.2 The Electronic Nose

There are two paradigms for gas phase chemical sensors: highly-specific "lock-and-key" sensors and cross-responsive sensors. Lock-and-key type sensors utilize strong, often irreversible, chemical interactions or reactions to detect a single target vapor. While these sensors are both highly-specific and highly-sensitive, if an application demands that a large number of vapors be identified, the number of required elements in an array composed of lock-and-key type sensors becomes infeasible. Also, since lock-and-key sensors typically respond irreversibly, they cannot be easily integrated into a detection system, and would have to be replaced after each exposure to a chemical vapor.

Conversely, a cross-responsive sensor can interact reversibly with a large number of target vapors, so that a single sensor can be reused many times to detect a variety of vapors. Because cross-responsive sensors lack the high-specificity of lock-and-key type sensors they must be employed in a sensor array, where each element in the array is chemically distinct. Such sensor arrays are often called "electronic noses" or "artificial noses" because of the similarity in operating principle to the mammalian olfactory system. In mammalian olfaction, the olfactory receptors in the nasal passages respond upon contact with odorant molecules, sending signals to the olfactory bulb, which then processes the information and identifies the odor. While humans have 5-6 million total receptors,

they only possess about 350 distinct types of receptors, meaning that a response pattern, rather than a single response measured by a single receptor, is responsible for odor identification.[1]

A wide variety of chemical vapor sensor modalities have been developed for use in cross-responsive arrays, including chemiresistors,[2] chemicapacitors,[3] responsive photonic crystals,[4] surface acoustic wave (SAW) sensors,[5] as well as micro- and nanocantilevers.[6,7,8,9] The choice of sensor employed for a given application depends upon a number of factors such as the sensitivity required, the target vapor, the power consumption limitations, the environmental conditions, and any sensor life-time requirements. Despite several decades of research, electronic noses cannot yet approach the odorant identification capabilities of the canine or even human nose. One reason for this is that there is great variety in the molecular structure and properties of compounds that are recognized as falling into broad categories that humans can identify, such as fruity or flowery.[1] Despite the inability to replicate the versatility of a natural mammalian nose, electronic noses can be optimized for a specific task such as differentiating between the odors of fresh fish and spoiled fish, making strict food quality control economically feasible.[10] Where electronic noses surpass mammalian noses is in the detection of volatile compounds that we are not adapted to sense.

Analogous to the mammalian olfaction system, upon exposure to a vapor, each sensor in the electronic nose array will respond to a certain degree, resulting in a "fingerprint" response, as shown in Figure 1.2. This fingerprint response is then decoded, taking the highly multidimensional data and extracting the relevant variation in array responses between different vapors. In place of the olfactory bulb, data analysis is done by computer, using either statistical methods such as Principal Components Analysis (PCA) or Fischer Linear Discriminant (FLD), or a neural network algorithm. As shown in Figure 1.3, data analysis by PCA results in a 2D or 3D visualization of the sensor response that captures the greatest three dimensions of variance in the sensor array responses. When an electronic nose is operating well, the array responses to each individual vapor cluster tightly, and

there is sufficient distance between the clusters (responses to different vapors) such that it is possible to discriminate between the vapors.

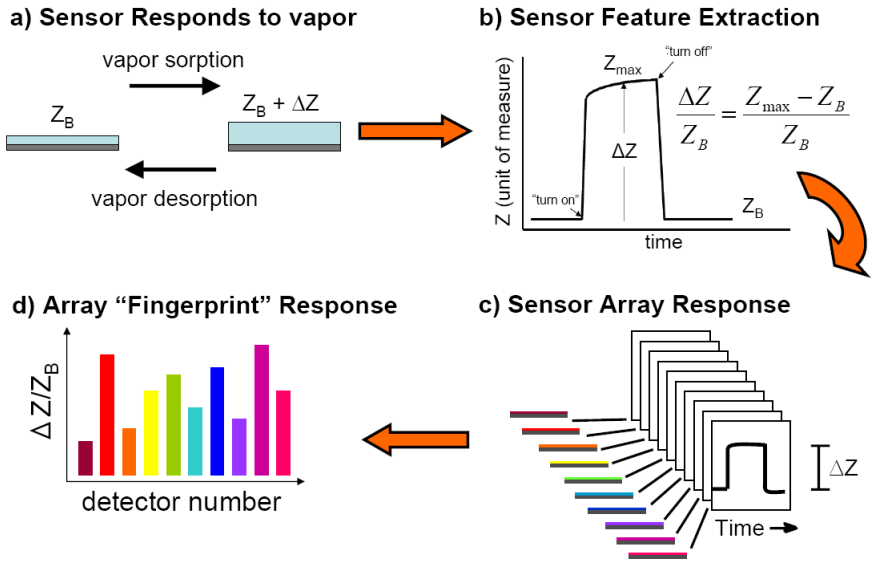

Figure 1.2: Schematic of an electronic nose. A chemical vapor sensor responds reversibly to a chemical vapor by a change in property Z, where Z_b is the baseline value of Z (a). The response signal is extracted; often in the form of the relative change in the relevant property of the sensor (b). A set of sensors with differing chemical coatings all produce responses to a single chemical vapor (c). The responses of the sensor array acts as a"fingerprint" for a chemical vapor (d).

1.3 Vapor Mixtures

One aspect of chemical vapor detection that is particularly challenging is the analysis of mixtures of chemical vapors. In the laboratory it is a simple task to generate a single, pure chemical vapor of known concentration and then direct it to come into contact with an array of sensors. Chemical vapor sensors operating outside of the laboratory must contend with simultaneously being exposed to tens or hundreds of chemical compounds, necessitating the development of strategies to analyze complex sensor responses induced by an additive mixture of vapors. Strategies for determining the components of vapor mixtures include introducing a spatiotemporal sensor chamber[12] and using high-specificity sensor coatings.[13]

Another strategy to handle vapor mixtures is to add a gas chromatography (GC) separation stage to the detection system upstream of the sensor array. While a mixture of vapors is introduced to the inlet, vapors are eluted individually such that the sensor array is only exposed to one vapor at a time, eliminating the need for complex data analysis.[14] While adding a GC greatly increases the complexity of a chemical vapor detection system, it enhances the flexibility of the system, and is likely to be mandatory for many applications.

1.4 Miniaturization of Chemical Vapor Sensors

Miniaturized chemical vapor detection systems embedded into handheld devices like smartphones, or even wearable packages, would put the power of chemical analysis, that today is confined to the laboratory, into the hands those working on the frontline of public health and safety. For example, doctors working in remote regions would be able to carry a handheld sensor system to detect the presence of biomarkers for contagious diseases, such as tuberculosis, on exhaled breath. If a patient tested positive, antibiotics could be prescribed immediately, a vast improvement from current standard diagnostic procedures which require cell culturing and a minimum of several days between sample collection and initiation of treatment.

Sensors in highly miniaturized systems must be capable of being fabricated small enough to be compatible with microfluidics while retaining sufficient sensitivity to detect the target vapors. Some well-studied macroscale sensors cannot achieve this. For example, as the dimensions of composite chemiresistors are decreased, their signal to noise ratio diminishes,[15] rendering them ineffective at the nanoscale. Additionally, sensor actuation and readout schemes must be compatible with size and power limitations. For example, sensors that rely on lasers or respond via color change are inappropriate for extreme miniaturization. A number of microscale chemical vapor sensors that are compatible with the constraints of miniaturized detection systems have been investi-

gated, including chemiresistors,[16,17,18,19,20] carbon nanotube chemicapacitors,[21,22] surface acoustic wave (SAW) devices,[23,24,25] organic thin film transistors,[26] metal oxide nanowires,[27] and microcantilevers (static and resonating).[28,29,30,31,31] Additionally, resonant nanocantilevers have been studied as detectors for ultra-fast GC as an intermediate step to integration with a portable micro-GC.[9] Figure 1.4 presents a schematic for a miniaturized vapor detection system along with a photograph of a prototype smartphone-based chemical vapor sensor array.

1.5 Micro- and Nanocantilever Sensors

Microcantilevers, and more recently nanocantilevers, have shown great promise for incorporation into miniaturized vapor detection systems. Cantilevers have a long history of being studied for use as chemical sensors, with macroscale cantilever chemical sensors for hydrogen gas measured by static deflection being reported as early as 1943.[33] But, due to their susceptibility to external vibrations, cantilever transducers attainted little practical appeal until microscale fabrication and precise readout methods became more widely available.[29] It was the advent of atomic force microscopy (AFM), which relies on resonance and deformation of microfabricated cantilever transducers to measure surface features at the nanoscale, that heralded renewed interest in cantilever sensors.[34]

A cantilever is a singly clamped suspended beam. Micro- and nanocantilevers are typically fabricated by either bulk micromachining (etching through a wafer from the backside to suspend the cantilever) or surface micromachining (etching the device side of the wafer to suspend the cantilever), and can be made using a variety of materials such as silicon nitride,[35] polymers,[36] and even nanowires.[37,38] Cantilever sensors can be operated either in static mode or dynamic mode, as shown in Figure 1.5. In the static mode, cantilever deflection is measured. Deflection can be caused by intrinsic stresses, such as when a bimaterial cantilever, comprised of two materials with different coefficients of thermal expansion, is heated. When operated statically as a chemical sensor, one

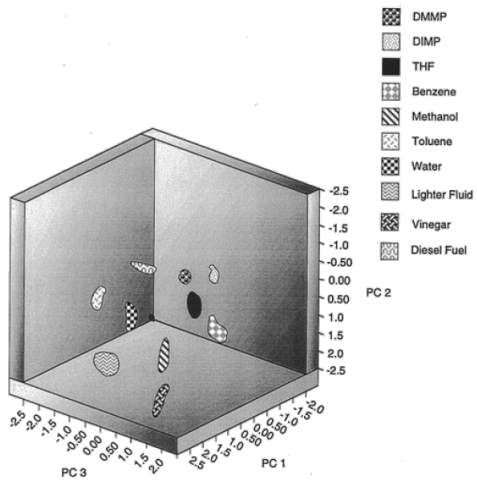

Figure 1.3: Example of electronic nose data analyzed using PCA: Data in principal component space of $\Delta R/R_b$ (relative change in electrical resistance) values produced when an eight-detector carbon black/polymer composite chemiresistor array was exposed to dimethylmethylphosphonate (DMMP), diisopropylphosphonate (DIMP), tetrahydrofuran (THF), benzene, methanol, toluene, water, lighter fluid, vinegar, or diesel fuel, each at P/P° = 0.010 (where P is the partial pressure and P° is the saturated vapor pressure), in an air background. The first three principal components contain 97% of the total variance in the data. The ellipsoids contain 95% of the data for each analyte. Each analyte was presented eight times to the array with the order of presentation randomized over all repetitions of all exposure types.[11]

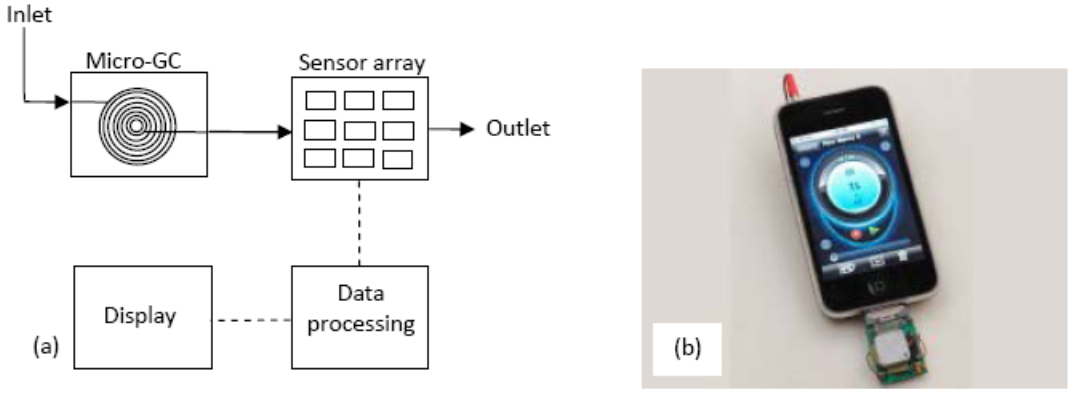

Figure 1.4: Schematic of chemical vapor detection system (a), and a photograph of a miniaturized chemical vapor sensor array (b), developed by NASA Ames Research Center (composed of sixteen nanosensors).[32]

surface of the cantilever is modified by applying a metal film, self assembled monolayer (SAM), or polymer film that will interact with the target chemical. The sorption of a chemical species onto the modified surface induces a change in surface stress, causing cantilever deflection.[6]

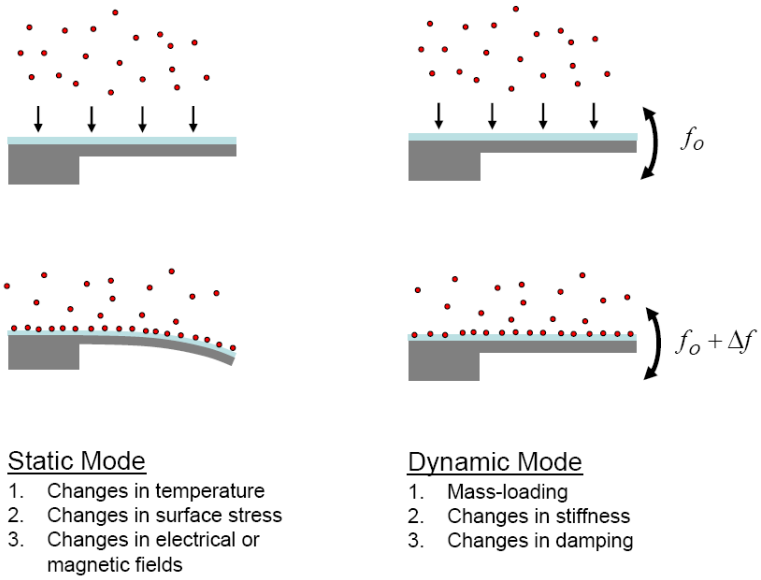

Figure 1.5: Static (a) vs. dynamic (b) cantilever operation. Flexible cantilevers are the most sensitive for static deformation experiments, while stiff cantilevers are preferred for dynamic resonant frequency shift experiments because mass responsivity improves with increasing resonant frequency.

In dynamic operation (in vacuum or gases) cantilevers can be treated as weakly damped oscillators, and resonant frequency is a function of the cantilever mass and stiffness:

$$f_0 = \frac{1}{2\pi}\sqrt{\frac{k}{m_{eff}}} \tag{1.1}$$

where f_0 is the fundamental resonance frequency, m_{eff} is the effective mass for the fundamental mode (the total mass multiplied by the integral of a normalized function describing the modal shape[39]) and k is the effective fundamental-mode stiffness (spring constant). It is often assumed, especially for microcantilevers, that the spring constant remains unchanged and thus mass-loading is the sole cause of observed shifts in resonance frequency.[40,41] Changes in spring constant must

be considered when thick sorptive films (relative to cantilever thickness) are applied,[8] when metal films undergo alloying,[42] and especially when cantilever dimensions are shrunk to the nanoscale.[43] In these cases, assuming ($\delta m_{eff} << m_{eff}$ and $\delta k << k$), the relative change in resonance frequency can be approximated as

$$\frac{\Delta f}{f_0} = \frac{\partial k}{2k} - \frac{\partial m_{eff}}{2m_{eff}} \tag{1.2}$$

where $\Delta f / f_0$ is the relative change in resonance frequency.[43] According to Equation 1.2, an increase in effective mass induces a negative frequency shift, while an increase in spring constant induces a positive frequency shift.

The resonance quality factor (Q) of a cantilever is the measure of damping, or energy loss. The higher the Q value, the greater the amplitude of vibration at the resonant frequency (f_0) and the smaller the bandwidth (the range of frequencies around f_0, at which the cantilever resonates). The Q of a resonant cantilever determines the minimum resolvable change in f_0, which in turn determines the minimum changes in mass and stiffness resulting from the sorption of vapor molecules, which can be measured, as shown in Figure 1.6. Thus the design and fabrication high Q cantilevers is essential for the production of highly sensitive chemical vapor sensors.

The displacements of cantilevers operating statically or dynamically can be measured using a number of methods. Optical detection of cantilever movement is very precise, but becomes inefficient when applied to nanocantilevers, and may not be compatible with portable detection systems. Electrical readout by piezoresistive, piezoelectric, capacitance, or electron tunneling methods is suitable for both micro- and nanocantilevers, and can be more readily integrated into a miniaturized vapor detection system.[29] The resonant frequency of the nanocantilevers used in this thesis was measured via piezoresistive readout, whereby the gold top surface of the cantilever undergoes elon-

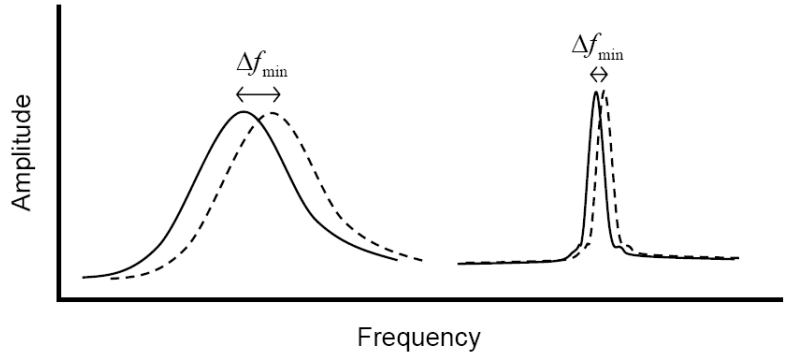

Figure 1.6: Low Q (a) vs high Q (b) resonance peaks. The higher the Q value, the smaller the resolvable shift in resonant frequency, and the more sensitive the cantilever to changes in mass and stiffness.

gation and compression with cantilever motion. By current biasing the gold film piezoresistor, the strain-induced resistance change is translated into a measurable voltage.[44] Additionally, the piezoresistor is used to downmix the displacement signal to a lower frequency, enabling the detection of nanocantilever displacement using standard circuitry.[45]

There are also a number of methods to actuate the resonance of micro- and nanocantilevers,[6] the choice of which can effect the Q of the sensor. For example, in the preliminary studies conducted to characterize the nanocantilevers used in this thesis, the sensors were mounted on a piezoshaker, which was used to actuate cantilever resonance. The piezoshaker introduced undesirable secondary resonances, and the nanocantilever resonance quality varied significantly. Upon noting these limitations, sensors were switched to thermal-elastic actuation, whereby cantilever resonance is driven by resistive heating and motion is induced because of the difference in coefficients of thermal expansion of the bilayer structure. Figure 1.7 illustrates the difference in resonance quality between the two actuation schemes. Thermal-elastic actuation resulted in much cleaner resonance peaks, improved sensor-to-sensor reproducibility, and enhanced sensitivity to chemical vapors.

Shrinking the dimensions of resonant cantilevers to the nanoscale has a number of benefits.

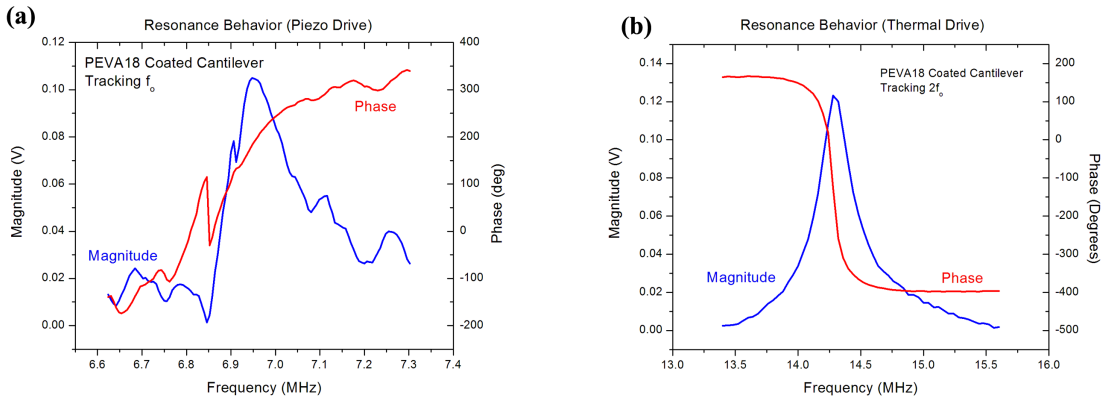

Figure 1.7: The resonance peaks of the same nanocantilever actuated via piezoshaker (a) and then driven by the thermal-elastic effect (b). Switching from the piezoshaker to thermal-elastic drive improved the signal to noise ratio of sensor responses to chemical vapors, but introduced greater baseline noise.

Firstly, by shrinking the cantilevers, more sensors can be packed into the same area. Large sensor arrays with multiple redundant cantilevers and a variety of different chemically functional coatings can be achieved while maintaining a footprint small enough for integration into microfluidics. Secondly, shrinking the cantilevers enhances their sensitivity. The minimum detectable mass change is described as

$$\delta m_{min} \approx 2\frac{m_{eff}}{\omega_0}\delta\omega_{min} \tag{1.3}$$

where δm_{min} is the minimum detectable change in mass, ω_0 is the resonance frequency, and $\delta\omega_{min}$ is the minimum resolvable shift in resonant frequency. Decreasing the effective mass of the cantilever (shrinking its dimensions) while maximizing its resonant frequency (fabricating the sensor from a stiff material) leads to the most sensitive mass detection.[39] This extreme responsivity to changes in mass that occurs upon shrinking cantilevers to the nanoscale outweighs the effects of simultaneously reducing the vapor capture area. Lastly, nanoscale cantilevers have an additional attribute: they maintain high Q in ambient conditions, enabling small shifts in resonant frequency,

correlating to small changes in mass and stiffness, to be resolved.[44]

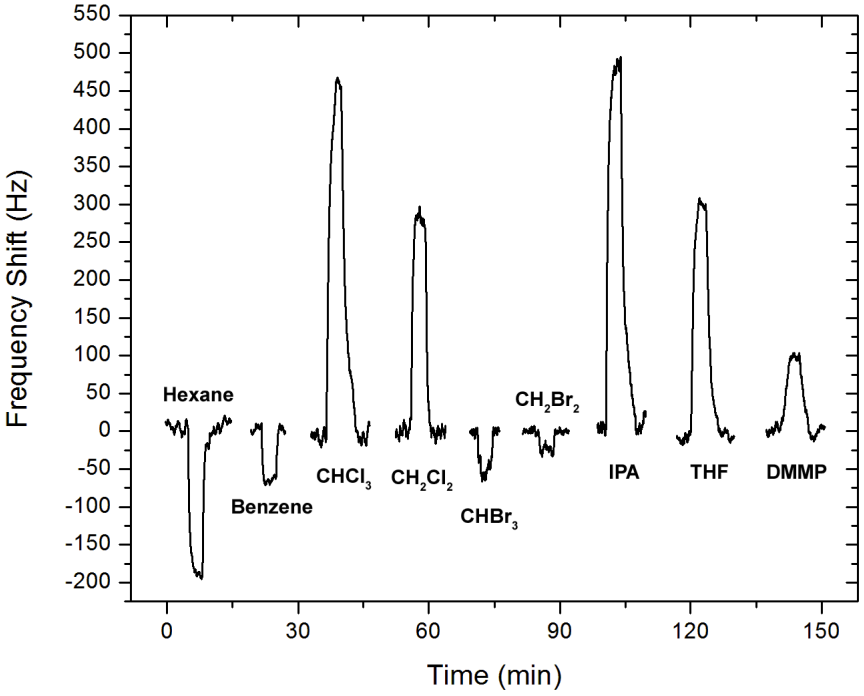

Figure 1.8: Preliminary nanocantilever responses to a series of chemical vapors. The cantilever was coated with a 2-10 nm thick, dropcast film of poly(ethylene oxide), and was actuated by a piezoshaker. The vapors were presented at $P/P^{\circ} = 0.020$, and the exposure time was 200 s. Abbreviations: IPA = isopropanol, THF = tetrahydrofuran, and DMMP = dimethylmethylphosphonate. The sensor responses that consisted of positive shifts in resonance frequency revealed that mass-loading was not the only response mechanism at play. Additionally, the clear differences in responses between the vapors showed that polymer-coated nanocantilevers might be suitable for a nanoscale electronic nose.

One complication of shrinking cantilevers to the nanoscale is that their surface area to volume ratio increases, leading them to become more likely to exhibit "anomalous" frequency shift responses to chemical stimuli that cannot be accounted for by mass-loading alone. For example, nanocantilever biosensors exhibited positive frequency shifts upon absorption of bacteria, which was attributed to an increase in cantilever stiffness.[46,47] Similar anomalous responses were observed with resonant nanocantilevers exposed to chemical vapors during preliminary experiemnts,

as shown in Figure 1.8, promting an detailed exploration of the underlying causes behind these early observations. To date, no models have been developed that satisfactorily explain the mechanisms behind nanocantilever responses that cannot be explained by mass-loading alone, and it remains an active research area.[43]

1.6 Outline of this Thesis

This thesis is comprised of three projects that were undertaken to develop resonant nanocantilever sensors for use in highly-miniaturized vapor detection systems. Chapter 2 covers the creation and testing of a five sensor nanocantilever electronic nose. The sensor and array performance of the nanocantilevers was compared to that of an array of macroscale chemiresistive sensors, which acted as a standard to benchmark the strengths and weaknesses of the nanocantilevers. Chapter 3 describes the use of surface initiated atom transfer radical polymerization (SI-ATRP) to grow thick, uniform films of poly(methyl methacrylate) on nanocantilever chemical vapor sensors in order to improve sensitivity and reproducibility. Chapter 4 builds on the work of Chapter 3 by comparing the behavior of nanocantilevers coated with SI-ATRP grown films of rubbery and glassy polymers. Additionally, SI-ATRP is combined with a chromium masking and passivation scheme to localize the growth of polymer films to either the free end or the clamped end of the nanocantilevers to determine whether mass-loading or changes in stiffness dominates the observed sensor response behavior. Finally, Chapter 5 presents a brief summary of the work, relating it to the overall field, and gives ideas for future research directions necessary to realize nanocantilevers as practical chemical vapor sensors.

Bibliography

[1] T. C. Pearce, S. S. Schiffman, H. T. Nagle, and J. W. Gardner. *Handbook of Machine Olfaction - Electronic Nose Technology*. John Wiley & Sons, 2003.

[2] N. S. Lewis. Comparisons between mammalian and artificial olfaction based on arrays of carbon black-polymer composite vapor detectors. *Accounts of Chemical Research*, 37(9):663–672, 2004.

[3] S. Dimopoulos, M. Kitsara, D. Goustouridis, S. Chatzandroulis, and I. Raptis. A chemocapacitive sensor array system for gas sensing applications. *Sensor Letters*, 9(2):577–583, 2011.

[4] L. D. Bonifacio, G. A. Ozin, and A. C. Arsenault. The photonic nose: A versatile platform for sensing applications. In T. George, M. S. Islam, and A. K. Dutta, editors, *Micro- and Nanotechnology Sensors, Systems, and Applications III*, volume 8031 of *Proceedings of SPIE*. Spie-Int Soc Optical Engineering, Bellingham, 2011.

[5] J. W. Grate and B. M. Wise. Chemical information from polymer-coated acoustic wave sensor arrays. In S. Buttgenbach, editor, *Chemical Microsensors and Applications Ii*, volume 3857 of *Proceedings of the Society of Photo-Optical Instrumentation Engineers (SPIE)*, pages 170–173. Spie-Int Soc Optical Engineering, Bellingham, 1999.

[6] A. Boisen, S. Dohn, S. S. Keller, S. Schmid, and M. Tenje. Cantilever-like micromechanical sensors. *Reports on Progress in Physics*, 74(3):30, 2011.

[7] M. Zougagh and A. Rios. Micro-electromechanical sensors in the analytical field. *Analyst*, 134(7):1274–1290, 2009.

[8] T. Thundat, G. Y. Chen, R. J. Warmack, D. P. Allison, and E. A. Wachter. Vapor detection using resonating microcantilevers. *Analytical Chemistry*, 67(3):519–521, 1995.

[9] M. Li, E. B. Myers, H. X. Tang, S. J. Aldridge, H. C. McCaig, J. J. Whiting, R. J. Simonson, N. S. Lewis, and M. L. Roukes. Nanoelectromechanical resonator arrays for ultrafast, gas-phase chromatographic chemical analysis. *Nano Letters*, 10(10):3899–3903, 2010.

[10] C. Di Natale, G. Olafsdottir, S. Einarsson, E. Martinelli, R. Paolesse, and A. D'Amico. Comparison and integration of different electronic noses for freshness evaluation of cod-fish fillets. *Sensors and Actuators B-Chemical*, 77(1-2):572–578, 2001.

[11] A. R. Hopkins and N. S. Lewis. Detection and classification characteristics of arrays of carbon black/organic polymer composite chemiresistive vapor detectors for the nerve agent simulants dimethylmethylphosphonate and diisopropylmethylphosponate. *Analytical Chemistry*, 73(5):884–892, 2001.

[12] M. D. Woodka, B. S. Brunschwig, and N. S. Lewis. Use of spatiotemporal response information from sorption-based sensor arrays to identify and quantify the composition of analyte mixtures. *Langmuir*, 23(26):13232–13241, 2007.

[13] L. A. Pinnaduwage, W. Zhao, A. C. Gehl, S. L. Allman, A. Shepp, K. K. Mahmud, and J. W. Leis. Quantitative analysis of ternary vapor mixtures using a microcantilever-based electronic nose. *Applied Physics Letters*, 91(4):044105, 2007.

[14] R.L. Grob and E.F. Barry. *Modern Practice of Gas Chromatography*. Wiley-Interscience, 2004.

[15] S. M. Briglin, M. S. Freund, P. Tokumaru, and N. S. Lewis. Exploitation of spatiotemporal information and geometric optimization of signal/noise performance using arrays of carbon black-polymer composite vapor detectors. *Sensors and Actuators B-Chemical*, 82(1):54–74, 2002.

[16] E. Covington, F. I. Bohrer, C. Xu, E. T. Zellers, and C. Kurdak. Densely integrated array of chemiresistor vapor sensors with electron-beam patterned monolayer-protected gold nanoparticle interface films. *Lab on a Chip*, 10(22):3058–3060, 2010.

[17] C. J. Lu, W. H. Steinecker, W. C. Tian, M. C. Oborny, J. M. Nichols, M. Agah, J. A. Potkay, H. K. L. Chan, J. Driscoll, R. D. Sacks, K. D. Wise, S. W. Pang, and E. T. Zellers. First-generation hybrid MEMS gas chromatograph. *Lab on a Chip*, 5(10):1123–1131, 2005.

[18] K. J. Albert, N. S. Lewis, C. L. Schauer, G. A. Sotzing, S. E. Stitzel, T. P. Vaid, and D. R. Walt. Cross-reactive chemical sensor arrays. *Chemical Reviews*, 100(7):2595–2626, 2000.

[19] F. J. Ibañez, U. Gowrishetty, M. M. Crain, K. M. Walsh, and F. P. Zamborini. Chemiresistive vapor sensing with microscale films of gold monolayer protected clusters. *Analytical Chemistry*, 78(3):753–761, 2006.

[20] R. S. Jian, R. X. Huang, and C. J. Lu. A micro GC detector array based on chemiresistors employing various surface functionalized monolayer-protected gold nanoparticles. *Talanta*, 88:160–167, 2012.

[21] E. S. Snow, F. K. Perkins, E. J. Houser, S. C. Badescu, and T. L. Reinecke. Chemical detection with a single-walled carbon nanotube capacitor. *Science*, 307(5717):1942–1945, 2005.

[22] J. A. Robinson, E. S. Snow, and F. K. Perkins. Improved chemical detection using single-

walled carbon nanotube network capacitors. *Sensors and Actuators A-Physical*, 135(2):309–314, 2007.

[23] J. W. Grate. Acoustic wave microsensor arrays for vapor sensing. *Chemical Reviews*, 100(7):2627–2647, 2000.

[24] P. R. Lewis, R. P. Manginell, D. R. Adkins, R. J. Kottenstette, D. R. Wheeler, S. S. Sokolowski, D. E. Trudell, J. E. Byrnes, M. Okandan, J. M. Bauer, R. G. Manley, and G. C. Frye-Mason. Recent advancements in the gas-phase MicroChemLab. *IEEE Sensors Journal*, 6(3):784–795, 2006.

[25] Jay W. Grate, Susan L. Rose-Pehrsson, David L. Venezky, Mark Klusty, and Hank Wohltjen. Smart sensor system for trace organophosphorus and organosulfur vapor detection employing a temperature-controlled array of surface acoustic wave sensors, automated sample preconcentration, and pattern recognition. *Analytical Chemistry*, 65(14):1868–1881, 1993.

[26] L. Wang, D. Fine, and A. Dodabalapur. Nanoscale chemical sensor based on organic thin-film transistors. *Applied Physics Letters*, 85(26):6386–6388, 2004.

[27] P. C. Chen, F. N. Ishikawa, H. K. Chang, K. Ryu, and C. Zhou. A nanoelectronic nose: a hybrid nanowire/carbon nanotube sensor array with integrated micromachined hotplates for sensitive gas discrimination. *Nanotechnology*, 20(12):8, 2009.

[28] L. A. Pinnaduwage, H. F. Ji, and T. Thundat. Moore's law in homeland defense: An integrated sensor platform based on silicon microcantilevers. *IEEE Sensors Journal*, 5(4):774–785, 2005.

[29] N. V. Lavrik, M. J. Sepaniak, and P. G. Datskos. Cantilever transducers as a platform for chemical and biological sensors. *Review of Scientific Instruments*, 75(7):2229–2253, 2004.

[30] H. P. Lang, M. K. Baller, R. Berger, Ch Gerber, J. K. Gimzewski, F. M. Battiston, P. Fornaro, J. P. Ramseyer, E. Meyer, and H. J. Gntherodt. An artificial nose based on a micromechanical cantilever array. *Analytica Chimica Acta*, 393(1-3):59–65, 1999.

[31] Peter J. Chapman, Frank Vogt, Pampa Dutta, Panos G. Datskos, Gerald L. Devault, and Michael J. Sepaniak. Facile hyphenation of gas chromatography and a microcantilever array sensor for enhanced selectivity. *Analytical Chemistry*, 79(1):364–370, 2006.

[32] NASA Ames Scientist Develops Cell Phone Chemical Sensor. `http://www.nasa.gov/centers/ames/news/features/2009/cell_phone_sensors.html`, 2009. (Accessed September 3, 2012).

[33] F.J. Norton. Gas Analyzer, 1943.

[34] G. Binnig, C. F. Quate, and C. Gerber. Atomic force microscope. *Physical Review Letters*, 56(9):930–933, 1986.

[35] R. Datar, S. Kim, S. Jeon, P. Hesketh, S. Manalis, A. Boisen, and T. Thundat. Cantilever sensors: Nanomechanical tools for diagnostics. *MRS Bulletin*, 34(6):449–454, 2009.

[36] J. Tamayo, D. Ramos, J. Mertens, and M. Calleja. Effect of the adsorbate stiffness on the resonance response of microcantilever sensors. *Applied Physics Letters*, 89(22):3, 2006.

[37] M. D. Dai, C. W. Kim, and K. Eom. Finite size effect on nanomechanical mass detection: the role of surface elasticity. *Nanotechnology*, 22(26):10, 2011.

[38] J. R. Montague, M. Dalberth, J. M. Gray, D. Seghete, K. A. Bertness, S. M. George, V. M. Bright, C. T. Rogers, and N. A. Sanford. Analysis of high-Q, gallium nitride nanowire resonators in response to deposited thin films. *Sensors and Actuators A-Physical*, 165(1):59–65, 2011.

[39] K. L. Ekinci and M. L. Roukes. Nanoelectromechanical systems. *Review of Scientific Instruments*, 76(6), 2005.

[40] M. Maute, S. Raible, F. E. Prins, D. P. Kern, H. Ulmer, U. Weimar, and W. Gopel. Detection of volatile organic compounds (VOCs) with polymer-coated cantilevers. *Sensors and Actuators B-Chemical*, 58(1-3):505–511, 1999.

[41] S. Singamaneni, M. C. LeMieux, H. P. Lang, C. Gerber, Y. Lam, S. Zauscher, P. G. Datskos, N. V. Lavrik, H. Jiang, R. R. Naik, T. J. Bunning, and V. V. Tsukruk. Bimaterial microcantilevers as a hybrid sensing platform. *Advanced Materials*, 20(4):653–680, 2008.

[42] T. Thundat, E. A. Wachter, S. L. Sharp, and R. J. Warmack. Detection of mercury-vapor using resonating microcantilevers. *Applied Physics Letters*, 66(13):1695–1697, 1995.

[43] K. Eom, H. S. Park, D. S. Yoon, and T. Kwon. Nanomechanical resonators and their applications in biological/chemical detection: Nanomechanics principles. *Physics Reports-Review Section of Physics Letters*, 503(4-5):115–163, 2011.

[44] M. Li, H. X. Tang, and M. L. Roukes. Ultra-sensitive NEMS-based cantilevers for sensing, scanned probe and very high-frequency applications. *Nature Nanotechnology*, 2(2):114–120, 2007.

[45] I. Bargatin, E. B. Myers, J. Arlett, B. Gudlewski, and M. L. Roukes. Sensitive detection of nanomechanical motion using piezoresistive signal downmixing. *Applied Physics Letters*, 86(13):3, 2005.

[46] D. Ramos, J. Tamayo, J. Mertens, M. Calleja, and A. Zaballos. Origin of the response of nanomechanical resonators to bacteria adsorption. *Journal of Applied Physics*, 100(10):3, 2006.

[47] D. Ramos, M. Calleja, J. Mertens, A. Zaballos, and J. Tamayo. Measurement of the mass and rigidity of adsorbates on a microcantilever sensor. *Sensors*, 7(9):1834–1845, 2007.

Chapter 2

Nanocantilever Chemical Vapor Sensor Array for Detection and Discrimination of Volatile Organic Compounds (VOCs)

Miniaturized chemical vapor sensor arrays require the development of ultra-sensitive detectors that enable real-time detection and chemical identification. Here, we present a five-element array of resonating, polymer-coated nanocantilevers capable of discriminating among seven volatile organic compound (VOC) vapors, under both dry and slightly humid conditions. To confirm the quality of the nanocantilever array's performance, its sensitivity and discrimination capability were compared to that of a composite chemiresistor array that utilized the same polymers as the nanocantilever array. The chemiresistors required a minimum footprint of 1.17 mm^2 per detector to match the signal to noise ratio (SNR) of the nanocantilevers, which have a 1.5 μm^2 footprint each; a factor of 10^6 difference in area. The nanocantilever responses shifted when humidity was introduced to the background, which was attributed to the physisorption of water vapor onto the nanocantilever surface, and into the hydrophilic polymer films. The nanocantilever array successfully discriminated between all seven analyte vapors under dry background conditions, but failed to differentiate between some vapors in a humid background. However, with their extreme sensitivity, strong discrimination

capability, and small dimensions, resonating nanocantilever arrays are ideal candidates for minaturized electronic nose applications.

2.1 Introduction

Chemical vapor sensors are utilized in diverse fields such as defense, healthcare, environmental monitoring, and food quality control.[1] Sensors are either designed to be highly specific, utilizing strong lock-and-key type chemical interactions or reactions to detect a single compound or class of compounds, or broadly-cross reactive, such that a single sensor will respond to a variety of analytes. Cross-reactive sensors reflect less-specific interactions, such as Van Der Waals forces and hydrogen bonding, and are often used in arrays such that each sensor will respond to a certain degree to most analytes presented.[2,3] Upon exposure to an odorant, the pattern of responses produced by the sensors in the array yields a fingerprint for the vapor, mimicking the principles of mammalian olfaction and leading these arrays to be called electronic noses. Pattern recognition algorithms can then be used to differentiate between analytes of varying molecular weight, polarity, chirality, other physiochemical properties, and concentration,[4,5,6,6] and with training are capable of classifying a range of organic and inorganic vapors for a variety of applications.[7,8,9]

Recently, there has been much interest in using electronic noses in field environments via either incorporation into everyday products, such as cell phones,[10,11,12,13,14] or inclusion in a lab-on-a-chip apparatus, such as with micro-gas chromatographs.[15,16] The challenge of utilizing the maximum number of sensors in the minimum amount of space has prompted the study of micro- and nanoscale chemical vapor sensors that can be multiplexed into arrays.[17,18,19,20,21] Microscale sensors, however, must be extremely sensitive to offset their small capture areas,[22] and be readily functionalizable to introduce response selectivity. A number of microscale chemical vapor sensors have been investigated including chemiresistors,[3,17,23,24] carbon nanotube chemicapacitors,[25,26] sur-

face acoustic wave (SAW) devices,[21,27,28] organic thin film transistors,[29] metal oxide nanowires,[19] and both static and resonating microcantilevers.[20,30,31,32,33]

Of these, nanocantilever and other nanoelectromechanical systems (NEMS) resonators show great promise for these applications, as they are small enough to operate within microanalytical systems, can be multiplexed in arrays, and have demonstrated mass sensitivity at and below the zeptogram scale (10^{-21} g) in vacuum.[34,35,36] Resonating nanocantilever sensors detect the sorption of vapor molecules through resonant frequency shifts that can be attributed to changes in mass, stiffness, surface stress, and surface elasticity.[37] Coating nanocantilevers with thin polymer films increases the quantity of vapor that can be adsorbed onto the sensor, and introduces selectivity by harnessing specific chemical interactions between the polymer films and the analytes. In previous work, the minimum resolvable mass change was calculated to be below 1 attogram (10^{-18} g) for a poly(methyl methacrylate) coated nanocantilever exposed to 1,1-difluoroethane in ambient conditions.[38] More recently, a two element nanocantilever array was combined with ultrafast-GC to analyze thirteen chemicals within a 5 s time window and demonstrated detection of sub-parts per billion (ppb) of diisopropyl methylphosphonate (DIMP), a nerve agent simulant.[16] Here, we conduct an in-depth study of a nanocantilever chemical vapor sensor array's discrimination performance based only on the sensitivity and selectivity inherent in the sensors. This work demonstrates that nanocantilever-based chemical vapor sensor arrays are capable of performing many vapor discrimination tasks on par with an array of well-developed macroscale sensors, and thus provide a viable option to achieving an integrated, field-deployable nanoscale electronic nose.

In this work the sensitivity and discrimination performance of a five element array of polymer-coated nanocantilever sensors exposed to seven different volatile organic compounds (VOCs) was examined. To provide a baseline for performance evaluation, an array of chemiresistive sensors, coated with the same set of polymers as the nanocantilevers, was tested under the same conditions

as the nanocantilevers. Chemiresistors were chosen for this comparison because their ability to detect and discriminate between VOCs has been studied extensively.[39,40,41,42,43] The chemiresistors used in this study are a composite material composed of conductive carbon black particulates and an insulating polymer, which swells upon exposure to analyte vapors. The polymer film swelling decreases the number of conductive pathways across the film, inducing a measurable increase in resistance across the film.[2] The seven analytes tested (hexane, benzene, chloroform, dichloromethane, bromoform, dibromomethane, and isopropanol) include closely related compounds to challenge the discrimination capability of the arrays. Sensor arrays were exposed to analyte vapors in both dry nitrogen and humid air background to determine the effect of humidity on response and discrimination. Individual sensor performance was evaluated in terms of response magnitude and signal to noise ratio (SNR), which correlates to the minimum detectable level (MDL), the lowest detectable concentration of analyte vapor. Array discrimination performance was analyzed using Principle Components Analysis (PCA), to visualize response clustering, and Fisher's Linear Discriminant (FDL), to quantify the discrimination between pairs of analytes. This study demonstrated that high array discrimination performance was maintained with nanoscale sensors when operated in dry conditions, and that polymer coatings applied to nanocantilever sensors must be appropriately matched to the expected background conditions as well as target analytes.

2.2 Experimental

2.2.1 Materials

Polybutadiene (variable MW) (PBD) and hydroxypropylcellulose (MW = 60k) (HPC) were purchased from Scientific Polymer Products, Poly(ethylene-co-vinyl acetate) (18% vinyl acetate) (variable MW) (PEVA) and Polysulfone (MW = 30k) (PSul) were purchased from Polysciences, and

Polystyrene (GPC Standard MW = 2,460) (PS) was purchased from Aldrich. Carbon black (Black Pearls 2000) (CB) was donated by Cabot, Inc. Reagent grade benzene (Ben), bromoform (CHBr3), dibromomethane (DBM), and n-hexane (Hex), were purchased from Aldrich. Reagent grade chloroform (CHCl3), dichloromethane (DCM), and isopropanol (IPA) were obtained from VWR. All chemicals were used as received.

2.2.2 Sensors

2.2.2.1 Nanocantilevers

Silicon nitride nanocantilevers (Figure 2.1) with integrated piezoresistive readouts were used in this study. The fabrication of this type of nanocantilever has been described in detail previously.[38,44] Briefly, the cantilever shapes were patterned with electron beam lithography onto a 100 nm thick layer of SiN on a silicon substrate, followed by gold film deposition, and then liftoff. A dry plasma etch was then used to release the sensors. The gold overlayer served as both etch mask during fabrication and later as a piezoresistive transducer.[45] Nanocantilevers had a typical fundamental resonance frequency of 10–12 MHz, quality (Q) factors of 100–200 in ambient conditions, and a capture area of 1.5 μm^2. Resonance was actuated thermoelastically.[46] Nanocantilever sensors were operated with home-built, LabView-controlled electronics[45] which tracked each sensor's resonance frequency using parallel, independent phase-locked loops, and were capable of operating five sensors simultaneously. Thin polymer films were deposited by dropcasting from dilute solutions (5 mg/mL polymer in toluene), resulting in 2-10 nm thick films as measured by ellipsometry.[38] Sorption of vapor molecules into the polymer films changed sensor mass and stiffness, inducing a resonance frequency shift. Cantilevers were imaged with a scanning electron microscope (SEM) to verify fabrication quality *before* coating, as the electron beam can damage polymer films.

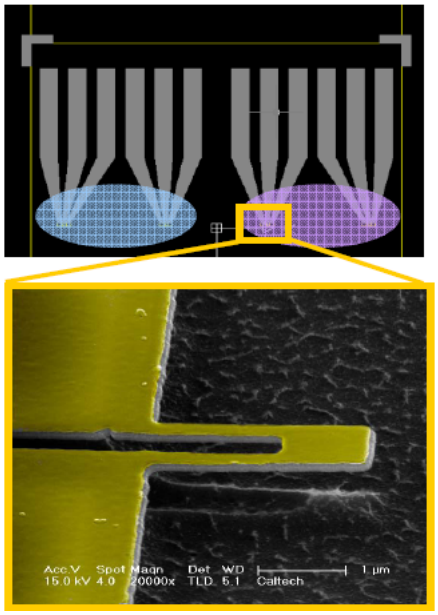

Figure 2.1: (a) Illustration of a nanocantilever chip (1 cm across), containing eight sensors, with two dropcast polymer films. (b) False-color SEM image of 2.5 μm long self-sensing SiN nanocantilever with gold top layer for piezoresistive readout.

2.2.2.2 Chemiresistors

Chemiresistors were prepared by depositing a polymer/CB film across a 5 mm gap between two gold leads that had been evaporated onto a glass microscope slide. Chemiresistive composite materials were composed of an 80:20 mass ratio of polymer to carbon black dissolved in THF. To form solutions, 160 mg of polymer was added to 20 mL of THF and sonicated until dissolved. Then 40 mg of CB was added and the solution sonicated until CB was suspended. The solutions were sprayed onto the sensor substrates with an airbrush, resulting in films with resistances of 18-48 kΩ, a range shown to reliably produce repeatable responses.[47] Sorption of vapor molecules into the composite chemiresistive film caused the film to swell, increasing the sensor's resistance. The DC resistance across each chemiresistor was measured by a digital multimeter (Keithley Model 2002) connected to a multiplexing unit (Keithley Model 7001).

2.2.3 Sensor Arrays

Five element sensor arrays of nanocantilevers and chemiresistors were created for comparison experiments as this was the maximum number of nanocantilevers that could be operated simultaneously with our custom-built electronics. Polymers were chosen from a chemiresistor array of ten polymers spanning a range of chemical functionalities according to Linear Solvation Energy Relationships (LSER) principles.[48,49] From this group the five best polymers, in terms of sensitivity, response time, and unique response pattern across analyte vapors, were selected for the array comparison experiments (see Figure 2.2 for selected polymers). The chemiresistor and nanocantilever sensor arrays consisted of one sensor using each polymer.

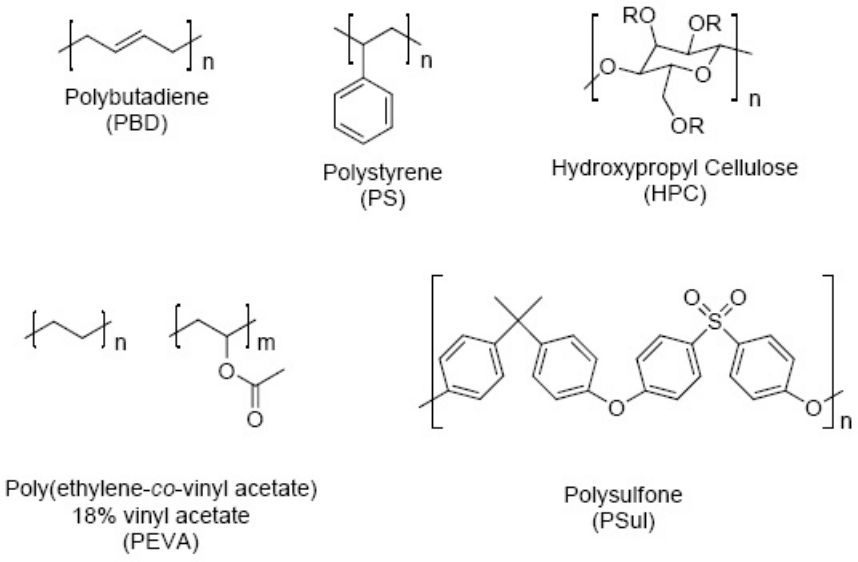

Figure 2.2: Repeat units of polymers used in this work.

2.2.4 Measurements

The computer-controlled (LabVIEW) analyte vapor generation and delivery system is described in detail elsewhere.[41] Briefly, carrier gas was passed through analyte bubblers to produce a saturated

vapor stream which was then diluted to the desired concentration and delivered to the sensor chamber. Analyte vapors were delivered in random order at 0.02 P/P°, where P and P° are the partial pressure and the saturated vapor pressure of the analyte, respectively, with a 2.5 L/min background flow of either dry nitrogen (cylinder) or oil-free house compressed air containing 1.10 ± 0.15 ppth water vapor (8–10% relative humidity). Temperature was not specifically controlled, but was stable at 21 ± 1°C. Each analyte exposure consisted of 70 s of pure carrier gas, 200 s of analyte vapor exposure, and 410 s of carrier gas purge. Pure carrier gas was run through the sensor chamber for 500 s before the first exposure to bring all sensors to a stable baseline. A single experimental run consisted of twelve exposures to each of seven analyte vapors, with a total time of 16 h. Nanocantilevers and chemiresistor arrays were tested in separate runs.

Chemiresistors were housed in a rectangular, stainless steel and Teflon sensor chamber with an interior volume of 2,047.5 cm^3, while nanocantilevers were housed in a brass chamber with an interior volume of 100 cm^3. Teflon tubing and stainless steel fittings were used throughout the vapor delivery system. The nanocantilever frequency was sampled every 0.5 s and the chemiresistor resistance was sampled every 4–6 s.

2.2.5 Data Analysis

2.2.5.1 Response Extraction

All data analysis was performed using custom written scripts in MATLAB.51 Nanocantilever sensor responses were calculated as the maximum relative frequency change, $\Delta f_{max}/f_0$, where f_0 is the baseline-corrected resonance frequency and Δf_{max} is the maximum frequency change upon exposure to an analyte. Chemiresistor sensor responses were calculated as the maximum relative resistance change, $\Delta R_{max}/R_B$, where R_B is the baseline resistance and ΔR_{max} is the maximum resistance change upon exposure to an analyte, for chemiresistors. Previous work shows that

$\Delta R_{max}/R_B$ is a more consistent metric than ΔR_{max},[50,51] and $\Delta f_{max}/f_0$ is used to normalize for differences in f_0 among nanocantilevers.[52] Raw data was corrected for baseline drift with a linear fit to the baseline average using the first 25 s of the pre-exposure and the last 25 s of the post exposure data. Signal to noise ratios (SNR) were calculated as the ΔR_{max} or Δf_{max} for a given sensor divided by three times the standard deviation of the baseline frequency or resistance as noise measurement, and the minimum detectable level (MDL) was calculated as the analyte concentration that would elicit a sensor response of three times the baseline noise, assuming a linear correlation between analyte concentration and sensor response magnitude.

2.2.5.2 Principal Components Analysis (PCA)

PCA is a means to visualize a sensor array's ability to differentiate between analyte vapors. Data were first sum-normalized[53] to compensate for differences in response magnitude, then transformed so that the variance within the data set was captured by the minimum number of dimensions. The most variance is captured by the first principal component (PC), the second-most by the second PC, etc. The data were projected along the first three PCs to observe the clustering of array responses to each analyte.

2.2.5.3 Fisher's Linear Discriminant (FLD)

FLD was used to evaluate each sensor array's ability to discriminate between pairs of analytes. FLD projects the multidimensional array data onto a vector that maximizes the distance between the average array responses to a pair of analytes while minimizing the variance within each cluster. The optimal separation vector is found by maximizing the resolution factor, *rf*,[54]

$$rf = \frac{d}{\left(\sigma_1^2 + \sigma_2^2\right)^{1/2}} \tag{2.1}$$

where d is the distance between the population means, and σ_1 and σ_2 are the standard deviations of the array response to the two analytes. An *rf* = 1 indicates 72% correct assignment, *rf* = 2 indicates 92% correct assignment, and *rf* = 3 indicates 98% correct assignment. FLD was applied to all pairwise combinations of analytes, with the first six exposures to each analyte used to determine the projection vector that maximized *rf* and to determine the decision boundary. This decision boundary was used to classify the last six exposures to the pair of analytes.

2.3 Results

2.3.1 Sensor Responses with Nitrogen Carrier Gas

Figure 2.3 (a) shows nanocantilever $\Delta f_{max}/f_0$ values in response to analyte exposures with dry nitrogen background, while Figure 2.3 (c) shows the corresponding SNR values. Nanocantilevers coated with PEVA, HPC, and PS exhibited only positive frequency shifts, while cantilevers coated with PBD and PSul exhibited both positive and negative shifts. The nanocantilever array fingerprint was similar for closely related compounds (e.g. $CHCl_3$ and DCM) and showed significant variation for chemically distinct compounds (e.g. Hex and IPA). Figure 2.3 (b) and (d) show the corresponding chemiresistor $\Delta R/R_b$ and SNR values, respectively, for analytes exposed with dry nitrogen background. Nanocantilever and chemiresistor responses were reversible, and both sensor types returned to baseline values post-exposure on the same time scale. Nanocantilevers exhibited lower response and SNR values than chemiresistors, which led to higher MDLs than chemiresistors. Response, SNR, and MDL values for both nanocantilever and chemiresistive sensors are tabulated in Tables 2.1 and 2.2, respectively.

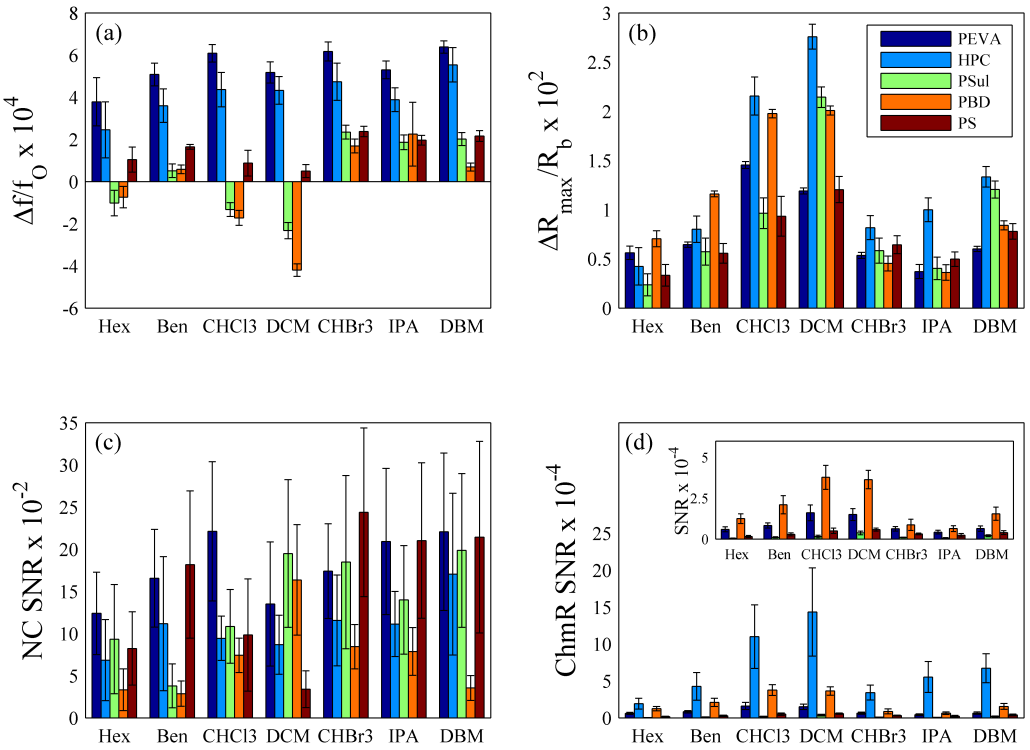

Figure 2.3: Responses of sensors exposed with dry nitrogen background. (a) and (c) $\Delta f_{max}/f_0$ and SNR respectively of nanocantilever sensors. (b) and (d) $\Delta R_{max}/R_B$ and SNR respectively of chemiresistive sensors (inset in (d) shows SNR without HPC). Analyte fingerprints differ between sensor types due to difference in response mechanisms.

Table 2.1: Nanocantilever array $\Delta f_{max}/f_0$, SNR, and MDL values for vapor exposures conducted with dry nitrogen background. Outliers were removed to calculate average SNR, and those values were used to calculate average MDL.

(a) Nanocantilever Array $\Delta f_{max}/f_0$ x 10^5 (N_2 background)					
	PBD	PS	PEVA	HPC	PSul
Hex	-7.52 ± 4.43	8.33 ± 5.34	32.63 ± 9.10	24.78 ± 10.69	9.24 ± 5.78
Ben	4.30 ± 0.86	15.63 ± 1.50	$49.20 \pm .15$	35.38 ± 3.52	6.43 ± 1.37
$CHCl_3$	-19.25 ± 1.90	8.10 ± 1.38	$56.10 \pm .27$	40.13 ± 2.98	-13.72 ± 1.38
DCM	-43.18 ± 2.60	32.69 ± 1.22	50.33 ± 2.65	42.69 ± 3.31	-23.41 ± 1.88
$CHBr_3$	15.56 ± 2.42	21.10 ± 1.16	55.93 ± 2.72	45.83 ± 3.60	22.67 ± 2.22
IPA	16.30 ± 1.73	17.57 ± 0.95	48.82 ± 2.56	39.36 ± 2.33	16.86 ± 1.80
DBM	5.11 ± 1.59	19.35 ± 1.38	59.66 ± 2.53	53.01 ± 3.42	19.36 ± 2.00
(b) Nanocantilever Array SNR (N_2 background)					
	PBD	PS	PEVA	HPC	PSul
Hex	52 ± 25	74 ± 35	121 ± 50	59 ± 36	181 ± 120
Ben	37 ± 3	282 ± 108	349 ± 55	213 ± 50	78 ± 21
$CHCl_3$	134 ± 56	115 ± 52	349 ± 73	189 ± 53	273 ± 64
DCM	222 ± 57	16 ± 7	166 ± 133	142 ± 94	355 ± 196
$CHBr_3$	127 ± 12	363 ± 125	226 ± 106	237 ± 73	473 ± 160
IPA	88 ± 32	227 ± 83	219 ± 116	158 ± 60	282 ± 82
DBM	38 ± 10	187 ± 97	274 ± 145	314 ± 23	306 ± 87
(c) Nanocantilever Array MDL in P/P$^\circ$ (N_2 background)					
	PBD	PS	PEVA	HPC	PSul
Hex	3.8 x 10^{-4}	2.7 x 10^{-4}	1.7 x 10^{-4}	3.4 x 10^{-4}	1.1 x 10^{-4}
Ben	5.4 x 10^{-4}	7.1 x 10^{-5}	5.1 x 10^{-5}	9.4 x 10^{-5}	2.6 x 10^{-5}
$CHCl_3$	1.5 x 10^{-4}	1.7 x 10^{-4}	5.7 x 10^{-5}	1.1 x 10^{-4}	7.3 x 10^{-5}
DCM	9.0 x 10^{-5}	1.3 x 10^{-3}	1.2 x 10^{-4}	1.4 x 10^{-4}	5.6 x 10^{-5}
$CHBr_3$	1.6 x 10^{-4}	5.5 x 10^{-5}	8.8 x 10^{-5}	8.4 x 10^{-5}	4.2 x 10^{-5}
IPA	2.3 x 10^{-4}	8.8 x 10^{-5}	9.1 x 10^{-5}	1.3 x 10^{-4}	7.1 x 10^{-5}
DBM	5.2 x 10^{-4}	1.1 x 10^{-4}	7.3 x 10^{-5}	6.4 x 10^{-5}	6.5 x 10^{-5}

Table 2.2: Chemiresistor array $\Delta R_{max}/R_B$ values, SNR, and MDL for vapor exposures conducted with dry nitrogen background.

(a) Chemiresistor Array $\Delta R_{max}/R_B$ x 10^3 (N_2 background)

	PBD	PS	PEVA	HPC	PSul
Hex	6.51 ± 0.53	2.08 ± 0.97	3.24 ± 0.92	5.55 ± 0.43	2.76 ± 0.52
Ben	11.60 ± 0.22	4.73 ± 0.99	7.07 ± 0.84	6.43 ± 0.21	4.94 ± 0.43
$CHCl_3$	19.72 ± 0.33	8.56 ± 0.87	20.10 ± 1.37	14.41 ± 0.17	8.29 ± 1.04
DCM	19.78 ± 0.41	20.99 ± 0.58	26.90 ± 0.77	11.92 ± 0.14	11.26 ± 0.65
$CHBr_3$	4.23 ± 0.54	5.20 ± 0.78	7.19 ± 0.79	5.33 ± 0.20	5.78 ± 0.59
IPA	3.34 ± 0.68	3.37 ± 0.65	9.06 ± 0.88	3.57 ± 0.60	4.43 ± 0.44
DBM	8.25 ± 0.33	11.01 ± 0.39	12.51 ± 0.57	6.03 ± 0.21	7.25 ± 5.32

(b) Chemiresistor Array SNR (N_2 background)

	PBD	PS	PEVA	HPC	PSul
Hex	845 ± 313	28 ± 7	229 ± 35	699 ± 245	136 ± 87
Ben	2648 ± 1427	115 ± 38	401 ± 37	880 ± 324	326 ± 218
$CHCl_3$	3605 ± 889	173 ± 80	689 ± 24	2223 ± 703	740 ± 428
DCM	4014 ± 1904	377 ± 71	2000 ± 242	1548 ± 450	912 ± 314
$CHBr_3$	842 ± 399	96 ± 32	350 ± 30	852 ± 329	345 ± 72
IPA	373 ± 167	65 ± 23	486 ± 43	419 ± 167	141 ± 109
DBM	1202 ± 188	247 ± 171	786 ± 81	682 ± 123	280 ± 65

(c) Chemiresistor Array MDL in P/P$^\circ$ (N_2 background)

	PBD	PS	PEVA	HPC	PSul
Hex	2.4 x 10^{-5}	7.1 x 10^{-4}	8.7 x 10^{-5}	2.9 x 10^{-5}	1.5 x 10^{-4}
Ben	7.6 x 10^{-6}	1.7 x 10^{-4}	5.0 x 10^{-5}	2.3 x 10^{-5}	6.1 x 10^{-5}
$CHCl_3$	5.5 x 10^{-6}	1.2 x 10^{-4}	2.9 x 10^{-5}	9.0 x 10^{-6}	2.7 x 10^{-5}
DCM	5.0 x 10^{-6}	5.3 x 10^{-5}	1.0 x 10^{-5}	1.3 x 10^{-5}	2.2 x 10^{-5}
$CHBr_3$	2.4 x 10^{-5}	2.1 x 10^{-4}	5.7 x 10^{-5}	2.3 x 10^{-5}	5.8 x 10^{-5}
IPA	5.4 x 10^{-5}	3.1 x 10^{-4}	4.1 x 10^{-5}	4.8 x 10^{-5}	1.4 x 10^{-4}
DBM	1.7 x 10^{-5}	8.1 x 10^{-5}	2.5 x 10^{-5}	2.9 x 10^{-5}	7.1 x 10^{-5}

2.3.2 Array Discrimination with Nitrogen Carrier Gas

Figure 2.4 shows the PCA projection of the sum-normalized nanocantilever array responses to analytes exposed with a dry nitrogen background projected on the first three PCs, along with the variance captured in each PC. Hex and DCM were less tightly clustered than other analytes. Slight cluster overlap was observed for $CHBr_3$ and IPA. Figure 2.5 shows a plot of chemiresistor array responses to analytes exposed with a dry nitrogen background plotted along the first three PCs of the responses. Slight cluster overlap was observed for Hex and Ben.

Table 2.3(a) shows rf values calculated for the nanocantilever array with respective discrimination performance shown in parentheses, where *rf* = 3 signifies 98% correct discrimination, *rf* = 2 for 92% correct discrimination, and *rf* = 1 for 72% correct discrimination. The nanocantilever array achieved rf values of three or higher for almost all pairwise comparisons, but struggled to discriminate Hex from Ben and $CHCl_3$ and also between $CHBr_3$ and IPA. Table 2.3(b) shows *rf* values calculated for the chemiresistor array. Two pairwise comparisons resulted in $rf < 2$: discrimination between Hex and $CHCl_3$ and between $CHBr_3$ and DBM.

2.3.3 Sensor Response and Array Discrimination with Humid Air Background

Figure 2.6 shows the difference in nanocantilever sensor response between dry nitrogen and humid air carrier gas experiments. Operating nanocantilevers in a humid air background containing a small amount of water vapor caused $\Delta f_{max}/f_0$ values to shift negatively relative to $\Delta f_{max}/f_0$ values from nanocantilevers operated in a dry nitrogen background. The HPC coated nanocantilever responded poorly to analyte vapors under these conditions. To verify that the shift in nanocantilever responses was due to changes in humidity and not any other differences between the nitrogen and the laboratory air, an in-line drying column was inserted in the airflow path prior to the mass flow controllers during an experimental run using humid air background. Nanocantilever responses col-

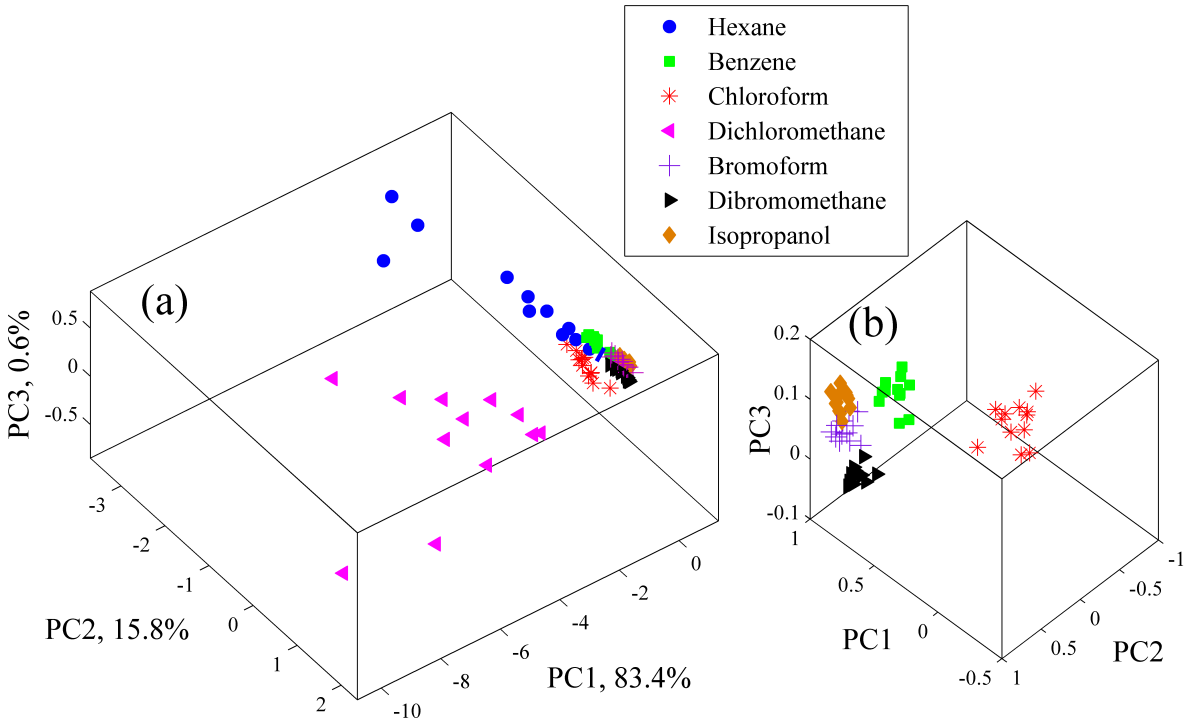

Figure 2.4: Nanocantilever array responses to analyte vapors with dry nitrogen background projected along the first three PCs, along with the variance captured in each PC. (b) Zoomed-in view of tightly clustered analytes. Large standard deviation in hexane responses led to cluster spread, while distinct, strong, negative responses led to separation of DCM cluster from other vapors.

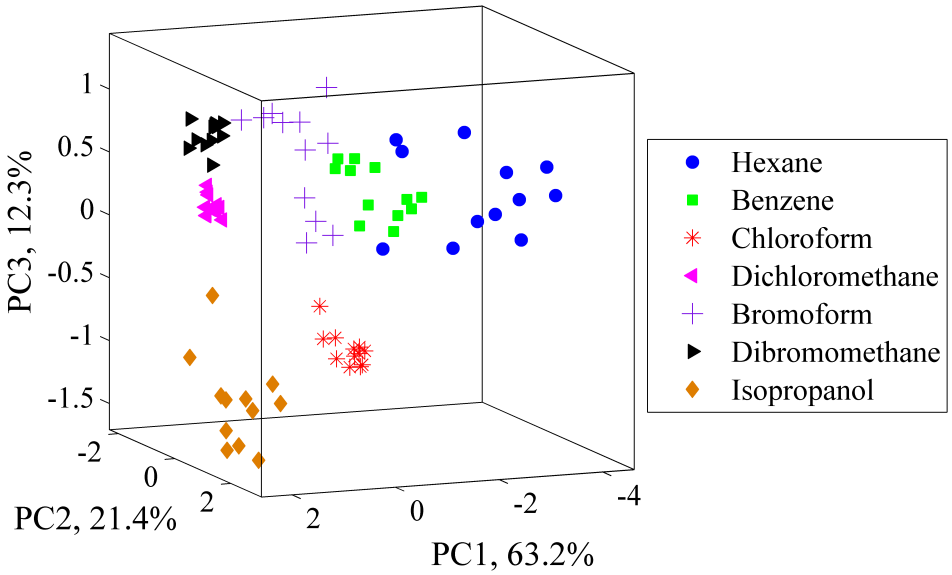

Figure 2.5: Chemiresistor array responses to analyte vapors with dry nitrogen background projected along the first three PCs, along with the variance captured in each PC, shows non-overlapping clustering of seven analytes captured with a five element array.

Table 2.3: *rf* values for nanocantilever and chemiresistor arrays exposed to analytes in dry nitrogen and humid air backgrounds. An *rf* = 3 corresponds to 98% correct pairwise discrimination.

(a) Nanocantilever Array with Dry Nitrogen Background

	Ben	CHCl3	DCM	CHBr3	IPA	CHBr2
Hex	0.87	1.09	3.48	4.17	3.48	3.22
Ben		6.29	11.06	5.05	2.1	2.56
$CHCl_3$			3.81	15.28	7.72	7.2
DCM				21.36	4.2	10.14
$CHBr_3$					0.92	2.59
IPA						2.45

(b) Chemiresistor Array with Dry Nitrogen Background

	Ben	CHCl3	DCM	CHBr3	IPA	CHBr2
Hex	4.93	1.64	5.17	5.72	9.11	5.7
Ben		2.5	4.05	7.25	8.82	4.25
$CHCl_3$			8.02	4.09	6.6	8.55
DCM				2.31	5.3	3.72
$CHBr_3$					3.43	1.97
IPA						5.4

(c) Nanocantilever Array with Humid Air Background

	Ben	CHCl3	DCM	CHBr3	IPA	CHBr2
Hex	1.94	2.22	2.57	5.24	2.77	1.23
Ben		1.81	4.03	3.03	1.17	1.24
$CHCl_3$			2.43	5.63	2.03	0.47
DCM				10.18	3.69	1.43
$CHBr_3$					1.97	5.33
IPA						2.56

(d) Chemiresistor Array with Humid Air Background

	Ben	CHCl3	DCM	CHBr3	IPA	CHBr2
Hex	3.82	2.55	14.73	4.53	5.34	6.37
Ben		2.55	13.79	2.64	3.26	3.43
$CHCl_3$			12.46	3.02	2.16	5.47
DCM				4.99	3.91	4.84
$CHBr_3$					3.1	2.5
IPA						2.78

lected with the dried air background were shifted positively relative to the humid air background. A negative shift in response was also observed for uncoated nanocantilever sensors exposed to analyte vapors in a humid air background as compared to in a dry nitrogen background. Figure 2.7 shows $\Delta f_{max}/f_0$ and SNR values for the nanocantilever array operated in an air background, and Table 2.4 shows tabulated response, SNR, and MDL values.

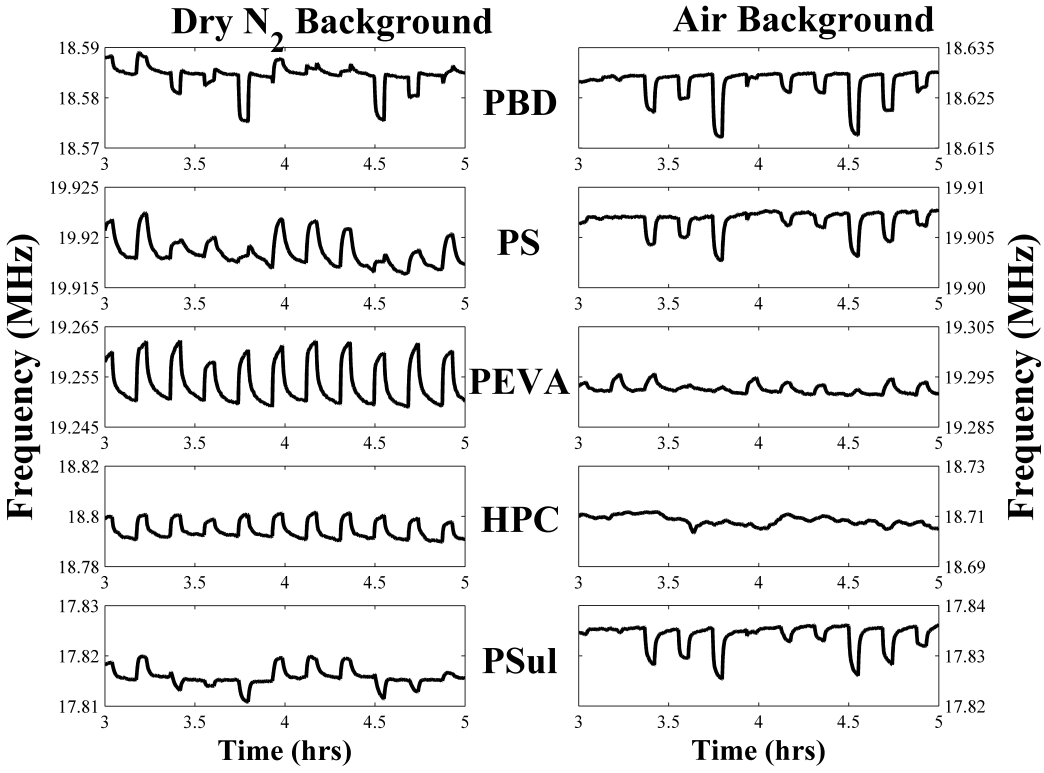

Figure 2.6: Nanocantilever response data to analytes exposed in random order shows negative shift in $\Delta f_{max}/f_0$ values upon switching from dry nitrogen to humid air background due to sorption of water vapor on sensor surfaces and into hydrophilic polymer films.

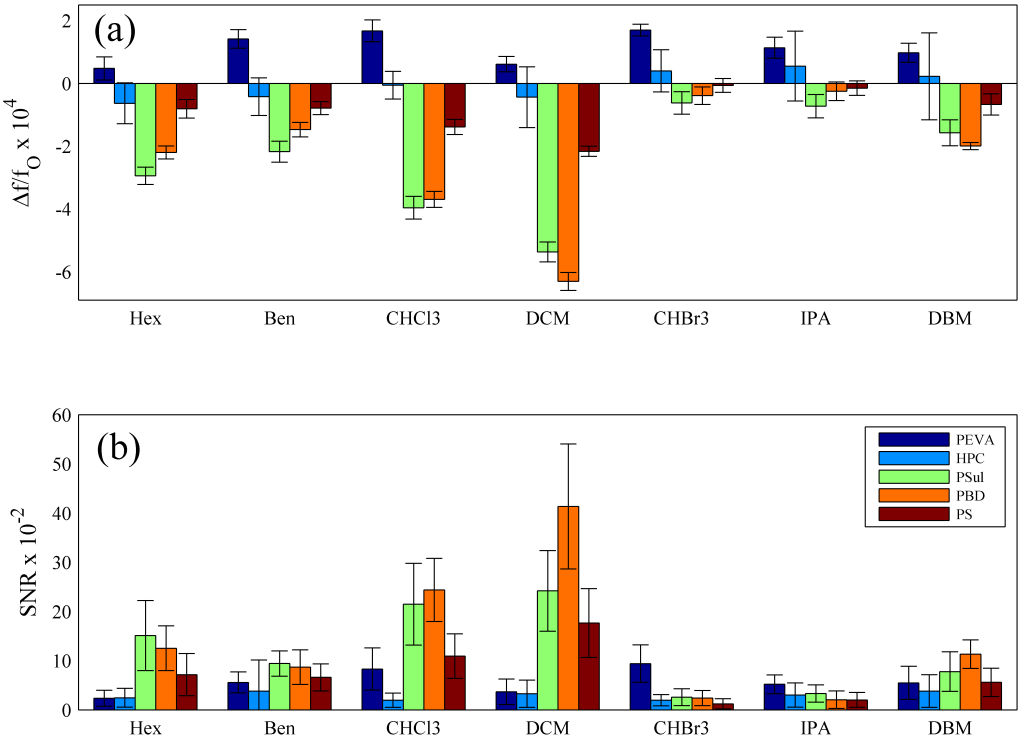

Figure 2.7: (a) $\Delta f_{max}/f_0$ and (b) SNR values of nanocantilevers exposed to analyte vapors with humid air background.

Table 2.4: Nanocantilever array $\Delta f_{max}/f_0$, SNR, and MDL values for vapor exposures conducted with humid air background.

(a) Nanocantilever Array $\Delta f_{max}/f_0$ x 10^5 (air background)					
	PBD	PS	PEVA	HPC	PSul
Hex	-21.37 ± 1.07	-9.40 ± 0.87	3.23 ± 1.26	-3.70 ± 3.38	-29.55 ± 0.84
Ben	-14.32 ± 0.63	-6.58 ± 0.61	11.19 ± 0.92	0.93 ± 2.76	-20.41 ± 0.64
$CHCl_3$	-36.14 ± 0.90	-12.79 ± 0.70	15.79 ± 1.05	2.57 ± 2.73	-38.61 ± 0.98
DCM	-61.58 ± 1.82	-20.63 ± 0.51	5.47 ± 0.82	-5.42 ± 4.06	-51.45 ± 1.48
$CHBr_3$	-4.32 ± 0.87	-0.20 ± 0.88	16.16 ± 1.33	5.83 ± 6.33	-4.32 ± 1.21
IPA	-2.97 ± 1.49	-2.31 ± 0.91	10.64 ± 1.93	4.82 ± 2.72	-7.42 ± 1.79
DBM	-19.67 ± 0.61	-6.52 ± 0.59	9.76 ± 0.91	3.52 ± 4.92	-15.67 ± 0.80
(b) Nanocantilever Array SNR (air background)					
	PBD	PS	PEVA	HPC	PSul
Hex	225 ± 78	129 ± 69	34 ± 16	31 ± 13	216 ± 99
Ben	143 ± 31	109 ± 33	71 ± 22	5 ± 19	212 ± 63
$CHCl_3$	409 ± 50	201 ± 58	117 ± 54	17 ± 24	397 ± 171
DCM	514 ± 140	386 ± 112	55 ± 10	77 ± 60	478 ± 202
$CHBr_3$	26 ± 8	6 ± 4	161 ± 67	53 ± 40	33 ± 17
IPA	31 ± 15	38 ± 17	118 ± 52	54 ± 27	68 ± 29
DBM	164 ± 47	99 ± 28	64 ± 14	25 ± 20	199 ± 42
(c) Nanocantilever Array MDL in P/P$^\circ$ (air background)					
	PBD	PS	PEVA	HPC	PSul
Hex	8.9 x 10^{-5}	1.6 x 10^{-4}	5.8 x 10^{-4}	6.4 x 10^{-4}	9.2 x 10^{-5}
Ben	1.4 x 10^{-4}	1.8 x 10^{-4}	2.8 x 10^{-4}	3.9 x 10^{-3}	9.4 x 10^{-5}
$CHCl_3$	4.9 x 10^{-5}	1.0 x 10^{-4}	1.7 x 10^{-4}	1.2 x 10^{-3}	5.0 x 10^{-5}
DCM	3.9 x 10^{-5}	5.2 x 10^{-5}	3.7 x 10^{-4}	2.6 x 10^{-4}	4.2 x 10^{-5}
$CHBr_3$	7.7 x 10^{-4}	3.3 x 10^{-3}	1.2 x 10^{-4}	3.8 x 10^{-4}	6.1 x 10^{-4}
IPA	6.5 x 10^{-4}	5.2 x 10^{-4}	1.7 x 10^{-4}	3.7 x 10^{-4}	3.0 x 10^{-4}
DBM	1.2 x 10^{-4}	2.0 x 10^{-4}	3.1 x 10^{-4}	7.9 x 10^{-4}	1.0 x 10^{-4}

Figure 2.8 shows a plot of the nanocantilever array responses to analytes exposed with a humid air background projected on the first three PCs. IPA was poorly clustered and overlapped slightly with $CHBr_3$. Little overlap was observed for the other analytes, but clusters were not widely separated. Table 2.3 (c) shows *rf* values calculated for the nanocantilever array operated in air. Cluster separation improved for some analyte pairs and was poorer for others relative to rf values calculated for the nanocantilever array run with nitrogen background.

Chemiresistor performance changed little when the array was run with humid air rather than dry nitrogen. Figure 2.9 shows there was an overall trend of decreased responses, with the PBD and PS chemiresistors being the most affected, resulting in change to the array's fingerprint response to hexane, benzene, and chloroform, shown in Figure 2.10 (a). Figure 2.10 (b) shows SNR values for the chemiresistor array operated in air, and Table 2.5 shows response, SNR, and MDL values. Figure 2.11 shows a plot of chemiresistor array responses to analytes exposed with an air background plotted on the first three PCs. No overlap between analyte clusters was observed.

2.4 Discussion

2.4.1 Nanocantilever Response Mechanism

Unlike the chemiresistors, the polymer-coated nanocantilever sensors in this study exhibited both positive and negative shifts in resonance frequency upon exposure to analyte vapors. Theoretical understanding of the response mechanisms responsible for observed frequency shifts in nanomechanical resonators is an active area of research and, recently, the subject of a thorough review.[37] In many resonant microcantilever studies, frequency shifts have been attributed only to the mass of sorbed species, though Thundat and coworkers observed positive resonance frequency shifts upon exposing a hydrogel coated V-shaped microcantilever to water vapor.[55] When resonator dimensions

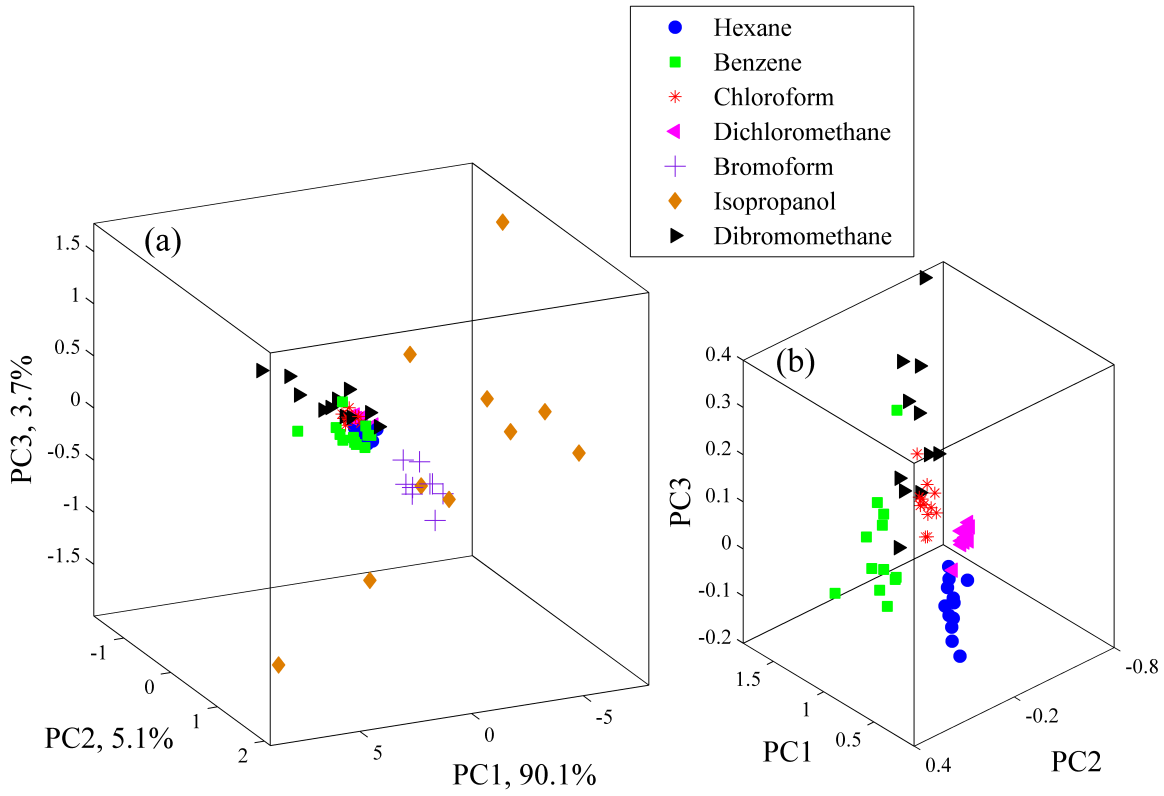

Figure 2.8: (a) Nanocantilever array responses to analyte vapors with humid air background projected along the first three PCs along with the variance captured in each PC. (b) Zoomed-in region of tightly clustered analytes. Discrimination is reduced due to the poor performance of the HPC-coated sensor.

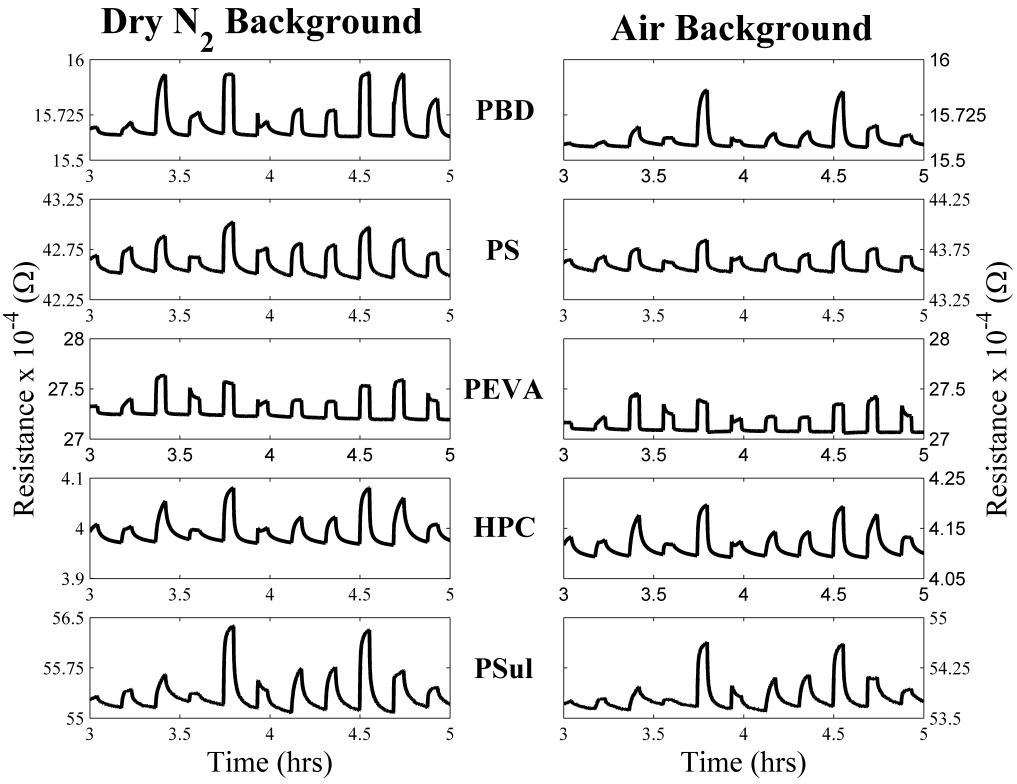

Figure 2.9: Chemiresistor responses were depressed upon switching carrier gas from dry nitrogen to humid air.

Table 2.5: Chemiresistor array $\Delta R_{max}/R_B$ values, SNR, and MDL for vapor exposures conducted with humid air background.

(a) Chemiresistor Array $\Delta R_{max}/R_B$ x 10^3 (air background)

	PBD	PS	PEVA	HPC	PSul
Hex	2.07 ± 0.38	1.50 ± 0.86	3.68 ± 1.08	5.48 ± 0.49	1.84 ± 0.34
Ben	2.98 ± 0.34	3.56 ± 1.10	6.74 ± 0.83	5.64 ± 0.27	3.11 ± 0.22
$CHCl_3$	5.85 ± 0.12	5.53 ± 0.37	18.61 ± 1.43	12.76 ± 0.20	4.94 ± 0.30
DCM	17.20 ± 0.34	16.94 ± 0.45	23.65 ± 0.87	10.35 ± 0.21	6.79 ± 0.25
$CHBr_3$	1.78 ± 0.26	3.24 ± 0.79	7.01 ± 0.60	4.52 ± 0.26	3.16 ± 0.16
IPA	1.41 ± 0.41	1.97 ± 0.34	9.15 ± 0.77	3.17 ± 0.61	2.66 ± 0.27
DBM	4.47 ± 0.24	8.17 ± 0.49	11.34 ± 0.68	5.22 ± 0.18	3.87 ± 0.13

(b) Chemiresistor Array SNR (air background)

	PBD	PS	PEVA	HPC	PSul
Hex	383 ± 159	19 ± 7	291 ± 73	678 ± 168	99 ± 43
Ben	535 ± 186	59 ± 38	488 ± 59	675 ± 137	158 ± 74
$CHCl_3$	559 ± 96	78 ± 43	872 ± 80	2222 ± 859	314 ± 69
DCM	3697 ± 1191	280 ± 120	2078 249	1667 ± 528	322 ± 166
$CHBr_3$	388 ± 99	45 ± 21	394 ± 33	760 ± 242	152 ± 31
IPA	279 ± 78	23 ± 6	591 ± 62	312 ± 40	172 ± 49
DBM	1047 ± 275	96 ± 9	935 ± 229	690 ± 211	205 ± 75

(c) Chemiresistor Array MDL in P/P$^\circ$ (air background)

	PBD	PS	PEVA	HPC	PSul
Hex	5.2 x 10^{-5}	1.1 x 10^{-3}	6.9 x 10^{-5}	2.9 x 10^{-5}	2.0 x 10^{-4}
Ben	3.7 x 10^{-5}	3.4 x 10^{-4}	4.1 x 10^{-5}	3.0 x 10^{-5}	1.3 x 10^{-4}
$CHCl_3$	3.6 x 10^{-5}	2.6 x 10^{-4}	2.3 x 10^{-5}	9.0 x 10^{-6}	6.4 x 10^{-5}
DCM	5.4 x 10^{-6}	7.2 x 10^{-5}	9.6 x 10^{-6}	1.2 x 10^{-5}	6.2 x 10^{-5}
$CHBr_3$	5.2 x 10^{-5}	4.4 x 10^{-4}	5.1 x 10^{-5}	2.6 x 10^{-5}	1.3 x 10^{-4}
IPA	7.2 x 10^{-5}	8.6 x 10^{-4}	3.4 x 10^{-5}	6.4 x 10^{-5}	1.2 x 10^{-4}
DBM	1.9 x 10^{-5}	2.1 x 10^{-4}	2.1 x 10^{-5}	2.9 x 10^{-5}	9.8 x 10^{-5}

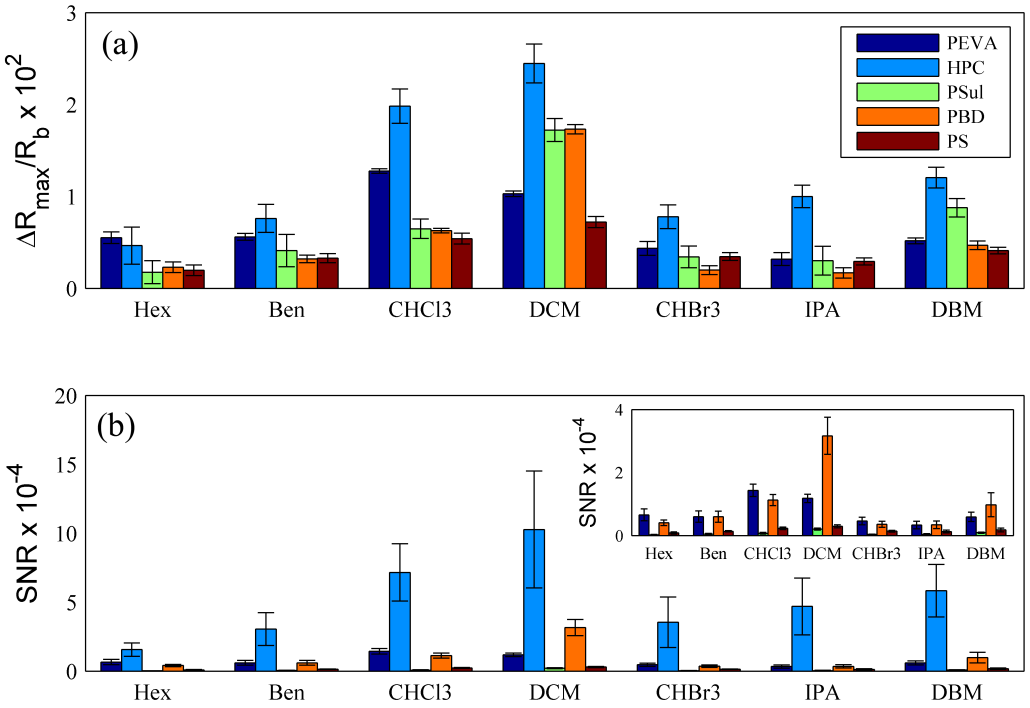

Figure 2.10: (a) $\Delta R_{max}/R_B$ and (b) SNR values of chemiresistors exposed to analyte vapors with humid air background. The fingerprint patterns of hexane and benzene exhibit the greatest change relative to sensor responses to analytes exposed with dry nitrogen background.

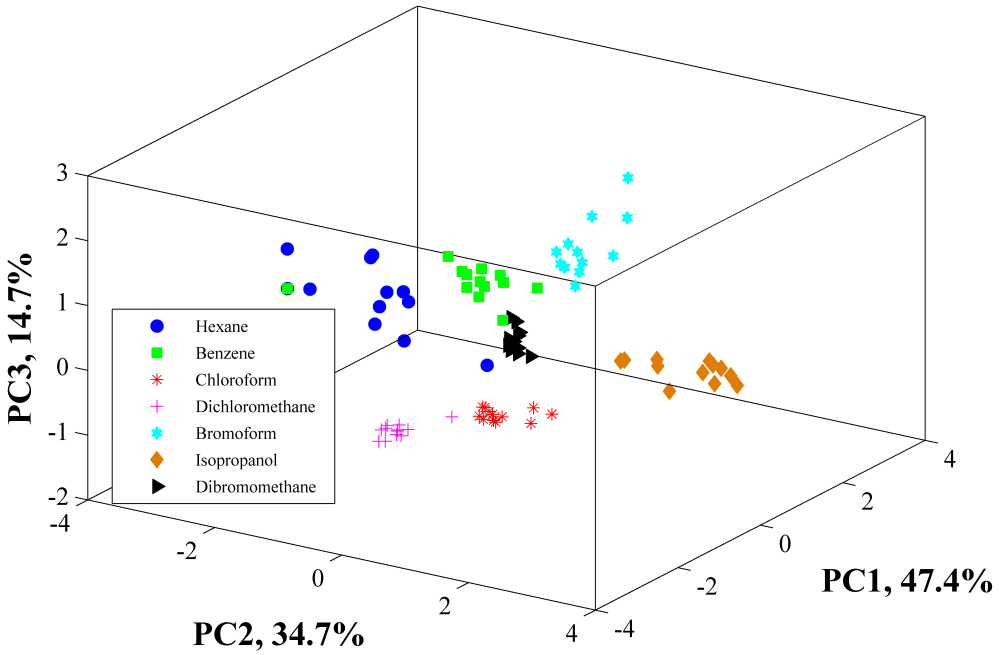

Figure 2.11: Chemiresistor array data from analyte exposures conducted with humid air background projected along the first three PCs shows no overlap between clusters.

are shrunk to the nanoscale, changes in stiffness (from factors such as polymer film swelling) and surface elasticity can induce positive shifts in resonance frequency. Positive frequency shifts have also been attributed to changes in surface stress, but this interpretation is controversial.[37] Nanocantilevers have shown positive shifts in resonance frequency upon sorption of viruses[56] and protein[57] near the clamped end of the resonator. The fundamental resonance frequency of cantilever sensors is related to effective mass and spring constant such that,

$$f_0 = \frac{1}{2\pi}\sqrt{\frac{k}{m_{eff}}} \tag{2.2}$$

where f_0 is the fundamental resonance frequency, m_{eff} is the effective mass for the fundamental mode (the total mass multiplied by the integral of a normalized function describing the modal shape[22]) and k is the effective fundamental mode stiffness (spring constant).[55] Only the fundamental resonant mode was used for all vapor exposure experiments. Assuming that $\delta m_{eff} << m_{eff}$ and $\delta k << k$, Equation 2.2 can be rearranged to show that the relative change in resonance frequency can be approximated as

$$\frac{\Delta f}{f_0} = \frac{\partial k}{2k} - \frac{\partial m_{eff}}{2m_{eff}} \tag{2.3}$$

where $\Delta f / f_0$ is the relative change in resonance frequency.[37] According to Equation 2, an increase in effective mass induces a negative frequency shift, while an increase in spring constant induces a positive frequency shift. Exposure to an analyte vapor increases both mass and spring constant, and will induce either a positive or negative Δf, depending on which factor dominates the response.[55] The direction of the observed frequency shift is dependent on polymer/analyte partition coefficient (the concentration ratio of analyte absorbed into the polymer relative to the analyte in the vapor phase),[47] the extent of polymer swelling relative to the mass of analyte sorbed,[40] polymer stiffness,

and the distribution of film thickness across the cantilever surface, the latter being a function of the dropcasting method employed in this study.

The nanocantilever's ability to respond in both directions aids in analyte discrimination. The nanocantilever's sensitivity to both changes in m_{eff} and k could also lead to suppression of the observed response if these two mechanisms are of similar magnitude, which might explain the $\Delta f_{max}/f_0$ values of the PS-coated nanocantilever exposed to DCM with nitrogen background, and IPA with air background. The response to changes in stiffness of the nanocantilevers was also observed upon coating the sensors with polymer films. Figure 2.12 shows that nanocantilever resonance frequency often increased upon dropcasting of polymer films, but the magnitude of the frequency shift was unpredictable due to differences in stiffness between the polymer films and the variation of film thickness (2-10 nm) across the sensors. General correlations between polymer properties, as well as polymer/analyte interactions, and observed frequency shifts cannot be made due to the non-uniformity of the polymer coating thickness on the nanocantilever sensors, and further study is necessary to fully understand the mechanisms responsible for the observed sensor responses. In previous work,[16] positive frequency shifts were not observed because all polar analytes tested in that study had high molecular weights, which consistently induced negative frequency shifts for both bare and polymer-coated nanocantilevers. Such polymer coatings, while of comparable thickness to the ones tested in this study, had glass transition temperatures (T_g) below the operating temperature of the nanocantilevers, rendering such coatings rubbery and thus less able to transmit strain due to swelling to the sensor, leading to responses dominated by the mass loading effect.

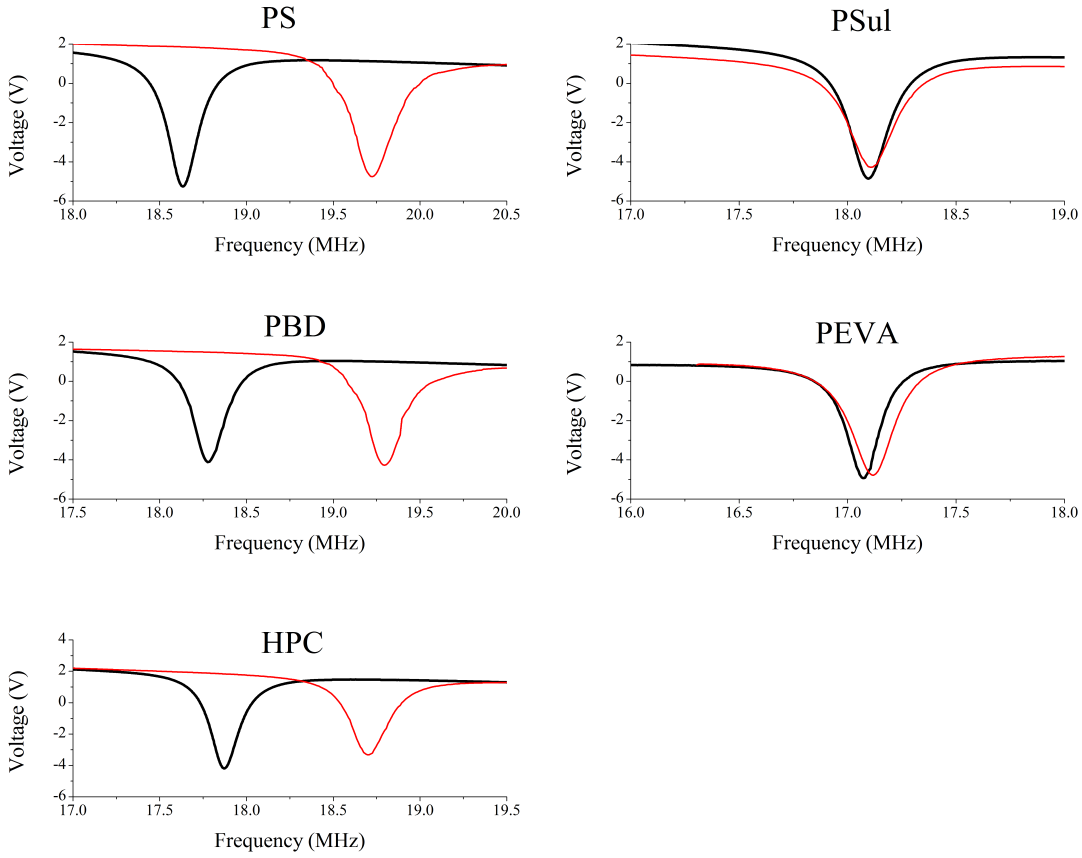

Figure 2.12: Resonance peaks of nanocantilevers used in array comparison experiments before (black) and after (red) dropcasting polymer film. Resonance frequency shift upon dropcasting was unpredictable, and quality factor often decreased upon coating due to damping. A second PS-coated cantilever exhibited a much smaller Δf upon coating, but responded poorly to analyte vapors so was not used in array comparison experiments.

2.4.2 Sensitivity Comparison

Directly comparing the sensitivity of nanocantilevers and chemiresistors presents challenges because the sensor types differ in response mechanism and the scaling of responsivity with size, but their sensitivity per area and the scaling of SNR by area can be evaluated. Nanocantilever sensitivity scales with f_0 and (directly with k_{eff} and inversely with m_{eff}), with the minimum detectable change in mass, and other quantities, improving with increasing resonance frequency. This sensitivity enhancement overwhelms the loss in capture area from shrinking cantilevers to the nanoscale.[52,58] Additionally, the nanocantilevers employed a very small volume of sorptive film compared to the chemiresistors. The maximum film thickness produced by dropcasting is approximately 10 nm, about twenty times thinner than the chemiresistive sensor films. Comparing sensitivity per sensor area, nanocantilevers are 10^7 more sensitive per area than chemiresistors, and in terms of sensitivity per volume of sorptive film, nanocantilevers are 10^3 more sensitive than chemiresistors.

For the case of chemiresistors exposed to high vapor pressure analytes in a large headspace volume, the conditions of this study, chemiresistor SNR scales as $A^{1/2}$, where A is the area of the composite chemiresistive film.[47] Assuming a constant thickness of the chemiresistive film, chemiresistors are required to have an area of 1.17 mm^2 each to match the average SNR of the nanocantilever sensors, which have capture areas of 1.5 μm^2 each. Nanocantilever SNR can be further improved by developing new techniques to apply thicker films to increase response magnitude, by using similarly-coated nanocantilever arrays,[59] and by employing alternate actuation and readout schemes[60] that have inherently lower baseline noise.

2.4.3 Discrimination Comparison

PCA plots for vapor exposure experiments with nitrogen background show that both nanocantilever and chemiresistor arrays have similar qualitative ability to produce separate clusters for each analyte, illustrating that the selectivity imparted by the specific polymers was not reduced when transferred from chemiresistors to nanocantilevers. Large variations in nanocantilever array responses to hexane and dichloromethane with nitrogen background were observed. The spread of the hexane data is likely due to the high standard deviation of responses, particularly for the HPC coated nanocantilever. Small array size leads to most variation being captured in the first two PCs, more so for the nanocantilever array than for the chemiresistor array, indicating that the two types of sensors require different sets of polymers for optimal discrimination performance. Figure 2.13 illustrates discrimination performance of nanocantilever and chemiresistor arrays would improve with increasing array size beyond five elements by plotting *rf* vs. the number of elements in the array.[61]

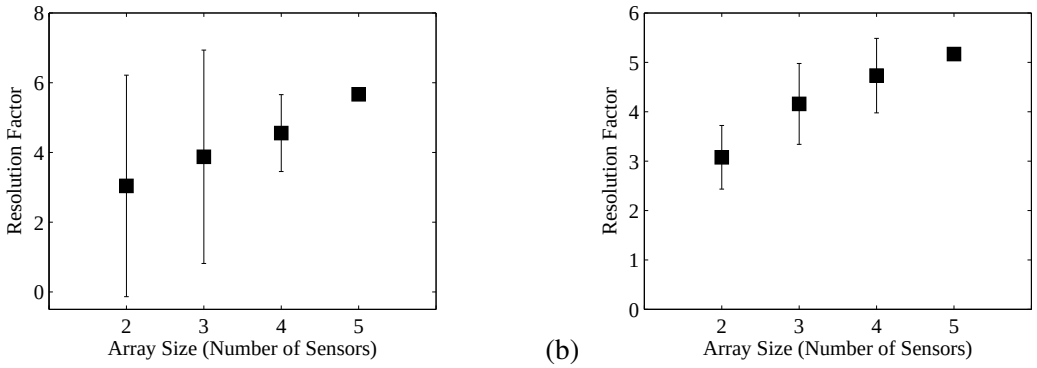

Figure 2.13: Average resolution factors, rf, for vapor exposures conducted with dry nitrogen background of (a) nanocantilever array and (b) chemiresistor array as a function of array size, showing that increasing the number of sensor elements would improve discrimination performance.

2.4.4 Humidity

Humidity affects the responses of a variety of sensor types,[62,63] and must be understood to enable optimal deployment of a sensor array. Nanocantilever sensors are affected by humidity though

the non-specific adsorption of water vapor molecules on the surface, which, like analyte vapors, can change effective spring constant (stiffening), surface stress, or surface elasticity, resulting in a positive shift in resonance frequency.[37]

Figure 2.14 shows that nanocantilevers employing hydrophilic polymers were more affected by switching carrier gas than those using hydrophobic polymers. The HPC coated nanocantilever was most affected, such that it only introduced noise into the array when run with humid air as the carrier gas. PCA performed after removing the HPC coated sensor from the analysis (Figure 2.15) shows marked improvement in qualitative discrimination. The chemiresistor array did not follow the same trend, as shown in Figure 2.16. $\Delta R_{max}/R_B$ values decreased similarly across the array for all analytes, with the PBD chemiresistor responses to hexane and benzene the most affected, altering the array fingerprint for these two vapors.

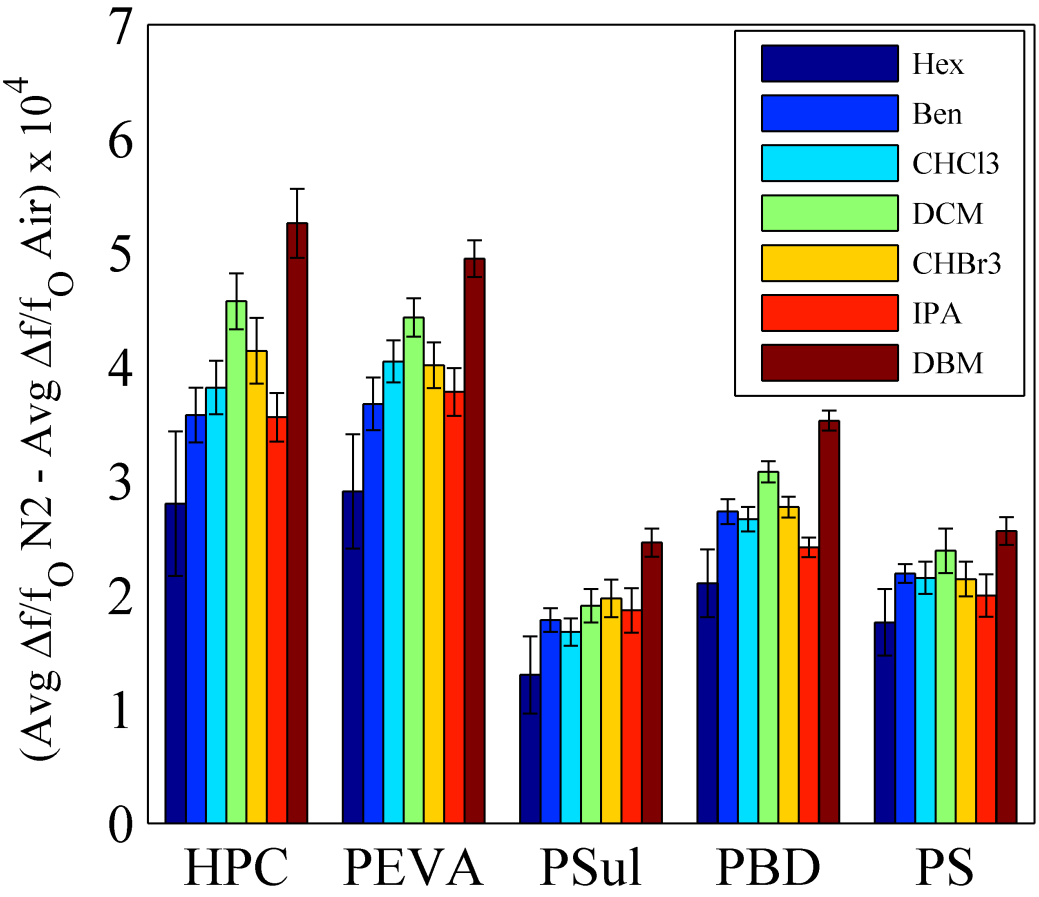

Figure 2.14: Nanocantilevers coated with hydrophilic polymers exhibit larger shift in $\Delta f_{max}/f_0$ values upon switching carrier gas than those coated with hydrophobic polymers, since water vapor will absorb into hydrophilic films as well as onto sensor surfaces.

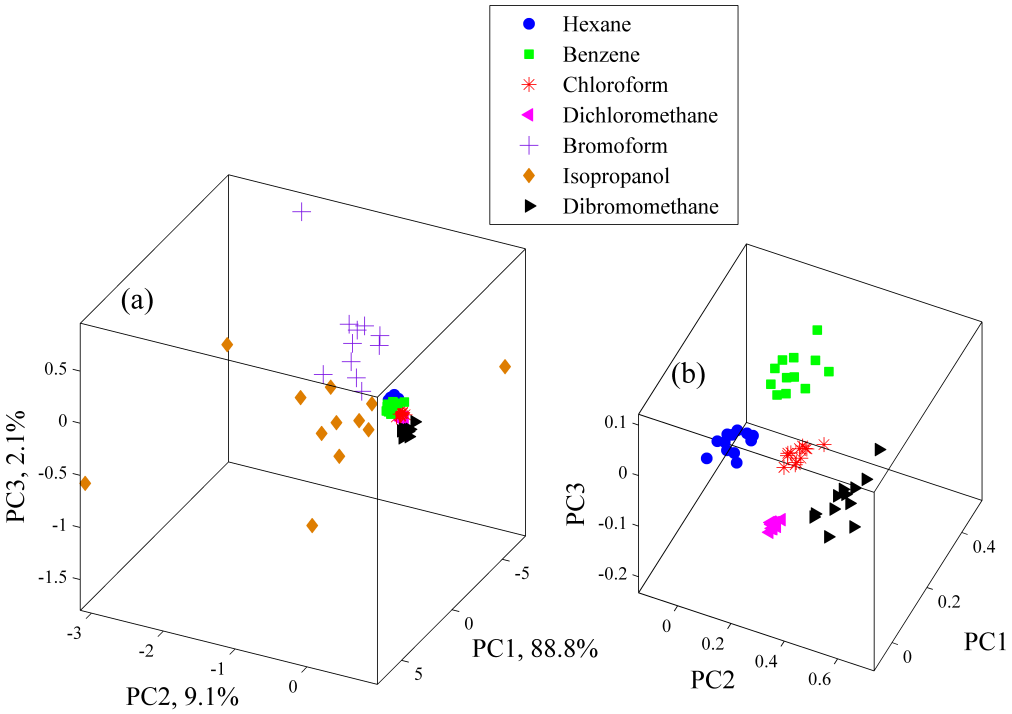

Figure 2.15: Excluding the HPC coated nanocantilever from PCA analysis of response data collected with humid air background improves analyte discrimination, increasing separation of closely spaced clusters. (a) PCA showing all analytes, and (b) the zoomed in region of tightly clustered analytes.

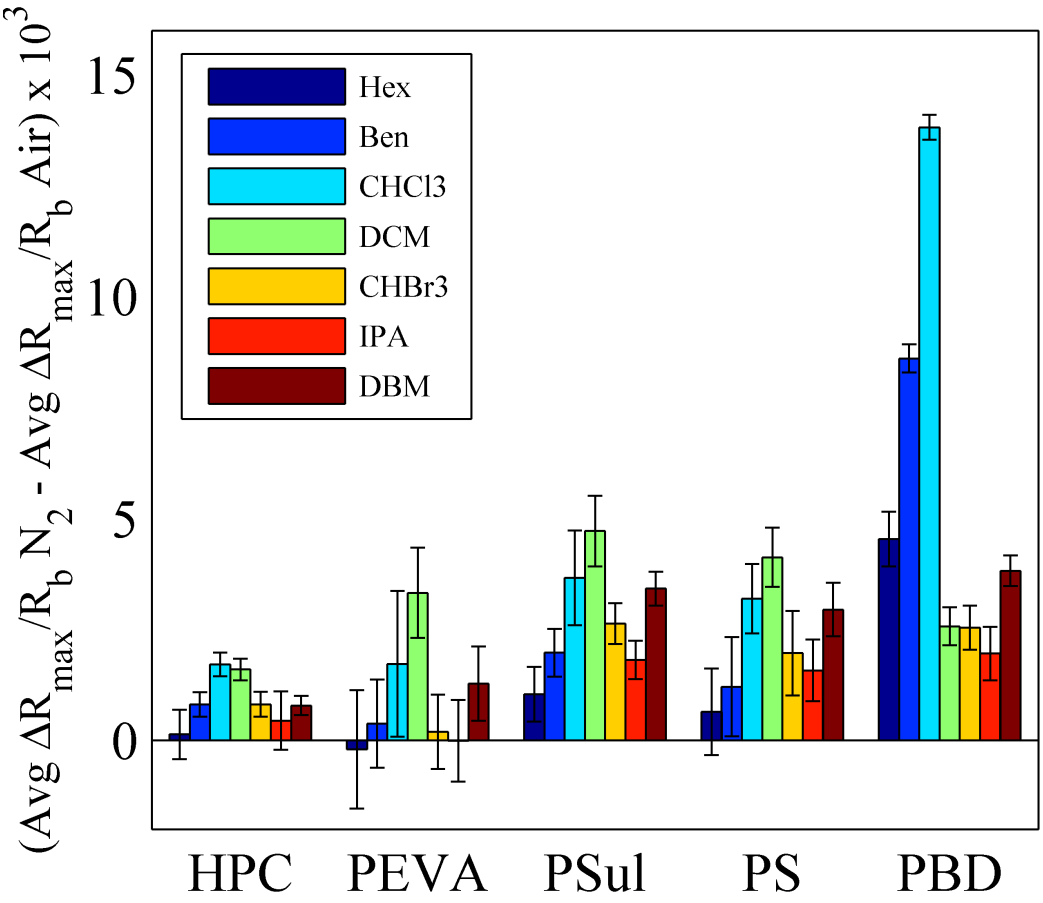

Figure 2.16: $\Delta R_{max}/R_B$ values for chemiresistors decreased across the array, most noticeably for the PBD chemiresistor exposed to hexane and benzene, which changed the array's fingerprint pattern for those two vapors.

Humidity suppresses the stiffening response mechanism, leading to frequency shifts that are more dominated by mass loading, which has the effect of shifting responses negatively. This indicates that nanocantilever responses to water vapor and VOCs are not purely additive, and that upon exposure to an analyte, the analyte molecules may displace a portion of the water molecules from the sensors.

2.5 Conclusions

The sensitivity and discrimination performance of a five-element array of polymer-coated resonating nanocantilever sensors compares favorably with that of a macroscale chemiresistor array utilizing the same polymers as the nanocantilever array. In direct comparison, the larger chemiresistors exhibit higher SNR than the nanocantilevers, but were calculated to require a minimum capture are of 1.17 mm^2 to match the SNR of the nanocantilevers, which have a capture area of 1.5 μm^2. A twenty element nanocantilever array, sufficient for most detection and discrimination tasks, could be housed in less than 100 μm^2 footprint, granting for 5 μm^2 for each sensor, while a 20 element array of chemiresistors with similar SNR values would require a minimum footprint of 23.4 mm^2. When exposed to analyte vapors with a dry nitrogen background both five element arrays produced clustered data of analyte vapors with little or no cluster overlap, as visualized by PCA, and FDL analysis shows both arrays produce *rf* > 3 for most pairwise combinations of analytes, indicating a better than 98% discrimination.

Nanocantilever $\Delta f_{max}/f_0$ values were shifted negatively when the carrier gas was switched from dry nitrogen to house air, which contains a low ppth concentration of water vapor. Adsorption of water vapor onto the nanocantilever surface and absorption into hydrophilic polymer films reduces the influence of surface elasticity and stiffness changes on responses to analytes, increasing the percentage of the response due to mass loading, which decreases resonance frequency. In this slightly humid setting, the HPC-coated nanocantilever did not respond to analyte vapors, degrading the array's discrimination performance, but data clustering, as seen in PCA, was restored if the HPC-coated nanocantilever was excluded from the analysis. This change in performance indicates that polymer coatings must be tailored for both analyte and environment to create an optimal nanocantilever array. With their extreme sensitivity, adjustable selectivity, and their small footprint,

nanocantilever chemical vapor sensors could pave the way to embedded sensor arrays in everyday products, and significant miniaturization of laboratory-scale analytical tools.

Bibliography

[1] F. Rock, N. Barsan, and U. Weimar. Electronic nose: Current status and future trends. *Chemical Reviews*, 108(2):705–725, 2008.

[2] N. S. Lewis. Comparisons between mammalian and artificial olfaction based on arrays of carbon black-polymer composite vapor detectors. *Accounts of Chemical Research*, 37(9):663–672, 2004.

[3] K. J. Albert, N. S. Lewis, C. L. Schauer, G. A. Sotzing, S. E. Stitzel, T. P. Vaid, and D. R. Walt. Cross-reactive chemical sensor arrays. *Chemical Reviews*, 100(7):2595–2626, 2000.

[4] J. A. Burns and G. M. Whitesides. Feedforward neural networks in chemistry - mathematical systems for classification and pattern-recognition. *Chemical Reviews*, 93(8):2583–2601, 1993.

[5] R.O Duda and P.E. Hart. *Pattern Classification and Scene Analysis*. John Wiley & Sons, New York, 1973.

[6] P. Geladi and B. R. Kowalski. Partial least-squares regression - a tutorial. *Analytica Chimica Acta*, 185:1–17, 1986.

[7] T. Gao, M. D. Woodka, B. S. Brunschwig, and N. S. Lewis. Chemiresistors for array-based vapor sensing using composites of carbon black with low volatility organic molecules. *Chemistry of Materials*, 18(22):5193–5202, 2006.

[8] S. Maldonado, E. Garcia-Berrios, M. D. Woodka, B. S. Brunschwig, and N. S. Lewis. Detection of organic vapors and nh3(g) using thin-film carbon black-metallophthalocyanine composite chemiresistors. *Sensors and Actuators B-Chemical*, 134(2):521–531, 2008.

[9] M. D. Woodka, B. S. Brunschwig, and N. S. Lewis. Use of spatiotemporal response information from sorption-based sensor arrays to identify and quantify the composition of analyte mixtures. *Langmuir*, 23(26):13232–13241, 2007.

[10] US Department of Homeland Security Cell-All Program.

[11] Synkera Technologies, Inc.

[12] Rhevision, Inc., in collaboration with Michael Sailor, UCSD.

[13] John Verrico. Cell phones that protect against deadly chemicals? Why not?, April 9, 2010.

[14] SR Chatterjee, M Chakraborty, and J Chakraborty. Cognitive radio sensor node empowered mobile phone for explosive trace detection. *International Journal of Communications, Network and System Sciences*, 4(1):33, 2011.

[15] Ronald Manginell, Joseph Bauer, Matthew Moorman, Lawrence Sanchez, John Anderson, Joshua Whiting, Daniel Porter, Davor Copic, and Komandoor Achyuthan. A monolithically-integrated μgc chemical sensor system. *Sensors and Actuators A-Physical*, 11(7):6517–6532, 2011.

[16] M. Li, E. B. Myers, H. X. Tang, S. J. Aldridge, H. C. McCaig, J. J. Whiting, R. J. Simonson, N. S. Lewis, and M. L. Roukes. Nanoelectromechanical resonator arrays for ultrafast, gas-phase chromatographic chemical analysis. *Nano Letters*, 10(10):3899–3903, 2010.

[17] F. J. Ibañez, U. Gowrishetty, M. M. Crain, K. M. Walsh, and F. P. Zamborini. Chemiresistive

vapor sensing with microscale films of gold monolayer protected clusters. *Analytical Chemistry*, 78(3):753–761, 2006.

[18] Forest I. Bohrer, Elizabeth Covington, Cagliyan Kurdak, and Edward T. Zellers. Characterization of dense arrays of chemiresistor vapor sensors with submicrometer features and patterned nanoparticle interface layers. *Analytical Chemistry*, 83(10):3687–3695, 2011.

[19] P. C. Chen, F. N. Ishikawa, H. K. Chang, K. Ryu, and C. Zhou. A nanoelectronic nose: a hybrid nanowire/carbon nanotube sensor array with integrated micromachined hotplates for sensitive gas discrimination. *Nanotechnology*, 20(12):8, 2009.

[20] Peter J. Chapman, Frank Vogt, Pampa Dutta, Panos G. Datskos, Gerald L. Devault, and Michael J. Sepaniak. Facile hyphenation of gas chromatography and a microcantilever array sensor for enhanced selectivity. *Analytical Chemistry*, 79(1):364–370, 2006.

[21] J. W. Grate. Acoustic wave microsensor arrays for vapor sensing. *Chemical Reviews*, 100(7):2627–2647, 2000.

[22] K. L. Ekinci and M. L. Roukes. Nanoelectromechanical systems. *Review of Scientific Instruments*, 76(6), 2005.

[23] E. Covington, F. I. Bohrer, C. Xu, E. T. Zellers, and C. Kurdak. Densely integrated array of chemiresistor vapor sensors with electron-beam patterned monolayer-protected gold nanoparticle interface films. *Lab on a Chip*, 10(22):3058–3060, 2010.

[24] C. J. Lu, W. H. Steinecker, W. C. Tian, M. C. Oborny, J. M. Nichols, M. Agah, J. A. Potkay, H. K. L. Chan, J. Driscoll, R. D. Sacks, K. D. Wise, S. W. Pang, and E. T. Zellers. First-generation hybrid MEMS gas chromatograph. *Lab on a Chip*, 5(10):1123–1131, 2005.

[25] E. S. Snow, F. K. Perkins, E. J. Houser, S. C. Badescu, and T. L. Reinecke. Chemical detection with a single-walled carbon nanotube capacitor. *Science*, 307(5717):1942–1945, 2005.

[26] J. A. Robinson, E. S. Snow, and F. K. Perkins. Improved chemical detection using single-walled carbon nanotube network capacitors. *Sensors and Actuators A-Physical*, 135(2):309–314, 2007.

[27] P. R. Lewis, R. P. Manginell, D. R. Adkins, R. J. Kottenstette, D. R. Wheeler, S. S. Sokolowski, D. E. Trudell, J. E. Byrnes, M. Okandan, J. M. Bauer, R. G. Manley, and G. C. Frye-Mason. Recent advancements in the gas-phase MicroChemLab. *IEEE Sensors Journal*, 6(3):784–795, 2006.

[28] Jay W. Grate, Susan L. Rose-Pehrsson, David L. Venezky, Mark Klusty, and Hank Wohltjen. Smart sensor system for trace organophosphorus and organosulfur vapor detection employing a temperature-controlled array of surface acoustic wave sensors, automated sample preconcentration, and pattern recognition. *Analytical Chemistry*, 65(14):1868–1881, 1993.

[29] L. Wang, D. Fine, and A. Dodabalapur. Nanoscale chemical sensor based on organic thin-film transistors. *Applied Physics Letters*, 85(26):6386–6388, 2004.

[30] L. A. Pinnaduwage, H. F. Ji, and T. Thundat. Moore's law in homeland defense: An integrated sensor platform based on silicon microcantilevers. *IEEE Sensors Journal*, 5(4):774–785, 2005.

[31] N. V. Lavrik, M. J. Sepaniak, and P. G. Datskos. Cantilever transducers as a platform for chemical and biological sensors. *Review of Scientific Instruments*, 75(7):2229–2253, 2004.

[32] H. P. Lang, M. K. Baller, R. Berger, Ch Gerber, J. K. Gimzewski, F. M. Battiston, P. Fornaro, J. P. Ramseyer, E. Meyer, and H. J. Gntherodt. An artificial nose based on a micromechanical cantilever array. *Analytica Chimica Acta*, 393(1-3):59–65, 1999.

[33] R. Datar, S. Kim, S. Jeon, P. Hesketh, S. Manalis, A. Boisen, and T. Thundat. Cantilever sensors: Nanomechanical tools for diagnostics. *MRS Bulletin*, 34(6):449–454, 2009.

[34] Y. T. Yang, C. Callegari, X. L. Feng, K. L. Ekinci, and M. L. Roukes. Zeptogram-scale nanomechanical mass sensing. *Nano Letters*, 6(4):583–586, 2006.

[35] H. Y. Chiu, P. Hung, H. W. C. Postma, and M. Bockrath. Atomic-scale mass sensing using carbon nanotube resonators. *Nano Letters*, 8(12):4342–4346, 2008.

[36] K. Jensen, K. Kim, and A. Zettl. An atomic-resolution nanomechanical mass sensor. *Nature Nanotechnology*, 3(9):533–537, 2008.

[37] K. Eom, H. S. Park, D. S. Yoon, and T. Kwon. Nanomechanical resonators and their applications in biological/chemical detection: Nanomechanics principles. *Physics Reports-Review Section of Physics Letters*, 503(4-5):115–163, 2011.

[38] M. Li, H. X. Tang, and M. L. Roukes. Ultra-sensitive NEMS-based cantilevers for sensing, scanned probe and very high-frequency applications. *Nature Nanotechnology*, 2(2):114–120, 2007.

[39] M. C. Lonergan, E. J. Severin, B. J. Doleman, S. A. Beaber, R. H. Grubb, and N. S. Lewis. Array-based vapor sensing using chemically sensitive, carbon black-polymer resistors. *Chemistry of Materials*, 8(9):2298–2312, 1996.

[40] E. J. Severin and N. S. Lewis. Relationships among resonant frequency changes on a coated quartz crystal microbalance, thickness changes, and resistance responses of polymer-carbon black composite chemiresistors. *Analytical Chemistry*, 72(9):2008–2015, 2000.

[41] E. J. Severin, B. J. Doleman, and N. S. Lewis. An investigation of the concentration depen-

dence and response to analyte mixtures of carbon black/insulating organic polymer composite vapor detectors. *Analytical Chemistry*, 72(4):658–668, 2000.

[42] A. R. Hopkins and N. S. Lewis. Detection and classification characteristics of arrays of carbon black/organic polymer composite chemiresistive vapor detectors for the nerve agent simulants dimethylmethylphosphonate and diisopropylmethylphosponate. *Analytical Chemistry*, 73(5):884–892, 2001.

[43] M. E. Koscho, R. H. Grubbs, and N. S. Lewis. Properties of vapor detector arrays formed through plasticization of carbon black-organic polymer composites. *Analytical Chemistry*, 74(6):1307–1315, 2002.

[44] Y. T. Yang, K. L. Ekinci, X. M. H. Huang, L. M. Schiavone, M. L. Roukes, C. A. Zorman, and M. Mehregany. Monocrystalline silicon carbide nanoelectromechanical systems. *Applied Physics Letters*, 78(2):162–164, 2001.

[45] I. Bargatin, E. B. Myers, J. Arlett, B. Gudlewski, and M. L. Roukes. Sensitive detection of nanomechanical motion using piezoresistive signal downmixing. *Applied Physics Letters*, 86(13):3, 2005.

[46] I. Bargatin, I. Kozinsky, and M. L. Roukes. Efficient electrothermal actuation of multiple modes of high-frequency nanoelectromechanical resonators. *Applied Physics Letters*, 90(9):3, 2007.

[47] S. M. Briglin, M. S. Freund, P. Tokumaru, and N. S. Lewis. Exploitation of spatiotemporal information and geometric optimization of signal/noise performance using arrays of carbon black-polymer composite vapor detectors. *Sensors and Actuators B-Chemical*, 82(1):54–74, 2002.

[48] J. W. Grate and M. H. Abraham. Solubility interactions and the design of chemically selective sorbent coatings for chemical sensors and arrays. *Sensors and Actuators B-Chemical*, 3(2):85–111, 1991.

[49] R. A. McGill, M. H. Abraham, and J. W. Grate. Choosing polymer-coatings for chemical sensors. *Chemtech*, 24(9):27–37, 1994.

[50] S. M. Briglin, T. Gao, and N. S. Lewis. Detection of organic mercaptan vapors using thin films of alkylamine-passivated gold nanocrystals. *Langmuir*, 20(2):299–305, 2004.

[51] B. C. Sisk and N. S. Lewis. Estimation of chemical and physical characteristics of analyte vapors through analysis of the response data of arrays of polymer-carbon black composite vapor detectors. *Sensors and Actuators B-Chemical*, 96(1-2):268–282, 2003.

[52] K. L. Ekinci, Y. T. Yang, and M. L. Roukes. Ultimate limits to inertial mass sensing based upon nanoelectromechanical systems. *Journal of Applied Physics*, 95(5):2682–2689, 2004.

[53] M Otto. *Statistics and Computer Application in Analytical Chemistry*. Wiley-VCH, New York, 1999.

[54] R.G. Brereton. *Chemometrics: Data Analysis for the Laboratory and Chemical Plant*. John Wiley & Sons, West Sussex, England, 2003.

[55] T. Thundat, G. Y. Chen, R. J. Warmack, D. P. Allison, and E. A. Wachter. Vapor detection using resonating microcantilevers. *Analytical Chemistry*, 67(3):519–521, 1995.

[56] A. K. Gupta, P. R. Nair, D. Akin, M. R. Ladisch, S. Broyles, M. A. Alam, and R. Bashir. Anomalous resonance in a nanomechanical biosensor. *Proceedings of the National Academy of Sciences of the United States of America*, 103(36):13362–13367, 2006.

[57] J. Tamayo, D. Ramos, J. Mertens, and M. Calleja. Effect of the adsorbate stiffness on the resonance response of microcantilever sensors. *Applied Physics Letters*, 89(22):3, 2006.

[58] K. L. Ekinci, X. M. H. Huang, and M. L. Roukes. Ultrasensitive nanoelectromechanical mass detection. *Applied Physics Letters*, 84(22):4469–4471, 2004.

[59] I. Bargatin, E. B. Myers, J. S. Aldridge, C. Marcoux, P. Brianceau, L. Duraffourg, E. Colinet, S. Hentz, P. Andreucci, and M. L. Roukes. Large-scale integration of nanoelectromechanical systems for gas sensing applications. *Nano Letters*, 12(3):1269–1274, 2012.

[60] Chang Liu. *Foundations of MEMS*. Prentice Hall, Upper Saddle River, N.J., 2nd edition, 2012.

[61] E. García-Berríos, T. Gao, J. C. Theriot, M. D. Woodka, B. S. Brunschwig, and N. S. Lewis. Response and discrimination performance of arrays of organothiol-capped au nanoparticle chemiresistive vapor sensors. *Journal of Physical Chemistry C*, 115(14):6208–6217, 2011.

[62] Z. Chen and C. Lu. Humidity sensors: A review of materials and mechanisms. *Sensor Letters*, 3(4):274–295, 2005.

[63] C. Y. Lee and G. B. Lee. Humidity sensors: A review. *Sensor Letters*, 3(1):1–15, 2005.

Chapter 3

Enhancing the Performance of Nanoelectromechanical Chemical Sensors through Surface-Initiated Polymerization

Improved coatings are critical for enhancing the sensitivity and selectivity of nanoscale chemical vapor sensors. Surface-initiated polymerization was used to grow thick, uniform poly(methyl methacrylate) (PMMA) films on nanocantilever chemical vapor sensors, which showed significantly greater sensitivity relative to bare cantilevers or those coated with dropcast polymer films, as well as a strong selectivity towards polar analytes. Our work suggests that surface-initiated polymerization can work as a straightforward, reproducible method for large-scale functionalization of nanosensors.

3.1 Introduction

Resonant micro- and nanocantilever sensors,[1,2] modified with self assembled monolayers (SAMs) or polymer films, have been used to detect a variety of biological and chemical targets,[3,4,5,6] including chemical vapors.[7,8,9,10,11] Sorption of a chemical vapor onto the surface of a cantilever changes factors such as mass and stiffness, which induce measurable shifts in resonant frequency.[2] The

smaller the dimensions of the resonant sensor, the more sensitive it becomes to the sorption of each vapor molecule,[12] so that nanocantilevers are able to detect mass changes at the attogram (10^{-18} g) scale in ambient conditions,[10] and at and below the zeptogram (10^{-21} g) scale in vacuum.[13,14,15,16]

Functionalizing nanocantilevers with polymer films increases sorption of chemical vapors onto the sensor relative to bare sensors and imparts a measure of selectivity to nanocantilever sensors based on the differences in chemical interactions of polymer/vapor pairs. The deposition of a thick polymer film is essential for producing high signal to noise ratio responses to chemical vapors in ambient conditions. Previous nanocantilever chemical vapor sensor studies have relied on thin, 2-10 nm dropcast polymer films,[10,11] which, while effective, limit the sensor's dynamic range in terms of both minimum detectable and maximum detectable vapor concentrations. All top-down coating techniques, such as microcapillary-pipette assisted dropcasting[17] and inkjet printing,[18] utilize solvent evaporation to produce solid films, which results in undesirable variation in film thickness across a single sensor and between adjacent sensors.

Surface initiated polymerization (SIP) has been widely used to grow polymers directly from a variety of substrates.[19] The resulting films are composed of polymer chains with one end tethered to a substrate, and when the inter-chain distance is small, steric repulsion leads to chain stretching, resulting in a brush-like conformation. Functionalizing nanocantilevers with SIP-grown films provides a method to deposit sorptive films. Surface Initiated Atom Transfer Radical Polymerization (SI-ATRP) is a particular polymer brush growth technique proven to have great ease of application and versatility for a wide range of functional groups.[20] SI-ATRP has been used to grow polymer brushes on microcantilevers that were subsequently used to detect changes in solvent quality,[21,22] pH,[22] and temperature,[22,23] as well as the presence of glucose in liquid,[24] and of saturated toluene vapor in nitrogen.[25] All of these microcantilever sensor measurements used static deflection of the cantilever beam rather than a resonant frequency shift to detect changes in their environments.

In this letter, we present a proof of concept use of surface initiated polymerization to grow thick, sorptive films on nanocantilever chemical vapor sensors. Poly(methyl methacrylate) (PMMA) was grown directly from the surface of nanocantilevers via SI-ATRP using a synthetic method which confines polymer formation to the cantilever surface. The SI-ATRP PMMA-coated cantilevers were then exposed to a series of seven organic vapors, along with both bare cantilevers and cantilevers functionalized with a dropcast PMMA film. The SI-ATRP PMMA-coated cantilever response to polar analytes was enhanced relative to bare and dropcast PMMA coated cantilevers, while all sensors exhibited similar magnitude responses to non-polar vapors. The thick polymer films grown with SI-ATRP on resonant nanocantilever sensors opens up a new area of study where sensor responses are dominated by analyte absorption into polymers and could be adapted for wafer scale processing.

3.2 Experimental

3.2.1 Materials

Methyl methacrylate (10–100 ppm MEHQ inhibitor), HQ/MEHQ inhibitor removal column packing, and poly(methyl methacrylate) (PMMA; T_g = 105 °C; MW = 35,000; ρ = 1.20 g/mL) were purchased from Scientific Polymer Products, Inc. Bis(2-[2'-bromoisobutyryloxy]ethyl) disulfide (BiBOEDS) (>90%) was purchased from ATRP Solutions. Methanol (anhydrous, 99.8%), copper (I) bromide (CuBr) (98%) and 2,2'-bypyridyl (>99%) were purchased from Aldrich. CuBr was purified by stirring with glacial acetic acid for 24 hrs at room temperature, followed by rinsing with ethanol and diethyl ether, and then drying overnight in vacuum. Purified CuBr was stored in a vacuum desiccator until use. Absolute ethanol was purchased from Decon Laboratories, Inc. Regent grade hexane, heptane, toluene, ethyl acetate, chloroform, tetrahydrofuran, isopropanol, and carbon tetrachloride were purchased from VWR, and were used to produce analyte vapors. All chemicals

were used as received unless otherwise stated. Ultrapure, deionized water (18 MΩ/cm) was used for all syntheses.

3.2.2 Nanocantilevers

The fabrication of silicon nitride nanocantilevers with integrated piezoresistive readouts has been described in detail previously.[10,26] Briefly, cantilever and bondpad shapes were pattered with electron beam lithography onto a 100 nm thick SiN layer on a silicon substrate, followed by gold film deposition, and then liftoff. Dry plasma etching was then used to release the cantilevers. The gold overlayer served as both etch mask during fabrication and later as a piezoresistive transducer.[27] Nanocantilevers had a typical fundamental resonance frequency of 10–12 MHz, quality (Q) factors of 100–200 in ambient conditions, and a capture area of 1.5 μm^2. Resonance was actuated thermoelastically.[28] Nanocantilever sensors were operated with home-built, LabView controlled, electronics[27] which tracked each sensor's resonance frequency using up to five parallel, independent phase-locked loops.

3.2.3 Initiator SAM Formation

Substrates were cleaned with hexane, acetone, tetrahydrofuran, methanol, and absolute ethanol, followed by a UV/ozone plasma clean for 8 min. After rinsing with deionized water and thoroughly drying with a stream of compressed air, substrates were immersed into a 5 mM solution of initiator in absolute alcohol. For a single chip, 2.5 mL of the solution (15 mg initiator), in a 20 mL scintillation vial was sufficient to fully immerse the substrate. The sealed vials were stored into the dark for 24–48 hrs to ensure the formation of a dense and ordered SAM.

3.2.4 Polymerization

Polymerization of MMA was done by water-accelerated SI-ATRP.[29] Neat MMA was first passed through an inhibitor removal column. The purified MMA was either used immediately, or was stored in sealed vials that were placed in a freezer until use. A two necked round bottom flask was charged with 7.5 mg purified MMA, 6 mL methanol, and 1.5 mL deionized water. The flask was sealed with septa and then the solution sonicated while sparging with nitrogen or argon for 45 min. The catalyst components, 258 mg of CuBr and 114 mg 2-bipy, were then added to the solution, which was then simultaneously sonicated and sparged until the catalyst dissolved, which generally took 30–45 min. Substrates were suspended with a flat alligator clip in a 20 mL scintillation vial equipped with a small stir bar and a septum. The clip was attached to a wire that was sufficiently long to bend over the rim of the vial, and was held in place with the septum. The vial was purged with nitrogen or argon for at least 45 min before introduction of the solution. The reaction solution was transferred via syringe from the round bottom flask to the vial containing the suspended substrate to prevent contact with oxygen. The reaction was allowed to proceed at room temperature with stirring and a constant inert gas purge. At the desired time the substrate was removed and thoroughly rinsed with tetrahydrofuran, methanol, and absolute ethanol.

3.2.5 Polymer Film Characterization

Films were characterized using ellipsometry and scanning electron microscopy (SEM). Flat substrates for ellipsometry measurements were prepared by evaporating 3 nm of chromium, followed by 30 nm of gold onto a silicon wafer coated with native oxide. Cleaning, SAM formation, and polymerization procedures were identical to those used for nanocantilevers. PMMA film thickness was measured with a Gaertner L166C ellipsometer, equipped with HeNe (633 nm wavelength) laser, at a 70° angle of incidence. The optical constants of the flat gold substrates were measured prior to

formation of the initiator SAM. Both initiator SAM and polymer film thickness were measured. The refractive index the SAM was assumed to be 1.46, and the refractive index of the PMMA film was assumed to be 1.49.[6] The thickness of the initiator SAM measured between 0-2 Å. SEM (ZEISS 1550 VP FESEM) was used to verify the quality of nanocantilever fabrication and the quality of the SI-ATRP grown polymer films.

3.2.6 Dropcast Polymer Films

PMMA solutions for dropcasting were formed by first making a concentrated solution by sonicating approximately 100 mg PMMA in 20 mL toluene until the polymer beads were dissolved. This concentrated solution was diluted 5 mM. A 10 μL micropipette was used to apply a 1.5 μL droplet of the dilute PMMA solution to the chip containing nanocantilever sensors, which was allowed to evaporate naturally.

3.2.7 Vapor Exposure Experiments

Nanocantilevers were exposed to analyte vapors using an automated vapor delivery system controlled by LabView.7 At least three sensors of each type (bare, dropcast PMMA, SI-ATRP PMMA) were tested. The analytes (hexane, toluene, heptane, ethyl acetate, chloroform, tetrahydrofuran, and isopropanol) were delivered at a concentrations of 0.005-0.08 P/P$^\circ$ (partial pressure divided by saturated vapor pressure), and each exposure consisted of 70 s of pure carrier gas, 400 s of analyte vapor exposure, followed by 630 s of carrier gas to purge the system. For single concentration experiments, a run consisted of five exposures to each analyte at 0.02 P/P$^\circ$. For linearity experiments, five exposures per concentration per analyte were delivered in the order 0.03, 0.01, 0.048, 0.005, 0.08, and 0.02 P/P$^\circ$ to prevent possible hysteresis from affecting linearity profile. The nanocantilevers were housed in a brass chamber with an internal volume of 100 mL. Between one and four sensors

were tested in each experimental run, and all sensors were "broken-in" prior to data collection by multiple exposures to each analyte. Temperature was not controlled, but was stable at $21 \pm 1\,^{\circ}\mathrm{C}$.

3.2.8 Data Analysis

Nanocantilever frequency data was corrected for baseline drift prior to extraction of sensor responses. Baseline noise was computed as the standard deviation of drift-corrected baseline frequency over a period of 10 s prior to sensor response. Signal to noise ratio was calculated conservatively as the average response divided by three times the baseline noise. Data analysis was done using OriginLab (Version 7.5). Nanocantilever sensor response data reported in figures and tables were recorded from single, representative sensors. Some variation was observed between individual sensors of each type, but it did not distort the reported trends.

3.2.9 Method for Determining Parition Coefficients of Dropcast and SI-ATRP Grown Polymer Films

Partition coefficients (K_{eq}) were determined by measuring the mass uptake of PMMA films applied to quartz crystal microbalances (QCMs). Each QCM was cleaned with hexane, acetone, and methanol before measurement of its initial resonance frequency, $F_{0,i}$. PMMA films were prepared either by spraycoating the QCM with a solution of PMMA (Scientific Polymer Products, Inc.) in tetrahydrofuran (160 mg / 20 mL) using an airbrush, or by SI-ATRP, as described above. All PMMA films were stored in a closed, but not sealed, container for at least 24 hrs after film formation to aid evaporation of any trapped solvent. Before data collection QCMs were broken-in by exposing them to a randomized series of vapor exposures for 12-18 hrs. QCMs were exposed to analyte vapors with an automated vapor delivery system.[7] Five exposures of the seven vapors at each of the five concentrations (P/P$^{\circ}$ = 0.01, 0.02. 0.04, 0.06, 0.08) were conducted in an order randomized for

both analyte identity and concentration. After an initial purge of 500 s, each exposure was 400 s in duration, with a 700 s purge between exposures. The change in resonance frequency due to polymer coating, $\Delta F_{polymer}$, was calculated as the difference of the resonance frequency before and after coating. The frequency change due to each vapor exposure, $\Delta F_{analyte}$, was calculated as the difference in frequency between the QCM during exposure relative to the baseline frequency. The baseline frequency was calculated as the average frequency during the 20 s prior to the specific vapor exposure, and the frequency during exposure was calculated as the average frequency between 350 and 398 s after the exposure had begun.

The calculation of the partition coefficient from the QCM frequency shift data has been described previously.[30] Briefly, first a line with a forced zero is fitted versus concentration data. The slope of this fit is then converted into a partition coefficient by,

$$K_{eq} = \frac{\rho RTm * 10^6}{M_W \Delta F_{polymer} P_{atm}} \tag{3.1}$$

where R is the ideal gas constant (1 atm mol^{-1} K^{-1}), ρ is the density (g mL^{-1}) of the polymer, T is the temperature (K), m is the slop4 of $\Delta F_{analyte}$ versus concentration (Hz/ppth in air), M_W is the molecular weight (g mol^{-1}) of the analyte, $\Delta F_{polymer}$ (Hz) is the frequency shift due to polymer coating, and P_{atm} is the atmospheric pressure (atm). The density of PMMA used in the K_{eq} calculations was 1.20 g/mL for QCMs with both spraycoated and SI-ATRP grown films.

3.2.10 Method for Ellipsometry of Polymer Film Swelling

Substrates coated with a either a dropcast or SI-ATRP grown PMMA film were placed into a vapor exposure chamber that was situated on the sample stage of the ellipsometer. The vapor exposure chamber consisted of a plastic box with ports for laser beam as well as vapor stream input. A glass window made from a microscope slide cover slip was installed in the top of the chamber to allow

for substrate alignment. Saturated analyte vapor was generated by passing a stream of laboratory air though a bubbler. A manual valve was used to switch the gas stream flowing through the sensor chamber between laboratory air and saturated analyte vapor. Substrates for PMMA film swelling measurement were QCMs that had been previously used to determine the K_{eq} of the films. The baseline film thickness of each sample was measured after exposure to a flow of laboratory air for 2 min. The flow was then switched to a stream of saturated analyte vapor for 6 min, and the film thickness was measured again. This procedure was repeated three times for each vapor.

3.3 Results

The sensors used in this work to investigate the benefits of SI-ATRP surface functionalization were piezoresistive, gold-coated silicon nitride nanocantilevers[10,26,27] with a typical fundamental resonance frequency of 10-12 MHz, quality (Q) factors of 100-200 in ambient conditions, and a capture area of 1.5 μm^2. Resonance was actuated thermoelastically.[28] Nanocantilever sensors were operated with home-built, LabView-controlled, electronics[27] which tracked each sensor's resonance frequency using parallel, independent phase-locked loops (PLLs). After thorough cleaning by UV/ozone plasma, the polymerization initiator bis(2-[2'-bromoisobutyryloxy]ethyl)disulfide (BiBOEDS) (ATRP Solutions) was tethered to the gold overlayer by self assembly by immersing the substrate in a 5 mM solution of BiBOEDS in absolute ethanol for 24-36 hr. The PMMA polymer brush was then grown using a room temperature, water-accelerated reaction[29] that was allowed to proceed between 30 min and 30 hr. Ellipsometry measurements, presented in Figure 3.1, of PMMA films grown on flat, gold-coated substrates show an initial linear relationship between reaction time and film thickness, which later slows due to chain termination, reaching a maximum film thickness of approximately 90 nm after 20 hr. SEM images of a nanocantilever coated with a 90 nm thick SI-ATRP PMMA film shows that the film is smooth, with a uniform thickness across the nanocan-

tilever, in comparison to a bare sensor and a dropcast PMMA film-coated sensor (Figure 3.2).

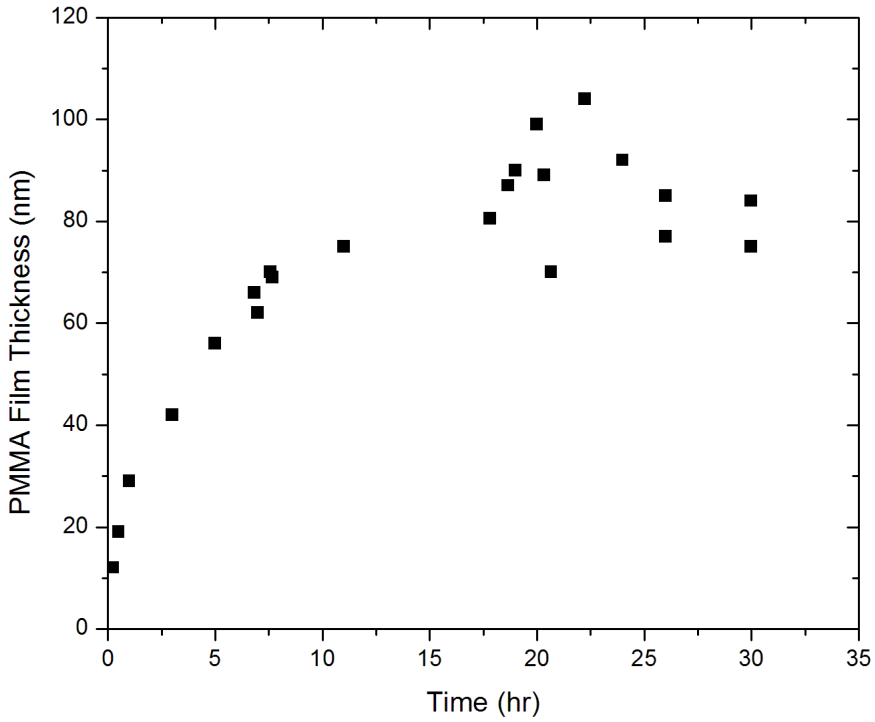

Figure 3.1: The growth of SI-ATRP PMMA films is linear for short reaction times, but levels out and reaches a maximum film thickness of approximately 90 nm at 20 h.

Nanocantilevers were exposed to analyte vapors using an automated vapor delivery system controlled by LabView-based software.[31] The analytes (hexane, toluene, heptane, ethyl acetate, chloroform, tetrahydrofuran, and isopropanol) were delivered at a concentrations of 0.005–0.08 P/P° (partial pressure divided by saturated vapor pressure), and each exposure consisted of 70 s of pure carrier gas, 400 s of analyte vapor exposure, followed by 630 s of carrier gas to purge the system. For single concentration experiments, a run consisted of five exposures to each analyte at 0.02 P/P°. For linearity experiments, five exposures per concentration per analyte were delivered in the order 0.03, 0.01, 0.048, 0.005, 0.08, and 0.02 P/P° to prevent possible hysteresis from affecting measured linearity profile. Additionally, SI-ATRP PMMA coated cantilevers were exposed to polar vapors

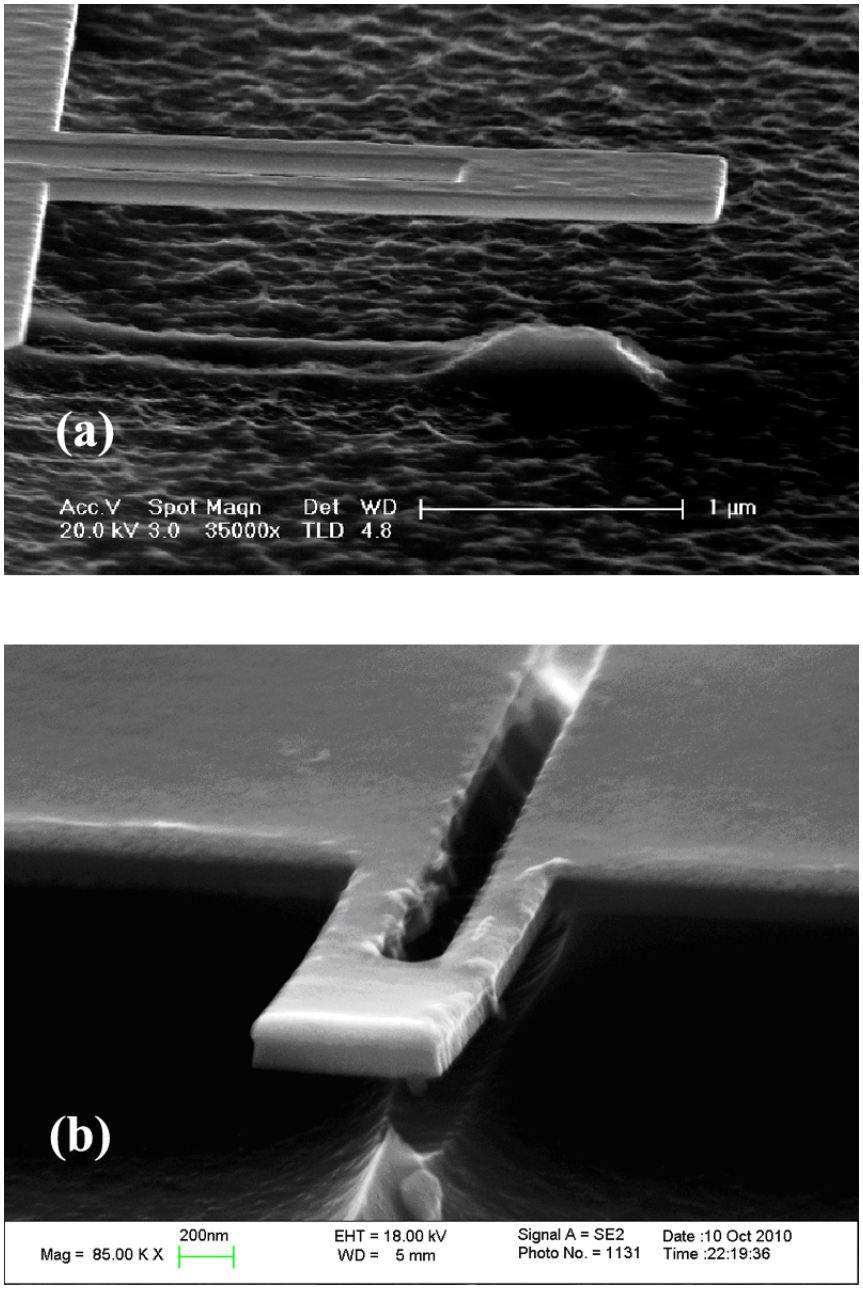

Figure 3.2: SEM images of nanocantilevers functionalized with (a) a 10 nm thick, dropcast polymer film and (b) a 90 nm thick, SI-ATRP grown PMMA film.

for longer times, up to 5000 s, to determine equilibrium response and response time.

For all vapor exposure experiments, the nanocantilevers were housed in a sealed brass chamber with an internal volume of 100 mL. Between one and four sensors were tested in each experimental run, and all sensors were broken-in prior to data collection by multiple exposures to each analyte. Temperature was not controlled, but was stable at $21 \pm 1\,^{\circ}\mathrm{C}$. Frequency data was corrected for baseline drift prior to extraction of sensor responses. Baseline noise was computed as the standard deviation of the drift-corrected baseline frequency over a period of 10 s prior to the sensor response. The signal to noise ratio (SNR) was calculated conservatively as the average response divided by three times the baseline noise.

The data from the 400 s exposure experiments (Figure 3.3) show that cantilevers coated with the SI-ATRP PMMA film produce stronger sensor responses to polar vapors compared to bare cantilevers and cantilevers coated with a dropcast PMMA film. No signal enhancement was observed for non-polar vapors. The response values for the nanocantilever sensors are reported in Table 3.1. The linearity of sensor response for 400 s exposures versus vapor concentration for a cantilever coated with SI-ATRP grown PMMA film is presented in Figure 3.4, and shows the response of the sensor to toluene vapor is nearly linear versus concentration, but the response of the sensor to ethyl acetate and isopropanol does not maintain linearity at higher concentrations. The following figures show baseline-drift corrected frequency traces for three cantilever sensors with different surface functionalization: bare gold (Figure 3.5), dropcast PMMA film (Figure 3.6), and SI-ATRP grown PMMA film (Figure 3.7). Each figure depicts the response of a single sensor to a series of exposures to analyte vapors at a concentration of 0.02 P/P$^{\circ}$. For these experiments, five sequential exposures to each of seven vapors were conducted in the order hexane, toluene, heptane, ethyl acetate, chloroform, isopropanol, and tetrahydrofuran.

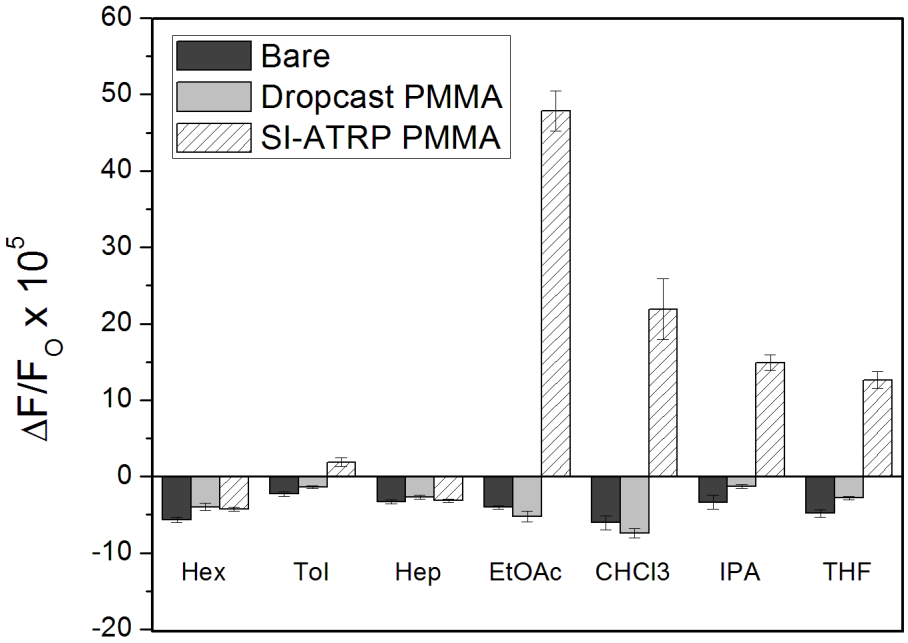

Figure 3.3: Responses of the nanocantilever sensors to a series of 400 s exposures to analyte vapors, delivered at 0.02 P/P°. Nanocantilevers coated with SI-ATRP grown PMMA films show enhanced sensitivity to polar analytes.

Table 3.1: Relative frequency shifts (a) and signal to noise ratio (b) for nanocantilevers with bare gold surface, dropcast PMMA film, and SI-ATRP PMMA film exposed to 400 s pulses of various analyte vapors.

(a) $\Delta f_{max}/f_0$ **x** 10^6			
Analyte	Bare	Dropcast PMMA	SI-ATRP PMMA
Hexane	-56.89 $\pm$ 3.34	-39.71 $\pm$ 4.63	-42.37 $\pm$ 2.62
Toluene	-22.96 $\pm$ 2.79	-13.73 $\pm$ 1.87	18.94 $\pm$ 5.45
Heptane	-33.02 $\pm$ 2.93	-26.83 $\pm$ 2.94	-31.67 $\pm$ 2.39
Ethyl Acetate	-40.45 $\pm$ 2.43	-52.31 $\pm$ 7.09	478.36 $\pm$ 26.47
Chloroform	-60.53 $\pm$ 9.34	-74.28 $\pm$ 6.29	219.21 $\pm$ 39.51
Isopropanol	-33.86 $\pm$ 9.22	-13.28 $\pm$ 2.52	149.13 $\pm$ 10..28
Tetrahydrofuran	-48.22 $\pm$ 4.55	-28.16 $\pm$ 1.83	126.52 $\pm$ 11.27

(b) SNR			
Analyte	Bare	Dropcast PMMA	SI-ATRP PMMA
Hexane	9.8 $\pm$ 0.6	6.9 $\pm$ 0.8	4.6 $\pm$ 0.05
Toluene	4.0 $\pm$ 0.5	2.4 $\pm$ 0.3	1.1 $\pm$ 0.1
Heptane	5.7 $\pm$ 0.5	4.6 $\pm$ 0.5	3.1 $\pm$ 0.3
Ethyl Acetate	7.0 $\pm$ 0.4	9.1 $\pm$ 1.2	49.6 $\pm$ 1.1
Chloroform	10.4 $\pm$ 1.6	12.9 $\pm$ 1.1	24.2 $\pm$ 1.1
Isopropanol	5.8 $\pm$ 1.6	2.3 $\pm$ 0.4	17.2 $\pm$ 2.0
Tetrahydrofuran	8.3 $\pm$ 0.8	4.9 $\pm$ 0.3	13.5 $\pm$ 0.6

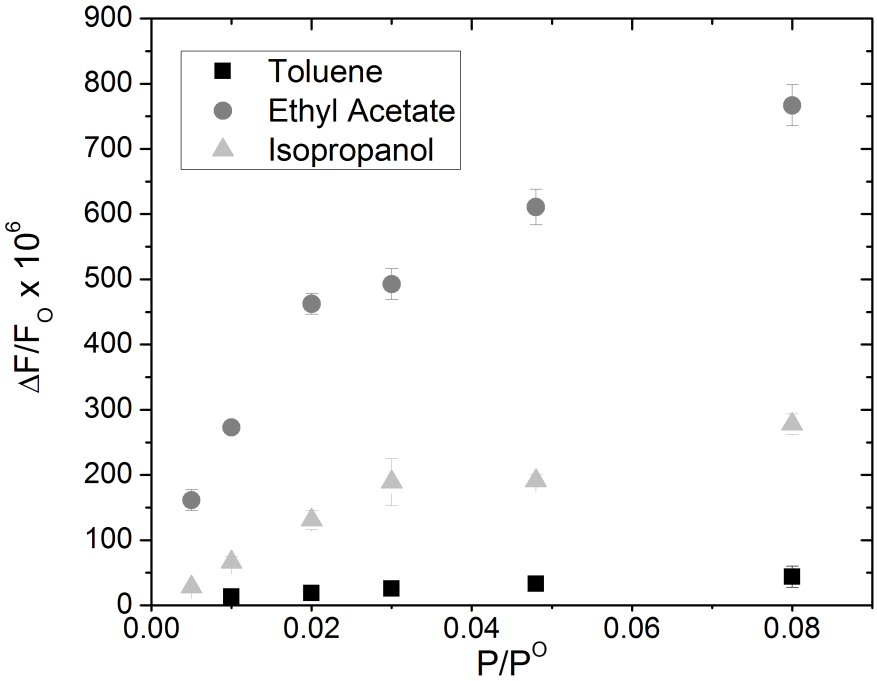

Figure 3.4: Linearity of sensor response for cantilevers coated with SI-ATRP grown PMMA films. Slow diffusion into the PMMA film by ethyl acetate and isopropanol leads to the departure from linearity exhibited by those two analytes.

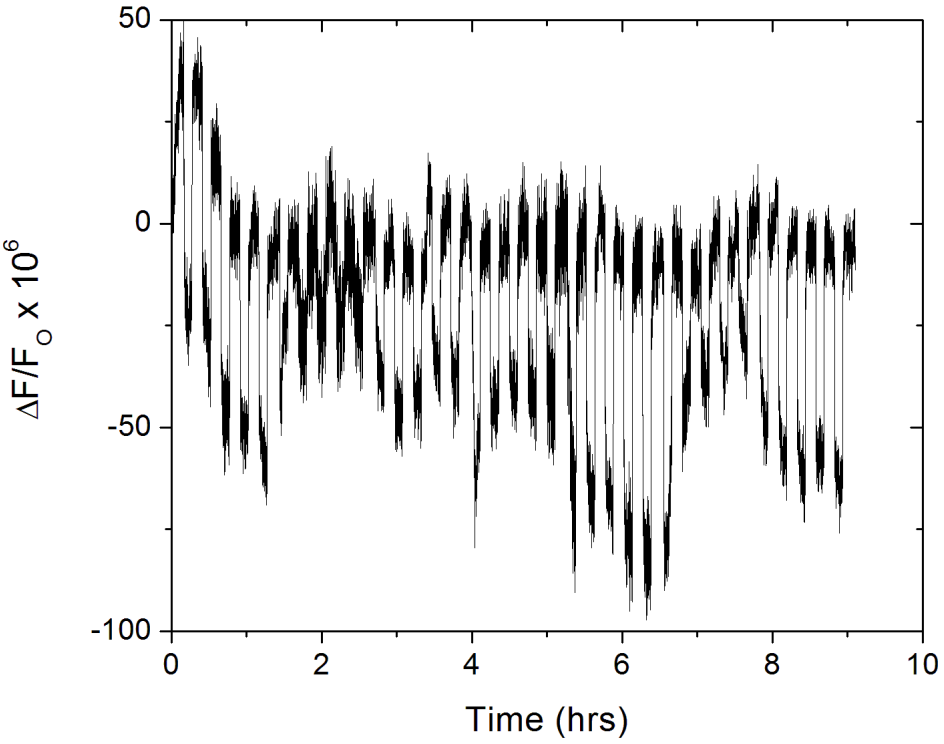

Figure 3.5: Responses of a bare cantilever to a series of analyte vapors delivered at 0.02 P/P°.

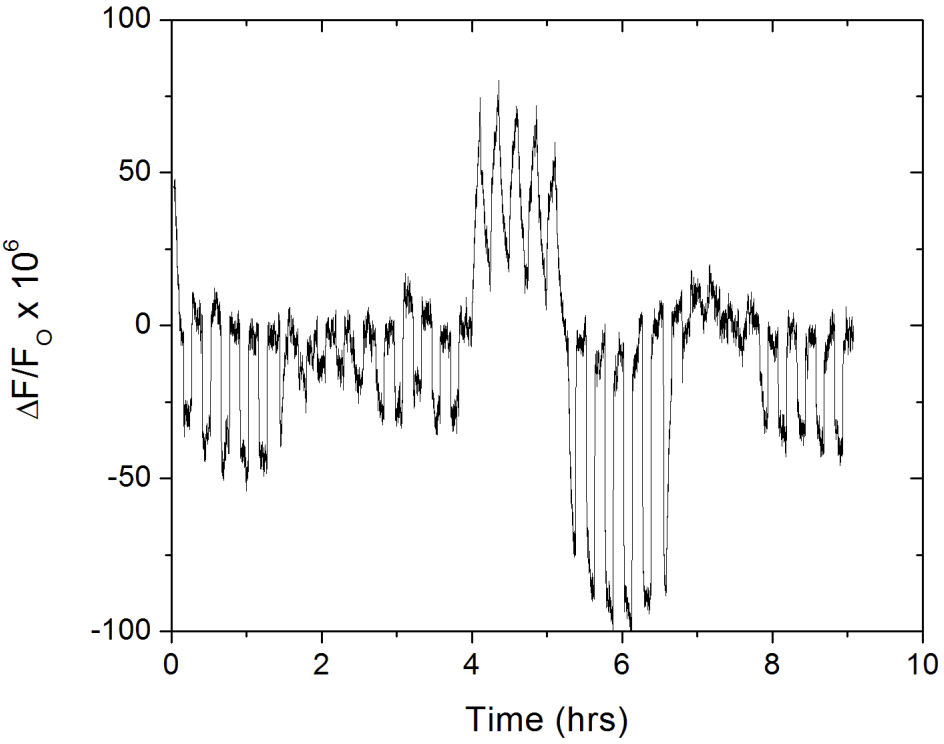

Figure 3.6: Responses of a cantilever functionalized with a dropcast film of PMMA to a series of analyte vapors delivered at 0.02 P/P°. Functionalizing the cantilever with a dropcast polymer film introduces selectivity and enhances sensitivity relative to a bare sensor.

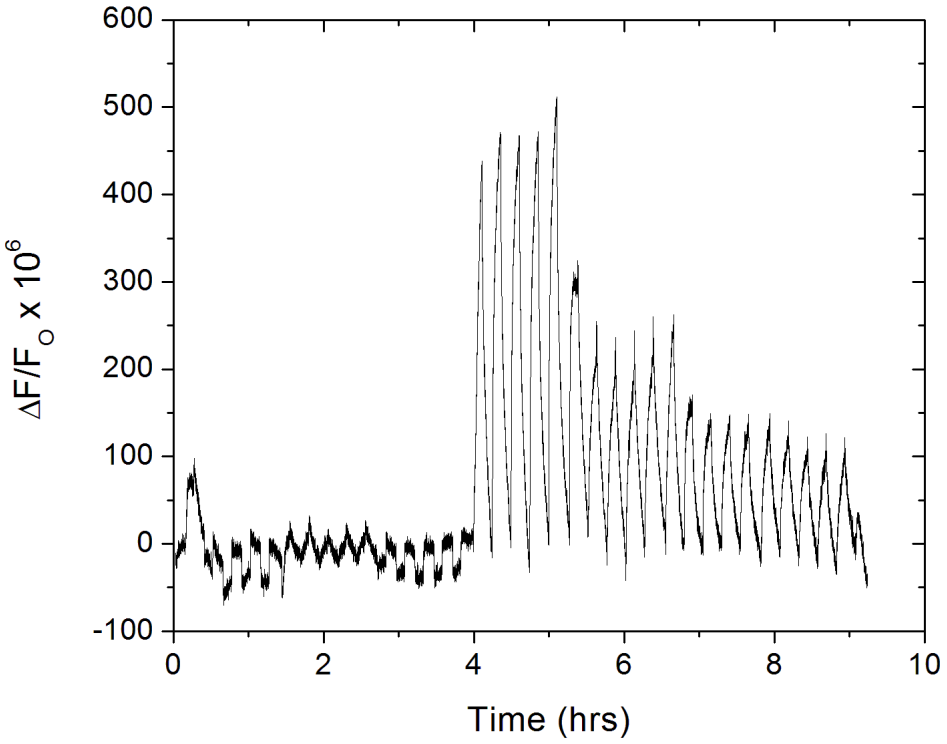

Figure 3.7: Responses of a cantilever functionalized with an SI-ATRP grown PMMA film to a series of analyte vapors delivered at 0.02 P/P°. The sensor's responsivity to polar vapors is greatly enhanced relative to a cantilever functionalized with a dropcast PMMA film.

3.4 Discussion

The increased sensitivity of the nanocantilever coated with an SI-ATRP grown PMMA film toward polar analytes, but not toward non-polar analytes is not explained by the difference in partition coefficient of polar and non-polar vapors absorbed in a PMMA film. The partition coefficient (K_{eq}) for an analyte/polymer pair is defined as,

$$K_{eq} = \frac{C_f}{C_v} \tag{3.2}$$

where C_f is the concentration of the analyte in the polymer film and C_v is the concentration of the analyte in the vapor phase.[32] Table 3.2 presents the K_{eq} values of both bulk PMMA and SI-ATRP PMMA for all analytes exposed to the nanocantilever sensors). This indicates that the number of molecules absorbed into the polymer film does not correlate with the response magnitude. Relative polymer film mass loading (calculated as the product of the partition coefficient and the molecular weight of the analyte) also does not correlate with response magnitude, meaning that other factors are influencing the sensor response.

Table 3.2: Calculated partition coefficients for bulk and SI-ATRP PMMA films. Due to the error inherrent in the measurement of QCM frequency shifts over the duration of the data collection, these values are best interpreted on the order of magnitude level (e.g. 4 x 10^2).

Partition Coefficients (K_{eq})		
Analyte	Spray Coated Bulk PMMA	SI-ATRP PMMA
Hexane	65	40
Toluene	540	375
Heptane	175	90
Ethyl Acetate	390	280
Chloroform	245	200
Isopropanol	415	350
Tetrahydrofuran	160	115

The SI-ATRP PMMA coated nanocantilever's enhanced sensitivity is also not explained by the vertical swelling of the polymer brush in response to the presence of analyte vapors (reported in Table 3.3). SI-ATRP PMMA films exhibited the strongest relative change in thickness when exposed to saturated chloroform vapor, followed by tetrahydrofuran, ethyl acetate, isopropanol, toluene, heptane, and finally hexane. The difference in magnitude of the relative thickness change does not correlate with the observed cantilever sensor responses. In addition, the ratio of the relative film swelling to the K_{eq} (reported in Table 3.3) for each vapor does not explain the enhanced response to polar analyte vapors since this ratio is an order of magnitude greater for chloroform and tetrahydrofuran, two good solvents for PMMA,[33] compared to all other analyte vapors.

Table 3.3: Relative swelling of SI-ATRP PMMA films exposed to saturated analyte vapors.

Relative Swelling (ΔH/H x 10^5)	
Analyte	SI-ATRP PMMA
Hexane	0.01
Toluene	0.12
Heptane	0.04
Ethyl Acetate	0.2
Chloroform	1.26
Isopropanol	0.18
Tetrahydrofuran	0.34

Table 3.4: Ratio of relative swelling to partition coefficient of SI-ATRP PMMA for various analyte vapors.

Relative Swelling ($(\Delta H/H)/K_{eq}$ x 100)	
Analyte	SI-ATRP PMMA
Hexane	2.5
Toluene	3.3
Heptane	4.3
Ethyl Acetate	7
Chloroform	63.3
Isopropanol	5.2
Tetrahydrofuran	29.7

The response magnitude of the SI-ATRP PMMA coated nanocantilevers does correlate somewhat with the dipole moment of the analyte vapors. To test this hypothesis, SI-ATRP PMMA coated cantilevers were additionally exposed to carbon tetrachloride, which is chemically similar to chloroform, but has a dipole moment of zero. While a 400 s exposure to chloroform induced relative frequency shift of 2.19 x 10^{-4}, a 400 s exposure to carbon tetrachloride only caused a relative frequency shift of -4.11 x 10^{-5}, as shown in Table 3.5. Analytes with non-zero dipole moments interact more strongly with PMMA, causing changes in the polymer film which are translated into increased sensor stiffness and are measured as large positive shifts in cantilever resonance frequency.

Table 3.5: The magnitude of the frequency shift of a SI-ATRP PMMA coated nanocantilever exposed to 400 s pulses of analyte vapors correlates with the dipole moment of the analyte. Analytes with a dipole moment of zero induce small frequency shifts, while analytes with non-zero dipoles induce large, positive frequency shifts.

SI-ATRP PMMA Nanocantilever Frequency Shift and Analyte Dipole Moment		
Analyte	$\Delta f_{max}/f_0$ x 10^6	Dipole moment (D/μ)[a]
Hexane	-42.37 $\pm$ 2.62	0
Toluene	18.94 $\pm$ 5.45	0.375 $\pm$ 0.010
Heptane	-31.67 $\pm$ 2.39	0
Ethyl Acetate	478.36 $\pm$ 26.47	1.78 $\pm$ 0.09
Chloroform	219.21 $\pm$ 39.51	1.04 $\pm$ 0.02
Isopropanol	149.13 $\pm$ 10..28	1.58 $\pm$ 0.03
Tetrahydrofuran	126.52 $\pm$ 11.27	1.75 $\pm$ 0.04
Carbon Tetrachloride	-41.13 $\pm$ 2.64	0

[a]Dipole moment values taken from the CRC Handbook of Chemistry and Physics, 82nd Edition.[34]

The positive shifts in nanocantilever resonance frequency in response to analyte exposure indicate that the sensors are experiencing an increase in effective stiffness. The change in resonance frequency of a cantilever is described by,

$$\frac{\Delta f}{f_0} = \frac{\partial k}{2k} - \frac{\partial m_{eff}}{2m_{eff}} \tag{3.3}$$

where Δf is the change in frequency, f_0 is the fundamental resonance frequency, k is the stiffness,

∂k is the change in stiffness, m_{eff} is the effective mass, and ∂m_{eff} is the change in effective mass.[7] The sorption of vapor molecules onto a nanocantilever will necessarily always result in an increase of mass, so for a positive frequency shift to be observed in response to the presence of an analyte vapor, the increase in stiffness must be greater than the effect of mass loading on the cantilever. This phenomenon has been observed in microcantilevers used for gas sensing,[7] as well as for nanocantilevers used to detect chemical vapors (see Chapter 2) and biological species.[35,36,37] Furthermore, it has been shown the resonant frequency of a microcantilever can either be increased or decreased by the evaporation of a gold film onto the device, depending on whether the gold was deposited at the clamped end or the free end.[38] In the case of vapor absorption into a glassy PMMA film, the effect of small molecules interpenetrating the polymer chains is transduced to the nanocantilever, which can result in an increase in sensor stiffness. The study of the exact mechanisms of nanocantilever stiffening is an active field, and further work is necessary to develop satisfactory models for the observed experimental responses.[2]

The shapes of nanocantilever linearity curves for ethyl acetate and isopropanol can be explained by the slow diffusion of strongly partitioning vapors into the 90 nm thick SI-ATRP grown PMMA film. Nanocantilever sensors operate at approximately 30 °C, whereas the glass transition temperature (T_g) of the bulk PMMA (Scientific Polymer Products, Inc: MW = 35k) used for the dropcast films is reported as 105 °C. Below the T_g, the individual chains of a polymer are locked into one configuration, rendering it "glassy" and decreasing the diffusion rate of vapor molecules into the film relative to the diffusion rate above the same polymer's T_g. Glassy polymers such as PMMA are known to exhibit non-Fickian diffusion characterized by a delayed relaxation of the polymer chains, which can greatly increase the time required for the absorbed analyte to reach its equilibrium concentration.[39,40,41,42] The responses of the nanocantilevers did not reach equilibrium during 400 s exposures to ethyl acetate at all concentrations, and for isopropanol at concentrations above

0.02 P/P°. It was determined that an equilibrium sensor response to ethyl acetate required a 5000 s exposure. The equilibrium response of the sensor to the polar analyte vapors increased by 53–138 % (as reported in Table 3.6) compared to the response generated by a 400 s exposure. The length of time to reach equilibrium is illustrated in Figure 3.8. Figure 3.9 shows the difference in sensor response between the 400 s and 5000 s vapor exposures. Furthermore, the response of SI-ATRP PMMA coated cantilevers to 5000 s exposures of ethyl acetate and isopropanol versus concentration remained non-linear. At higher concentrations, a 5000 s exposure was insufficient for the sensor to reach equilibrium. The PMMA film also exhibited pronounced history effect when exposed to ethyl acetate vapor, whereby an exposure to 0.03 P/P° ethyl acetate produced a smaller response than an exposure to 0.02 P/P° ethyl acetate later in the experiment, as shown in Figure 3.10.

Table 3.6: Equilibrium responses of a nanocantilever coated with an SI-ATRP PMMA film along with the percentage increase in response magnitude compared to the sensor response generated by a 400 s pulse of analyte vapor.

SI-ATRP PMMA Equilibrium Responses		
Analyte	$\Delta f_{max}/f_0$ x 10^6	Percent increase in response magnitude
Ethyl Acetate	714.73 $\pm$ 13.21	53%
Chloroform	508.05 $\pm$ 7.85	122%
Isopropanol	307.83 $\pm$ 61.40	90%
Tetrahydrofuran	305.51 $\pm$ 59.68	138%

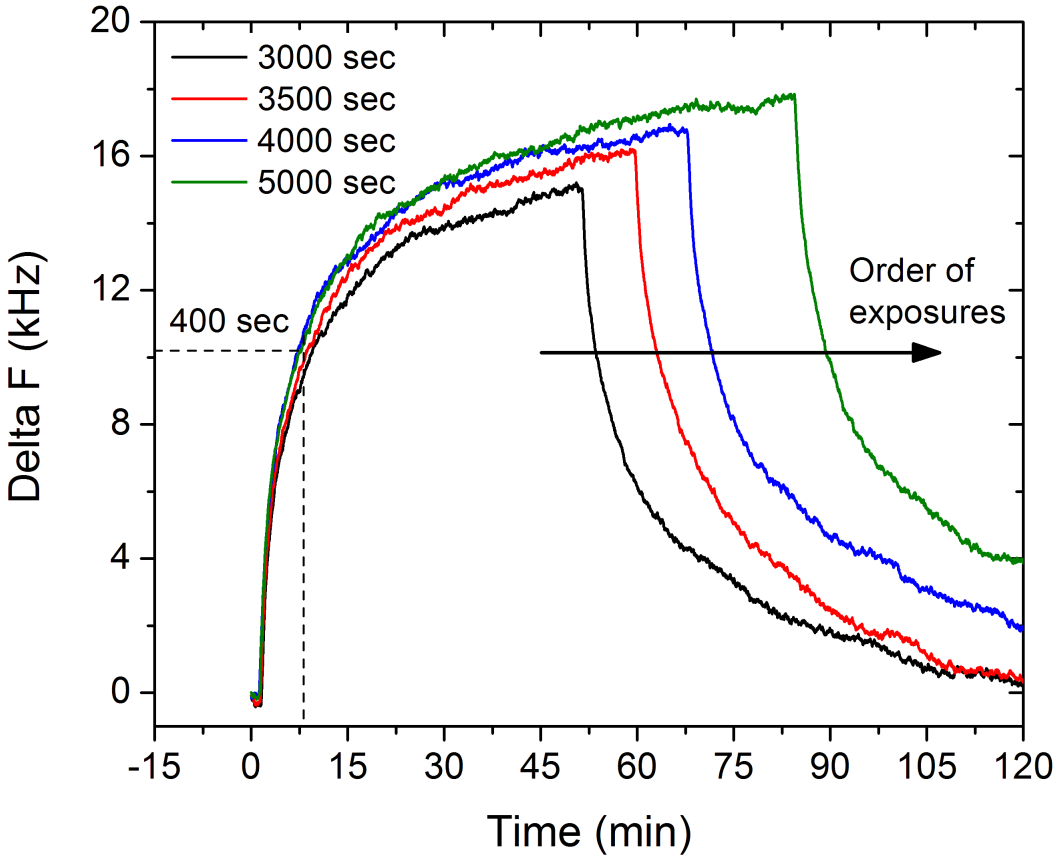

Figure 3.8: An SI-ATRP PMMA coated cantilever exposed to ethyl acetate vapor (0.02 P/P°) requires long exposure times to reach its new equilibrium frequency. The difference in response profile between the sensor responses also indicates that consecutive exposures to ethyl acetate affect the polymer film on a longer timescale. The sensor responded more rapidly during the later exposures, perhaps due to the PMMA being temporarily plasticized over the series of exposures.

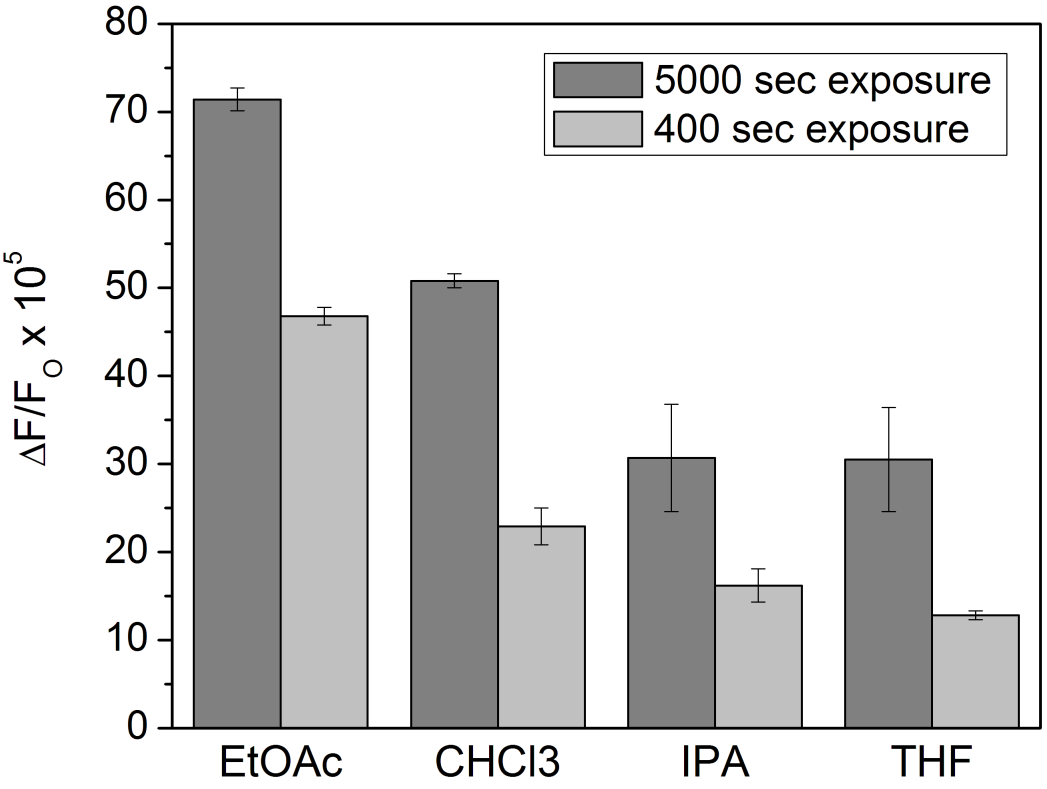

Figure 3.9: Comparison of SI-ATRP PMMA coated cantilever responses to polar vapors exposed for 400 s and 5000 s illustrates the slow diffusion of polar vapors into the PMMA film. When exposed to non-polar vapors, the same cantilever reached its equilibrium response within 400 s, as shown in Figure 3.7.

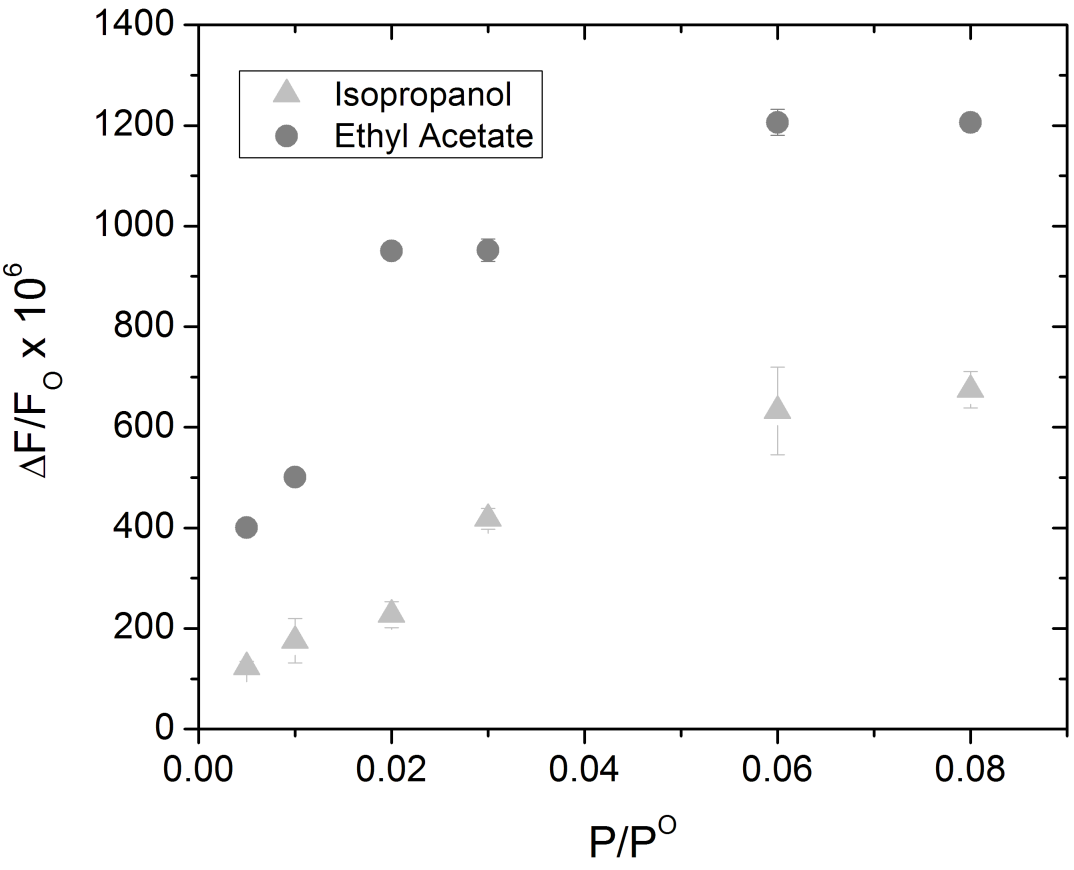

Figure 3.10: Longer exposure times (5000 s) to polar analyte vapors does not improve linearity because equilibrium is not reached for high vapor concentrations.

3.5 Conclusions

The work presented in this chapter demonstrates a proof of concept method for depositing thick, uniform polymer films on nanocantilevers to increase the amount of vapor absorbed onto the sensors. Growing polymer films with SI-ATRP circumvents the limitations of top-down functionalization schemes and creates an avenue to both improved sensitivity and saturation limit, while using techniques that preserve the option to tailor the physical and chemical properties of the polymer films for specific sensing applications. Chemical functionalization techniques, such as surface initiated

polymerization, that lead to improvements in concentration sensitivity are essential to realize the use of nanocantilevers in miniaturized vapor detection packages that can be incorporated into everyday life.

Bibliography

[1] A. Boisen, S. Dohn, S. S. Keller, S. Schmid, and M. Tenje. Cantilever-like micromechanical sensors. *Reports on Progress in Physics*, 74(3):30, 2011.

[2] K. Eom, H. S. Park, D. S. Yoon, and T. Kwon. Nanomechanical resonators and their applications in biological/chemical detection: Nanomechanics principles. *Physics Reports-Review Section of Physics Letters*, 503(4-5):115–163, 2011.

[3] N. V. Lavrik, M. J. Sepaniak, and P. G. Datskos. Cantilever transducers as a platform for chemical and biological sensors. *Review of Scientific Instruments*, 75(7):2229–2253, 2004.

[4] S. Singamaneni, M. C. LeMieux, H. P. Lang, C. Gerber, Y. Lam, S. Zauscher, P. G. Datskos, N. V. Lavrik, H. Jiang, R. R. Naik, T. J. Bunning, and V. V. Tsukruk. Bimaterial microcantilevers as a hybrid sensing platform. *Advanced Materials*, 20(4):653–680, 2008.

[5] M. Zougagh and A. Rios. Micro-electromechanical sensors in the analytical field. *Analyst*, 134(7):1274–1290, 2009.

[6] K. S. Hwang, S. M. Lee, S. K. Kim, J. H. Lee, and T. S. Kim. Micro- and nanocantilever devices and systems for biomolecule detection. *Annual Review of Analytical Chemistry*, 2:77–98, 2009.

[7] T. Thundat, G. Y. Chen, R. J. Warmack, D. P. Allison, and E. A. Wachter. Vapor detection using resonating microcantilevers. *Analytical Chemistry*, 67(3):519–521, 1995.

[8] M. Maute, S. Raible, F. E. Prins, D. P. Kern, H. Ulmer, U. Weimar, and W. Gopel. Detection of volatile organic compounds (VOCs) with polymer-coated cantilevers. *Sensors and Actuators B-Chemical*, 58(1-3):505–511, 1999.

[9] L. A. Pinnaduwage, H. F. Ji, and T. Thundat. Moore's law in homeland defense: An integrated sensor platform based on silicon microcantilevers. *IEEE Sensors Journal*, 5(4):774–785, 2005.

[10] M. Li, H. X. Tang, and M. L. Roukes. Ultra-sensitive NEMS-based cantilevers for sensing, scanned probe and very high-frequency applications. *Nature Nanotechnology*, 2(2):114–120, 2007.

[11] M. Li, E. B. Myers, H. X. Tang, S. J. Aldridge, H. C. McCaig, J. J. Whiting, R. J. Simonson, N. S. Lewis, and M. L. Roukes. Nanoelectromechanical resonator arrays for ultrafast, gas-phase chromatographic chemical analysis. *Nano Letters*, 10(10):3899–3903, 2010.

[12] K. L. Ekinci, Y. T. Yang, and M. L. Roukes. Ultimate limits to inertial mass sensing based upon nanoelectromechanical systems. *Journal of Applied Physics*, 95(5):2682–2689, 2004.

[13] Y. T. Yang, C. Callegari, X. L. Feng, K. L. Ekinci, and M. L. Roukes. Zeptogram-scale nanomechanical mass sensing. *Nano Letters*, 6(4):583–586, 2006.

[14] H. Y. Chiu, P. Hung, H. W. C. Postma, and M. Bockrath. Atomic-scale mass sensing using carbon nanotube resonators. *Nano Letters*, 8(12):4342–4346, 2008.

[15] K. Jensen, K. Kim, and A. Zettl. An atomic-resolution nanomechanical mass sensor. *Nature Nanotechnology*, 3(9):533–537, 2008.

[16] J.; Chaste, A.; Eichler, J.; Moser, G.; Ceballos, R.; Rurali, and A. Bachtold. A nanomechanical mass sensor with yoctogram resolution. *Nat Nano*, 7(5):301–304, 2012.

[17] Y. J. Wright, A. K. Kar, Y. W. Kim, C. Scholz, and M. A. George. Study of microcapillary pipette-assisted method to prepare polyethylene glycol-coated microcantilever sensors. *Sensors and Actuators B-Chemical*, 107(1):242–251, 2005.

[18] A. Bietsch, J. Y. Zhang, M. Hegner, H. P. Lang, and C. Gerber. Rapid functionalization of cantilever array sensors by inkjet printing. *Nanotechnology*, 15(8):873–880, 2004.

[19] Jürgen Rühe. Polymer brushes: On the way to tailor-made surfaces. In *Polymer Brushes*, pages 1–31. Wiley-VCH Verlag GmbH & Co. KGaA, 2005.

[20] K. Matyjaszewski and J. H. Xia. Atom transfer radical polymerization. *Chemical Reviews*, 101(9):2921–2990, 2001.

[21] G. G. Bumbu, M. Wolkenhauer, G. Kircher, J. S. Gutmann, and R. Berger. Micromechanical cantilever technique: A tool for investigating the swelling of polymer brushes. *Langmuir*, 23(4):2203–2207, 2007.

[22] N. I. Abu-Lail, M. Kaholek, B. LaMattina, R. L. Clark, and S. Zauscher. Micro-cantilevers with end-grafted stimulus-responsive polymer brushes for actuation and sensing. *Sensors and Actuators B-Chemical*, 114(1):371–378, 2006.

[23] C. Bradley, N. Jalili, S. K. Nett, L. Q. Chu, R. Forch, J. S. Gutmann, and R. Berger. Response characteristics of thermoresponsive polymers using nanomechanical cantilever sensors. *Macromolecular Chemistry and Physics*, 210(16):1339–1345, 2009.

[24] T. Chen, D. P. Chang, T. Liu, R. Desikan, R. Datar, T. Thundat, R. Berger, and S. Zauscher. Glucose-responsive polymer brushes for microcantilever sensing. *Journal of Materials Chemistry*, 20(17):3391–3395, 2010.

[25] G. G. Bumbu, G. Kircher, M. Wolkenhauer, R. Berger, and J. S. Gutmann. Synthesis and characterization of polymer brushes on micromechanical cantilevers. *Macromolecular Chemistry and Physics*, 205(13):1713–1720, 2004.

[26] Y. T. Yang, K. L. Ekinci, X. M. H. Huang, L. M. Schiavone, M. L. Roukes, C. A. Zorman, and M. Mehregany. Monocrystalline silicon carbide nanoelectromechanical systems. *Applied Physics Letters*, 78(2):162–164, 2001.

[27] I. Bargatin, E. B. Myers, J. Arlett, B. Gudlewski, and M. L. Roukes. Sensitive detection of nanomechanical motion using piezoresistive signal downmixing. *Applied Physics Letters*, 86(13):3, 2005.

[28] I. Bargatin, I. Kozinsky, and M. L. Roukes. Efficient electrothermal actuation of multiple modes of high-frequency nanoelectromechanical resonators. *Applied Physics Letters*, 90(9):3, 2007.

[29] D. M. Jones and W. T. S. Huck. Controlled surface-initiated polymerizations in aqueous media. *Advanced Materials*, 13(16):1256–1259, 2001.

[30] S. M. Briglin, M. S. Freund, P. Tokumaru, and N. S. Lewis. Exploitation of spatiotemporal information and geometric optimization of signal/noise performance using arrays of carbon black-polymer composite vapor detectors. *Sensors and Actuators B-Chemical*, 82(1):54–74, 2002.

[31] E. J. Severin, B. J. Doleman, and N. S. Lewis. An investigation of the concentration dependence and response to analyte mixtures of carbon black/insulating organic polymer composite vapor detectors. *Analytical Chemistry*, 72(4):658–668, 2000.

[32] J. W. Grate, A. Snow, D. S. Ballantine, H. Wohltjen, M. H. Abraham, R. A. McGill, and

P. Sasson. Determination of partition-coefficients from surface acoustic-wave sensor responses and correlation with gas-liquid chromatographic partition-coefficients. *Analytical Chemistry*, 60(9):869–875, 1988.

[33] E. J. Severin and N. S. Lewis. Relationships among resonant frequency changes on a coated quartz crystal microbalance, thickness changes, and resistance responses of polymer-carbon black composite chemiresistors. *Analytical Chemistry*, 72(9):2008–2015, 2000.

[34] *CRC Handbook of Chemistry and Physics*. CRC Press, 82nd edition, 2001.

[35] A. K. Gupta, P. R. Nair, D. Akin, M. R. Ladisch, S. Broyles, M. A. Alam, and R. Bashir. Anomalous resonance in a nanomechanical biosensor. *Proceedings of the National Academy of Sciences of the United States of America*, 103(36):13362–13367, 2006.

[36] J. Tamayo, D. Ramos, J. Mertens, and M. Calleja. Effect of the adsorbate stiffness on the resonance response of microcantilever sensors. *Applied Physics Letters*, 89(22):3, 2006.

[37] D. Ramos, J. Tamayo, J. Mertens, M. Calleja, and A. Zaballos. Origin of the response of nanomechanical resonators to bacteria adsorption. *Journal of Applied Physics*, 100(10):3, 2006.

[38] Dongkyu Lee, Seonghwan Kim, Namchul Jung, Thomas Thundat, and Sangmin Jeon. Effects of gold patterning on the bending profile and frequency response of a microcantilever. *Journal of Applied Physics*, 106(2):024310, 2009.

[39] M. Sanopoulou and J. H. Petropoulos. Systematic analysis and model interpretation of micro-molecular non-fickian sorption kinetics in polymer films. *Macromolecules*, 34(5):1400–1410, 2001.

[40] A. R. Berens and H. B. Hopfenberg. Diffusion of organic vapors at low concentrations in glassy pvc, polystyrene, and pmma. *Journal of Membrane Science*, 10(2-3):283–303, 1982.

[41] Maria-Chiara Ferrari, Enrico Piccinini, Marco Giacinti Baschetti, Ferruccio Doghieri, and Giulio C. Sarti. Solvent-induced stresses during sorption in glassy polycarbonate: Experimental analysis and model simulation for a novel bending cantilever apparatus. *Industrial & Engineering Chemistry Research*, 47(4):1071–1080, 2008.

[42] Maria Grazia De Angelis and Giulio C. Sarti. Solubility of gases and liquids in glassy polymers. *Annual Review of Chemical and Biomolecular Engineering*, 2(1):97–120, 2011.

Chapter 4

Nanocantilever Chemical Vapor Sensors Coated with Localized Rubbery and Glassy Polymer Brush Films: Sensing Changes in Stiffness

Highly-miniaturized chemical vapor detection systems, capable of near laboratory-quality analysis, could potentially be deployed widely, for applications in security, environmental monitoring, and disease biomarker detection on exhaled breath. Nanocantilever chemical vapor sensors, when coated with sorptive films, are ideal for such systems because of their ultra-small footprint, high sensitivity, and rapid response time. The deposition of well-controlled sorptive films is critical for optimizing sensor performance and enables the study of complex sensor response mechanisms. Towards this end, thick, uniform, and localized polymer films of poly(methyl methacrylate), poly(methyl acrylate), and poly(n-butyl methacrylate) were grown onto nanocantilevers via surface initiated atom transfer radical polymerization (SI-ATRP). Upon exposure to a series of chemical vapors at a concentration of 0.02 P/P° (where P is the partial pressure and P° is the saturated vapor pressure) the relative frequency shifts ($\Delta f / f_0$) of SI-ATRP polymer coated nanocantilevers were on the order of 5 – 200 x 10^5, two orders of magnitude greater than calculated frequency shift due to mass-loading alone.

To determine what section of the nanocantilever contributed the greatest portion of the observed response, polymer films were localized, by a chromium masking and passivation scheme, to selected regions of the nanocantilevers. Vapor sorption on the clamped end resulted in much stronger responses than vapor sorption on the tip, indicating that stiffness change, rather than mass-loading, is the predominant response mechanism. This information could be the key to improving future design and coating parameters for resonant nanocantilever sensors.

4.1 Introduction

Nanoscale chemical vapor sensors are an essential component of highly-miniaturized chemical detection systems.[1] Such systems have the potential to bring real-time, laboratory quality analysis to handheld devices, impacting fields as diverse as environmental monitoring, homeland security, and medical diagnostics.[2] A number of microscale chemical vapor sensors that are compatible with the constraints of miniaturized detection systems have been investigated, including chemiresistors,[3,4,5,6,7] carbon nanotube chemicapacitors,[8,9] surface acoustic wave (SAW) devices,[1,10,11] organic thin film transistors,[12] metal oxide nanowires,[13] and microcantilevers (static and resonating).[14,15,16,17,18] Of these, resonant nanocantilevers, and other nanoelectromechanical systems (NEMS), have been shown to be extremely sensitive to changes in mass,[19,20,21] and are able to detect mass loading on the attogram (10^{-18} g) scale in ambient conditions.[22]

The response mechanisms governing the behavior of NEMS sensors have been the subject of intense study,[23] and while experimentally observed shifts in resonance frequency are often attributed to mass loading, changes in the sensor's spring constant, especially when the thickness of the sorbed material is close to that of the nanocantilever, also contribute to frequency shifts. In particular, the effect of the modulus of the absorbate on nanocantilever resonant frequency has been observed

upon the absorption of self assembled monolayers (SAMs),[24] protein,[24] and bacterial cells,[25] as well as upon the patterning of gold films on cantilevers.[26] Similarly, the positive shifts in resonance frequency of gelatin-coated V-shaped microcantilevers upon exposure to water vapor has been attributed to stiffening of the gelatin film.[27] Previously, polymers have been deposited on nanocantilevers by dropcasting (see Chapter 2),[22,28] however, the resulting films were too thin, non-uniform, and irreproducible to draw conclusions about the polymer film's influence on sensor behavior.

One critical challenge that must be overcome to determine the effects of polymer films on the behavior of nanocantilever chemical vapor sensors is the development of a method to coat nanocantilevers, and other NEMS, with thick, uniform, and localized polymer films. Well-defined films composed of polymer brushes can be grown directly from substrates using surface initiated polymerization.[29] Polymer brushes are formed when polymer chains are tethered to a substrate in sufficient density that the chains are forced to stretch away from the surface, forming an anisotropic film resembling the upright fibers of a carpet. Previously, polymer brushes have been grown on static microcantilevers, and the deflection of the sensors used to detect phenomena such as changes in solvent quality,[30,31] pH,[31] and temperature,[31,32] as well as the presence of glucose in solution,[33] and of saturated toluene vapor in nitrogen.[34] Recently, a thick, uniform film of poly(methyl methacrylate) (PMMA) has been grown directly from the surface of nanocantilever sensors via surface initiated atom transfer radical polymerization (SI-ATRP) (see Chapter 3). Upon exposure to chemical vapors the SI-ATRP PMMA-coated nanocantilever exhibited strong positive shifts in resonance frequency, demonstrating that mass loading, which induces a decrease in the resonant frequency, was not the dominant response mechanism. However, these studies did not examine other underlying mechanistic questions that remain, such as whether mass-loading would be the dominant response mechanism for a nanocantilever coated with a rubbery polymer, and what sections of the nanocantilever would be the most sensitive to the sorption of vapor molecules.

In this study, surface initiated atom transfer radical polymerization (SI-ATRP) was used to grow thick, uniform films of two rubbery polymers, poly(methyl acrylate) (PMA), and poly(n-butyl methacrylate) (PBMA) on resonant nanocantilever chemical vapor sensors, which were then exposed to a series of chemical vapors. The response behavior of the nanocantilevers coated with rubbery polymers was compared to that of nanocantilevers coated with SI-ATRP grown films of the glassy polymer, PMMA, and thereafter compared to the calculated frequency shifts expected from mass-loading. Both the direction of the observed frequency shifts and the response time of the sensors were strongly influenced by whether the polymer film was rubbery or glassy.

The importance of stiffness change as a response mechanism was further shown when polymer films were localized to specific sections of the nanocantilever sensors through a chromium masking and passivation scheme to determine which part of the structure was responsible for the experimentally observed responses of the unmasked nanocantilevers. This work has revealed that nanocantilevers coated with SI-ATRP grown films respond to chemical vapors primarily through changes in stiffness, rather than via mass-loading. The importance of stiffness change as a response mechanism therefore should inform the design and coating of nanocantilevers for sensing applications.

4.2 Experimental

4.2.1 Cantilever Fabrication

The fabrication of silicon nitride nanocantilevers with integrated piezoresistive readouts has been described in detail previously.[22,35] Briefly, cantilever and bondpad shapes were pattered with electron beam lithography onto a 100 nm thick SiN layer on a silicon substrate, followed by gold film deposition, and then liftoff. Dry plasma etching was then used to release the cantilevers. The gold overlayer served as both etch mask during fabrication and later as a piezoresistive transducer.[36]

Chromium masked nanocantilevers were fabricated by first defining the bondpad and nanocantilever in gold, followed by a second electron beam lithography step to define the chromium areas, again followed by resist liftoff and then a release etch. Nanocantilevers had a typical fundamental resonance frequency of 10–12 MHz and quality (Q) factors of 120 in ambient conditions. Unmasked nanocantilevers had a capture area of 1.5 μm^2. Resonance was actuated thermoelastically.[37] Nanocantilever sensors were operated with home-built, LabView controlled, electronics,[36] which tracked each sensor's resonance frequency using parallel, independent, phase-locked loops.

4.2.2 Surface Chemistry

4.2.2.1 Materials

Methyl methacrylate (MMA), methyl acrylate (MA), and n-butyl methacrylate (BMA) (all containing 10-100 ppm MEHQ inhibitor), HQ/MEHQ inhibitor removal column packing, poly(methyl methacrylate) (PMMA; T_g = 105 °C; MW = 35,000; ρ = 1.20 g/mL), poly(methyl acrylate) (PMA; T_g = 5 °C; MW = 40,000; ρ = 1.22 g/mL), and poly(n-butyl methacrylate) (PBMA; T_g = 151 °C; MW = 180,000; ρ = 1.07 g/mL) were purchased from Scientific Polymer Products, Inc. Bis(2-[2'-bromoisobutyryloxy]ethyl) disulfide (BiBOEDS) (>90%) was purchased from ATRP Solutions. Methanol (anhydrous, 99.8%), n,n,n',n",n"-pentamethyldiethylenetriamine (PMDETA), copper (I) bromide (CuBr) (98%), copper (II) bromide ($CuBr_2$) (99.999%), and 2,2'-bypyridyl (2-bipy) (>99%) were purchased from Aldrich. CuBr was purified by stirring with glacial acetic acid for 24 hrs at room temperature, followed by rinsing with ethanol and diethyl ether, and then drying overnight in vacuum. Purified CuBr was stored in a vacuum desiccator until use. Absolute ethanol was purchased from Decon Laboratories, Inc. Regent grade hexane, heptane, toluene, ethyl acetate, chloroform, tetrahydrofuran, and isopropanol were purchased from VWR, and were used to produce analyte vapors. All chemicals were used as received unless otherwise stated. Ultrapure, deionized water

(18 MΩ/cm) was used for all syntheses. All quartz crystal microbalances (QCMs) and the QCM actuator were purchased from International Crystal Manufactures (ICM, Inc.).

4.2.2.2 Formation of SAMs

Solutions for SAM formation were prepared in 20 ml scintillation vials, consisting of 5 mM n-hexylphosphonic acid or BiBOEDS in absolute ethanol. Typically, each vial contained 2.5 – 5 mL of solution, which was sufficient to fully immerse the substrate. Solutions were stored in the dark to prevent potential degradation of the SAM forming molecules, particularly of the BiBOEDS, due to UV light.

Flat gold substrates were fabricated by evaporation of 30 nm gold film on silicon over a 10 nm chromium adhesion layer. Flat chromium substrates were fabricated by evaporation of a 30 nm chromium film on silicon, and were stored in air such that a native oxide was formed. All flat substrates, nanocantilevers, and QCMs were first thoroughly washed with hexane, acetone, tetrahydrofuran, and absolute ethanol, and then dried with compressed air. Organic contaminants were removed using an 8 min ozone plasma etch, followed by rinsing with deionized water (18 MΩ/cm), thorough drying with compressed air, and immediate immersion in the pre-prepared ethanol solution of either n-hexylphosphonic acid or BiBOEDS. To aid in the handling of the delicate QCMs, a sample holder consisting of an NMR tube cap with a slit cut with a razor blade was employed. A single QCM was slid into the slit, so that the cap could be handled with tweezers.

Substrates were soaked in each solution for at least 36 h to ensure the formation of an ordered SAM. Substrates were then rinsed with absolute ethanol and dried with compressed air. Substrates were characterized and then either immersed in a second SAM-formation solution or immediately prepared for use in a polymerization reaction. Unmasked nanocantilevers were not immersed in the n-hexylphosphonic acid solution.

4.2.2.3 ATRP of PMMA

Polymerization of MMA was conducted by water-accelerated SI-ATRP.[38] Neat MMA was first passed through an inhibitor removal column. The purified MMA was either used immediately, or was stored in sealed vials that were placed in a freezer until use. A two necked round bottom flask was charged with 7.5 mg purified MMA, 6 mL methanol, and 1.5 mL deionized water. The flask was sealed with septa and then the solution sonicated while sparging with nitrogen or argon for 45 min. The catalyst components, 258 mg of CuBr and 114 mg 2-bipy, were then added to the solution, which was then simultaneously sonicated and sparged for 30–45 min until the catalyst dissolved. Substrates were suspended with a flat alligator clip in a 20 mL scintillation vial equipped with a small stir bar and a septum. The clip was attached to a wire that was sufficiently long to bend over the rim of the vial, and was held in place with the septum. The vial was purged with nitrogen or argon for at least 45 min before introduction of the solution. The reaction solution was transferred via syringe from the round bottom flask to the vial containing the suspended substrate to prevent contact with oxygen. The reaction was allowed to proceed at room temperature with stirring and a constant inert gas purge. At the desired time (e.g. 20 h for a 90 nm thick film) the substrate was removed and thoroughly rinsed with tetrahydrofuran, methanol, and absolute ethanol.

4.2.2.4 ATRP of PMA

Polymerization of MA was conduced by bulk SI-ATRP,[39] and the reaction parameters adjusted from the original publication such that polymer growth occurred at $50\,^{\circ}\mathrm{C}$ to prevent desorption of the BiBOEDS SAM. MA was first passed through an inhibitor removal column. A round bottom flask was charged with 23 g MA (excess to account for evaporation during the long polymerization) and 432 mg PMDETA. The flask was sealed with a septum, and then the solution was sonicated while sparging with argon for 1 h. A large test tube fitted with a magnetic stir bar was charged with

257 mg CuBr and 15 mg $CuBr_2$. The substrate was suspended in the test tube with a flat clip that was wired to a metal needle. The needle was pierced through the septum which was then used to seal the test tube, allowing the substrate height to be controlled. The pointed tip of the needle was wrapped in parafilm to seal it, to prevent accidental injury, and prevent oxygen contamination. Substrate suspension allowed the solution to be stirred without damaging the substrate. The tube was purged continuously with argon. The test tube was maintained at $50\,^{\circ}\mathrm{C}$ by emersion in an oil bath for the duration of the reaction. The sparged solution was transferred to the test tube using a syringe. Care was taken to prevent solution from contacting the substrate, which was kept suspended above the liquid. After stirring the solution for 1 h at $50\,^{\circ}\mathrm{C}$ to dissolve the catalyst, the substrate was lowered into the reaction solution. The reaction was allowed to proceed for 48 hrs, which resulted in a 100 nm thick PMA film. The solution was exposed to air to stop the polymerization. Substrates were rinsed with chloroform, methanol, and absolute ethanol.

4.2.2.5 ATRP of PBMA

Polymerization of BMA was conducted by water accelerated SI-ATRP.[40] Neat BMA was first passed through an inhibitor removal column, and then used immediately. A two necked round bottom flask was charged with 10 mL purified BMA, 9 mL isopropanol, and 1 mL deionized water. The flask was sealed with septa and then the solution sonicated while sparging with argon for 45 min. The catalyst components, 52 mg of CuBr and 127 mg 2-bipy, were then added to the solution, which was then simultaneously sonicated and sparged until the catalyst dissolved (30–45 min). The remainder of the reaction proceeded as for ATRP of PMMA, with a typical reaction time of 12 h producing a 100 nm thick PBMA film.

4.2.2.6 Dropcast Polymer Films

Polymer solutions for creating dropcast films on nanocantilevers were made by first making a concentrated solution by sonicating approximately 100 mg polymer in 20 mL toluene until the polymer beads were dissolved, which was then diluted to 5 mM. A 10 μL micropipette was used to apply a 1.5 μL droplet of the dilute PMMA solution to the chip containing nanocantilever sensors, which was allowed to evaporate naturally. This dropcasting procedure resulted in 2–10 nm thick polymer films.

4.2.2.7 Characterization

Films were characterized using ellipsometry and scanning electron microscopy (SEM). Polymer film thickness was measured with a Gaertner L166C ellipsometer, equipped with HeNe (633 nm wavelength) laser, at a 70° angle of incidence. The optical constants of the flat gold substrates were measured prior to formation of the initiator SAM. Both initiator SAM and polymer film thickness were measured. The refractive index both the n-hexylphosphonic acid and BiBOEDS SAMs was assumed to be 1.46. The refractive index of PMMA assumed to be 1.49, the index of PMA to be 1.48, and the index of PBMA to be 1.48, based on values provided by Scientific Polymer Products, Inc. for bulk polymers. The thickness of the initiator SAM measured between 0-2 Å. SEM (ZEISS 1550 VP FESEM) was used to verify the quality of nanocantilever fabrication and the quality of the SI-ATRP grown polymer films.

4.2.3 Vapor Exposure Experiments

The nanocantilevers were exposed to analyte vapors using an automated vapor delivery system controlled by LabView.[41] At least three sensors of each type (e.g. unmasked nanocantilevers with dropcast PMMA films, Cr-legs nanocantilevers with SI-BPMA films) were tested. The analytes

(hexane, toluene, heptane, ethyl acetate, chloroform, tetrahydrofuran, and isopropanol) were delivered at a concentrations of 0.005-0.08 P/P$^{\circ}$ (partial pressure divided by saturated vapor pressure), and each exposure consisted of 70 s of pure carrier gas, 400 s of analyte vapor exposure, followed by 630 s of carrier gas to purge the system. For single concentration experiments, a run consisted of five exposures to each analyte at 0.02 P/P$^{\circ}$. For linearity experiments, five exposures per concentration per analyte were delivered in the order 0.03, 0.01, 0.048, 0.005, 0.08, and 0.02 P/P$^{\circ}$ to prevent possible hysteresis from affecting linearity profile. The response times of the nanocantilevers were determined by running the sensors "open-loop" and measuring the error signal, rather than tracking the resonance frequency with a PLL.[28] The nanocantilevers were housed in a brass chamber with an internal volume of 100 mL. Between one and four sensors were tested in each experimental run, and all sensors were broken in prior to data collection by multiple exposures to each analyte over a period of 12-24 h. Temperature was not controlled, but was stable at $21 \pm 1\,^{\circ}\mathrm{C}$.

4.2.4 Nanocantilever Data Analysis

Nanocantilever frequency data was corrected for baseline drift prior to extraction of sensor responses using OriginLab (Version 7.5). The baseline-corrected frequency data was then imported into MATLAB (Mathworks, Version R22008b) and the sensor responses extracted using custom scripts. Baseline noise was computed as the standard deviation of drift-corrected baseline frequency over a period of 10 s prior to sensor response. Signal to noise ratio was calculated conservatively as the average response divided by three times the baseline noise. Nanocantilever sensor response data reported in figures and tables were recorded from single, representative sensors. Some variation was observed between individual sensors of each type, but it did not distort the reported trends.

4.2.5 Determinination of Partition Coefficients

Partition coefficients (K_{eq}) were determined by measuring the mass uptake of PMMA films applied to quartz crystal microbalances (QCMs). Each QCM was cleaned with hexane, acetone, and methanol before measurement of its initial resonance frequency, $F_{0,i}$. Polymer films were prepared either by spraycoating the QCM with a solution of PMMA, PMA, or PBMA in tetrahydrofuran (160 mg / 20 mL) using an airbrush, or by SI-ATRP, as described above. All coated QCMs were stored in a closed, but not sealed, container for at least 24 hrs after film formation to aid evaporation of any solvent trapped in the films. Before data collection QCMs were broken-in by exposing them to a randomized series of vapor exposures for 12-18 hrs.

QCMs were exposed to analyte vapors with an automated vapor delivery system.[41] Five exposures of the seven vapors at each of the five concentrations (P/P$^\circ$ = 0.01, 0.02. 0.04, 0.06, 0.08) were conducted in an order randomized for both analyte identify and concentration. After an initial purge of 500 s, each exposure was 400 s in duration, with a 700 s purge between exposures. The change in resonance frequency due to polymer coating, $\Delta F_{polymer}$, was calculated as the difference of the resonance frequency before and after coating. The frequency change due to each vapor exposure, $\Delta F_{analyte}$, was calculated as the difference in frequency between the QCM during exposure relative to the baseline frequency. The baseline frequency was calculated as the average frequency during the 20 s prior to the specific vapor exposure, and the frequency during exposure was calculated as the average frequency between 350 and 398 s after the exposure had begun.

The calculation of the partition coefficient from the QCM frequency shift data has been described previously.[42] Briefly, first a line with a forced zero is fitted versus concentration data. The slope of this fit is then converted into a partition coefficient by,

$$K_{eq} = \frac{\rho RTm * 10^6}{M_W \Delta F_{polymer} P_{atm}} \tag{4.1}$$

where R is the ideal gas constant (1 atm mol^{-1} K^{-1}), ρ is the density (g mL^{-1}) of the polymer, T is the temperature (K), m is the slop of $\Delta F_{analyte}$ versus concentration (Hz/ppth in air), M_W is the molecular weight (g mol^{-1}) of the analyte, $\Delta F_{polymer}$ (Hz) is the frequency shift due to polymer coating, and P_{atm} is the atmospheric pressure (atm). The density of PMMA used in the K_{eq} calculations was 1.20 g/mL for QCMs with both spraycoated and SI-ATRP grown films.

4.2.6 Modeling

Assuming that the change in the stiffness of the cantilever is negligible, the fractional frequency shift is related to the effective mass of the resonator, such that

$$\frac{\Delta f}{f_0} = -\frac{\partial m_{eff}}{2m_{eff}} \tag{4.2}$$

where Δf is the change in resonance frequency, f_0 is the resonant frequency, and m_{eff} is the effective mass of the resonator. Rewriting Eqn. 4.2, we find

$$\Delta f = K_{eq} = -\frac{f_0}{2m_{eff}} \Delta m_{eff} \tag{4.3}$$

The change in effective mass caused by analyte absorption is position-dependent, as molecules absorbed closer to the cantilever base participate less in resonant motion and so have a smaller inertial effect. This dependence is directly related to the resonance mode shape as follows:

$$\delta m_{eff}(x) = \delta m(x) \phi^2(x), \tag{4.4}$$

where $\delta m(x)$ is the differential mass absorbed at position x along the length of the cantilever, and $\phi^2(x)$ is the normalized mode shape function.[43] $\delta m(x)$ is derived from the measured partition coefficient:

$$\delta m(x) = \frac{K_{eq} P M_W}{\rho R T} A(x) \partial x \tag{4.5}$$

Here P is the partial analyte vapor pressure delivered to the device (typically 0.02 x saturation vapor pressure) and $A(x)$ is the cross-sectional area of the polymer at length position x. To determine the effective mass Δm_{eff} added to a portion of the cantilever (e.g., the legs only or the head only), Equation 4.5 was integrated over the respective length. The mode shape function was determined by modeling the cantilever head and legs as connected elastic beam segments[44] and solving the resulting differential equations using a Mathematica script.

4.3 Results

4.3.1 SI-ATRP Polymer Films on Unmasked Nanocantilevers

SI-ATRP was used to grow films of PMMA (88 nm thick), PMA (110 nm thick), and PBMA (108 nm thick) on nanocantilever sensors, as shown in Figure 4.1. The thickness of the polymer brush films on the nanocantilevers was determined using scanning electron microscopy (SEM). Ellipsometry was also used to measure the thickness of PMMA and PBMA films grown on flat substrates (silicon wafer with a 30 nm gold film on top of a 10 nm chromium adhesion layer), but that technique was not used for PMA because of that film's greater surface roughness. The roughness of the PMA film was attributed to the grafting density of the polymer chains being lower than that of the PMMA and PBMA films. Previously, polymer film dimpling had been observed upon the drying and collapse of a brush with a low graft density due to the formation pinned micelles on

the surface, with each micelle being composed of a number of polymer chains.[45,46] PMMA is a glassy polymer (bulk Tg = 105 °C), while PMA (bulk Tg = 5 °C) and PBMA (bulk Tg = 15 °C) are rubbery at the operating temperature of the nanocantilever (approximately 30 °C).[47] Briefly, the polymer films were grown by first forming a self assembled monolayer (SAM) of Bis(2-[2'-bromoisobutyryloxy]ethyl)disulfide (BiBOEDS), an ATRP polymerization initiator, which spontaneously binds to the gold via the disulfide. The polymerization conditions were such that no sacrificial initiator (unbound initiator in the solution) was necessary to control the reaction, so polymerization only occurred on the gold, BiBOEDS-functionalized surface. The PMMA and PBMA were grown at room temperature for 10 h and 20 h, respectively, while the PMA film was grown at 50 °C for 48 h, as detailed in the Methods section. An elevated temperature was necessary for the reaction to proceed, but increasing the reaction temperature further was undesirable because the thiol bond is labile above 60 °C, which can result in chain termination due to thiol desorption.[48] Dropcast polymer films of PMMA, PMA, and PBMA were also applied to nanocantilevers for comparison to the corresponding SI-ATRP polymer films.

The self-sensing piezoresistive nanocantilevers used in this study were 2.5 μm long bilayer structures of silicon nitride (100 nm thick) with the top layer comprising a 30 nm gold film, over a 10 nm chromium adhesion layer. The gold was used as an etch mask in fabrication and then for the actuation of vibration and the readout of the frequency during sensor operation.[22] Bare nanocantilevers had an average resonance quality factor (Q) of 120 in ambient conditions, which remained unchanged within the standard deviation of the initial Q when coated with a 2-10 nm dropcast polymer film, with 10 nm being approximately the maximum film thickness possible for a dropcast film. Figure 4.2 shows that nanocantilevers coated with an SI-ATRP grown PMMA film (SI-PMMA) had an average Q of 100, while nanocantilevers with an SI-ATRP grown PMA film (SI-PMA) had an average Q of 90, and nanocantilevers coated with an SI-ATRP grown PBMA film

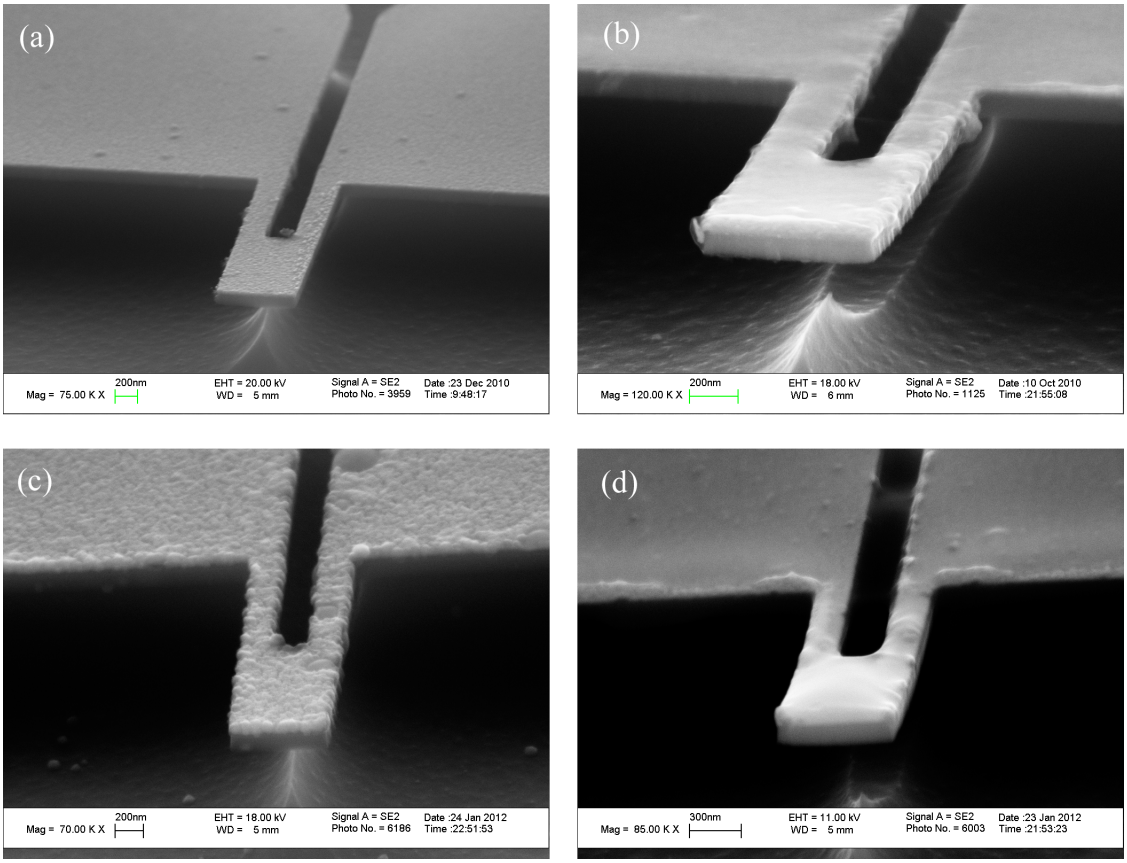

Figure 4.1: SEM images of unmasked nanocantilevers: as fabricated (a), coated with 88 nm SI-PMMA (b), coated with 110 nm SI-PMA (c), and coated with 108 nm SI-PBMA (d).

(SI-PBMA) had an average Q of 50. Three to eight cantilevers with each coating were used to calculate the average Q, and the error bars indicate the standard deviation of the average Q values.

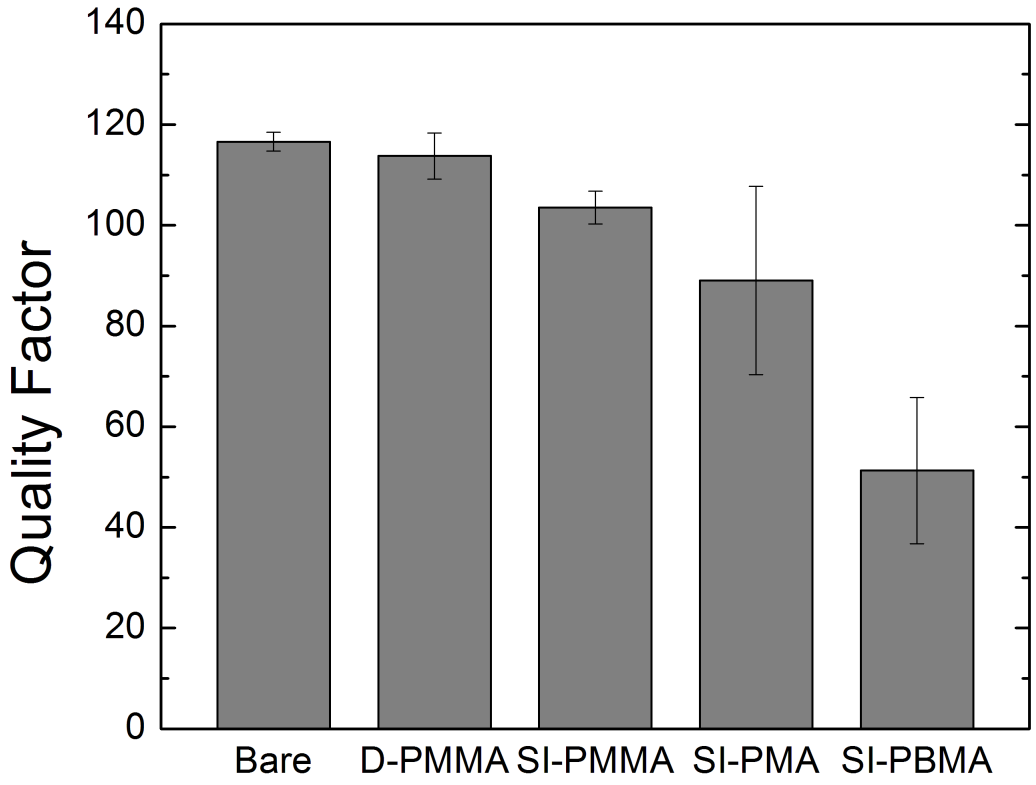

Figure 4.2: The resonance quality factor changes little upon coating nanocantilevers with D-PMMA and SI-PMMA films, but decreases when the nanocantilevers are coated with rubbery SI-PMA and SI-PBMA films.

4.3.2 Response of Unmasked Nanocantilever to Chemical Vapors

Nanocantilever sensors were exposed to 400 s pulses of a series of chemical vapors at 0.02 P/P° (where P is the partial pressure and P^o the saturated vapor pressure) in a background of laboratory air (1.10 ± 0.15 ppth water vapor). The chemical vapors were selected to include non-polar, polar, aromatic, and halogenated compounds. The resonant frequencies of nanocantilevers were tracked

using a phase-locked loop (PLL), enabling the real-time measurement of frequency shifts due to the sorption of chemical vapors.[22] Bare nanocantilevers and nanocantilevers coated with dropcast films of PMMA, PMA, and PBMA were tested along with nanocantilevers coated with SI-PMMA, SI-PMA, and SI-PBMA, as shown in Figure 4.3. The responses of nanocantilevers coated with dropcast PMA and PBMA are not shown for clarity, but they were on the same order of magnitude of the responses of nanocantilevers with the dropcast PMMA (D-PMMA) film. All nanocantilevers coated with SI-ATRP grown polymer films exhibited responses to all of the chemical vapors. Nanocantilevers coated with the glassy SI-PMMA exhibited positive shifts in resonance frequency when exposed to polar vapors, as previously described(see Chapter 3), while the nanocantilevers coated with SI-PMA and SI-PBMA exhibited negative frequency shifts upon exposure to all chemical vapors.

The response time of nanocantilevers coated with SI-ATRP grown polymer films was determined as the time necessary for the sensor to reach 90% of its equilibrium response upon exposure to 0.02P/P° of each tested vapor. Sensors coated with SI-PMA and SI-PBMA responded to all vapors within 50 s, while SI-PMMA coated nanocantilevers responded within 50 s for non-polar vapors, but required up to 1700 – 2600 s to reach 90% of equilibrium when exposed to polar vapors (Figure 4.4). The linearity of the sensor responses with respect to the concentration of toluene, isopropanol, and ethyl acetate was also tested in the range of 0.005 – 0.08 P/P°. Unlike SI-PMMA(see Chapter 3), nanocantilevers coated with both SI-PMA and SI-PBMA responded linearly to 400 s pulses of each chemical vapor, as shown in Figure 4.5. Nanocantilevers coated with SI- PMA and SI-PBMA also responded linearly to chloroform vapor, which induced the largest responses of any the vapor set.

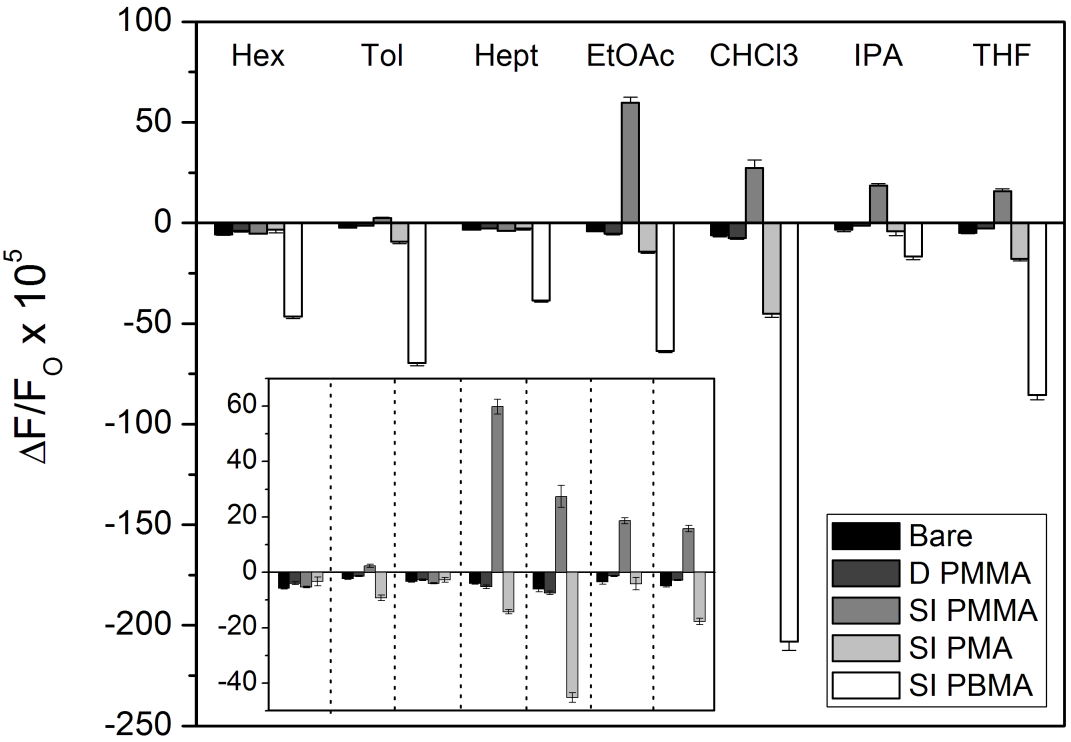

Figure 4.3: Responses of unmasked nanocantilevers to 400 s pulses of a series of chemical vapors at a concentration of 0.02 P/P°. Nanocantilevers coated with glassy SI-PMMA responded positively to polar vapors, while nanocantilevers coated with rubbery SI-PMA and SI-PBMA responded negatively to all vapors.

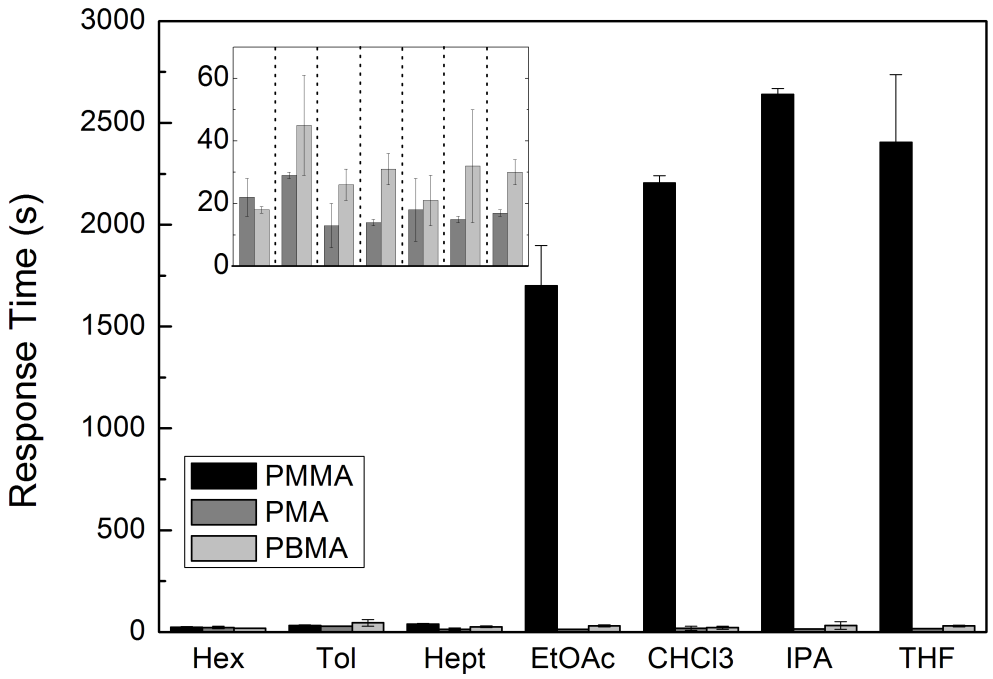

Figure 4.4: Nanocantilevers coated with rubbery SI-PMA and SI-PBMA responded to all vapors within 50 s, while nanocantilevers coated with glassy SI-PMMA required long exposures to reach equilibrium with polar vapors.

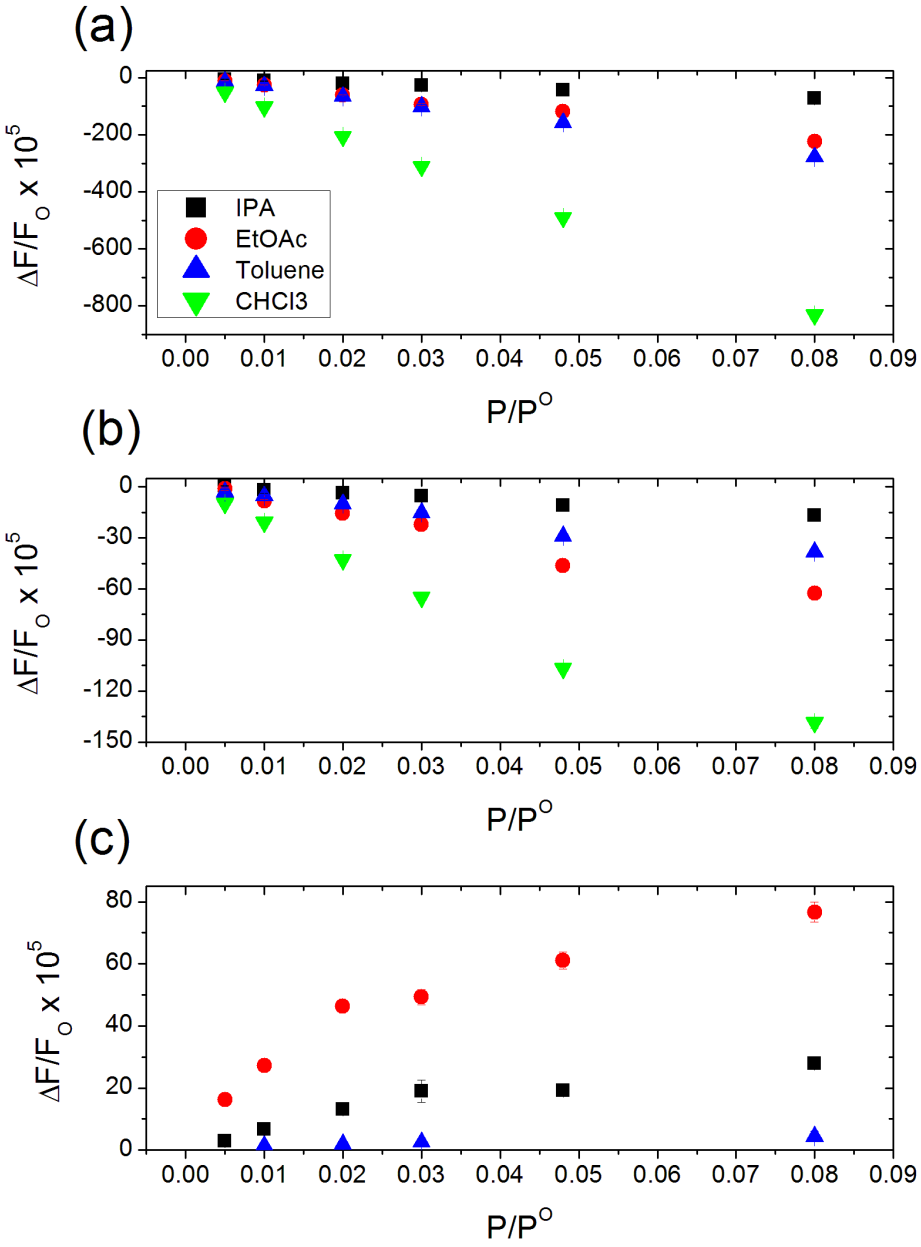

Figure 4.5: Linearity of sensor responses with respect to vapor concentration for unmasked nanocantilever coated with SI-PBMA (a), SI-PMA (b), and SI-PMMA (c).

4.3.3 Modeling of the Frequency Shift Caused by Mass Loading

To model the NEMS frequency shifts due to analyte mass loading, it was assumed that the polymer uniformly coats the top surface of the NEMS, with the additional mass absorbed into the polymer calculated according to the partition coefficient of each polymer/vapor pair. Partition coefficients were derived from the frequency shifts of quartz crystal microbalances (QCMs) coated with SI-ATRP grown polymer films. The resulting mass-induced frequency shifts were calculated using an analytical elastic continuum model for the polymer-coated cantilever; further details appear in the Methods section. The calculated relative frequency shifts ($\Delta f / f_0$) due to mass loading for a nanocantilever coated with 100 nm SI-PMMA ranged from -0.47 to -3.8 x 10^{-5} for hexane and chloroform, respectively, for SI-PMA -0.06 to -0.20 x 10^{-5} for heptane and chloroform, respectively, and for SI-PBMA -0.06 to -0.89 x 10^{-5} for heptane and chloroform, respectively. The comparison of calculated and experimental relative frequency shifts is presented in Table 4.1. The K_{eq} values for SI-PMMA, SI-PMA, and SI-PBMA are reported in Table 4.2

4.3.4 Chromium-Masked Nanocantilevers

Nanocantilevers with an additional masking layer of chromium on top of the gold surface were fabricated to study the effects of localizing SI-ATRP polymer films to sections of the nanocantilever structure. The chromium mask was applied to the nanocantilever tip (Cr-tip), legs and base (Cr-legs), or only base (Cr-base) via an additional electron-beam lithography step conducted prior to the nanocantilever release etch step. Additionally, prior to formation of the polymerization Bi-BOEDS SAM, the chromium was passivated with a SAM of n-hexylphosphonic acid. Without this treatment, significant polymer film growth ($>$10 nm) was measured on flat chromium surfaces via ellipsometry, and was visible in SEM images of chromium-masked cantilevers. Chromium passivation was tested by comparing the ratio of the thickness of an SI-PMMA brush film grown on

Table 4.1: Comparison of experimentally measured frequency shifts and calculated frequency shifts due to mass-loading for unmasked nanocantilever sensors.

Responses of Nanocantilevers: $\Delta f/f_0$ **x** 10^5		
	SI-PMMA	
Vapor	**Experimental**	**Calculated**
Hexane	-5.30 $\pm$ 0.26	-0.47
Toluene	2.37 $\pm$ 0.54	-1.07
Heptane	-3.96 $\pm$ 0.21	-0.28
Ethyl acetate	59.80 $\pm$ 2.65	-0.61
Chloroform	27.40 $\pm$ 3.95	-3.80
Isopropanol	18.60 $\pm$ 1.03	-0.23
Tetrahydrofuram	15.80 $\pm$ 1.13	-0.78
	SI-PMA	
Vapor	**Experimental**	**Calculated**
Hexane	- 3.32 $\pm$ 1.59	-0.13
Toluene	-9.21 $\pm$ 0.99	-0.14
Heptane	-2.72 $\pm$ 0.85	-0.06
Ethyl acetate	-14.22 $\pm$ 0.78	-0.16
Chloroform	-45.14 $\pm$ 1.72	-0.20
Isopropanol	-4.10 $\pm$ 2.28	-0.06
Tetrahydrofuram	-17.75 $\pm$ 1.13	-0.13
	SI-PBMA	
Vapor	**Experimental**	**Calculated**
Hexane	-46.45 $\pm$ 1.08	-0.13
Toluene	-69.67 $\pm$ 1.31	-0.20
Heptane	-38.55 $\pm$ 0.86	-0.07
Ethyl acetate	-63.57 $\pm$ 0.75	-0.43
Chloroform	-208.12 $\pm$ 4.40	-0.89
Isopropanol	-16.55 $\pm$ 1.59	-0.18
Tetrahydrofuram	-85.40 $\pm$ 2.56	-0.24

Table 4.2: Partition coefficients for dropcast and SI-ATRP grown polymer films.

Partition Coefficients (K_{eq})		
	PMMA	
Vapor	**Bulk PMMA**	**SI-PMMA**
Hexane	105	40
Toluene	525	375
Heptane	308	90
Ethyl acetate	108	280
Chloroform	46	200
Isopropanol	1037	350
Tetrahydrofuram	57	115
	PMA	
Vapor	**Bulk PMA**	**SI-PMA**
Hexane	56	41
Toluene	220	256
Heptane	160	76
Ethyl acetate	47	102
Chloroform	19	44
Isopropanol	593	106
Tetrahydrofuram	21	57
	PBMA	
Vapor	**Bulk PBMA**	**SI-PBMA**
Hexane	165	145
Toluene	2047	2014
Heptane	362	384
Ethyl acetate	438	399
Chloroform	875	853
Isopropanol	400	446
Tetrahydrofuram	402	376

flat gold and passivated-chromium substrates. All substrate-pairs for comparison studies underwent identical SAM formation steps, and were exposed to polymerization conditions together in the same reaction vial to minimize any differences in processing. The ratio of the thickness of the SI-PMMA films on gold and passivated-chromium substrates was measured as 20:1 by ellipsometry. When the n-hexylphosphonic acid SAM was formed prior to conducting SI-ATRP on chromium-masked nanocantilevers, no polymer was visible on the chromium-masked regions of the nanocantilevers while smooth, translucent polymer films had grown on the exposed gold, as shown in Figure 4.6. A similar high specificity of film growth was also observed for SI-PBMA (Figure 4.7), but SI-PMA was unable to be sufficiently localized to the gold for use in this study (Figure 4.8). The SI-PMMA films on the chromium-masked nanocantilevers was 74 nm thick, with the SI-PBMA films were 63 nm thick. Upon coating the chromium-masked nanocantilevers with SI-ATRP polymer films, the average shift in resonance frequency was within the standard deviation of the average resonance frequency of the uncoated nanocantilevers, though there was a slight increase in the average resonance frequency of the Cr-tip and Cr-base sensors (polymer grown on the clamped end), and a slight decrease in the resonance frequency of the Cr-legs sensors (polymer grown on the free end), as shown in Figure 4.9.

Chromium-masked nanocantilevers with SI-PMMA (Figure 4.10, Table 4.3) and SI-PBMA (Figure 4.11, Table 4.4), and SI-PMA (Figure 4.12) films were exposed to 400 s pulses of a series of chemical vapors at 0.02 P/P°, with the sensor responses of single, representative cantilevers. At least three nanocantilevers of each chromium-masking geometry and polymer coating were tested, and the representative chromium-masked sensors were from a single fabrication and polymerization batch to minimize processing differences. Chromium-masked nanocantilevers without polymer films responded to the chemical vapors similarly to bare, unmasked nanocantilevers. Of the chromium-masked nanocantilevers with an SI-PMMA film, the Cr-tip sensors responded more

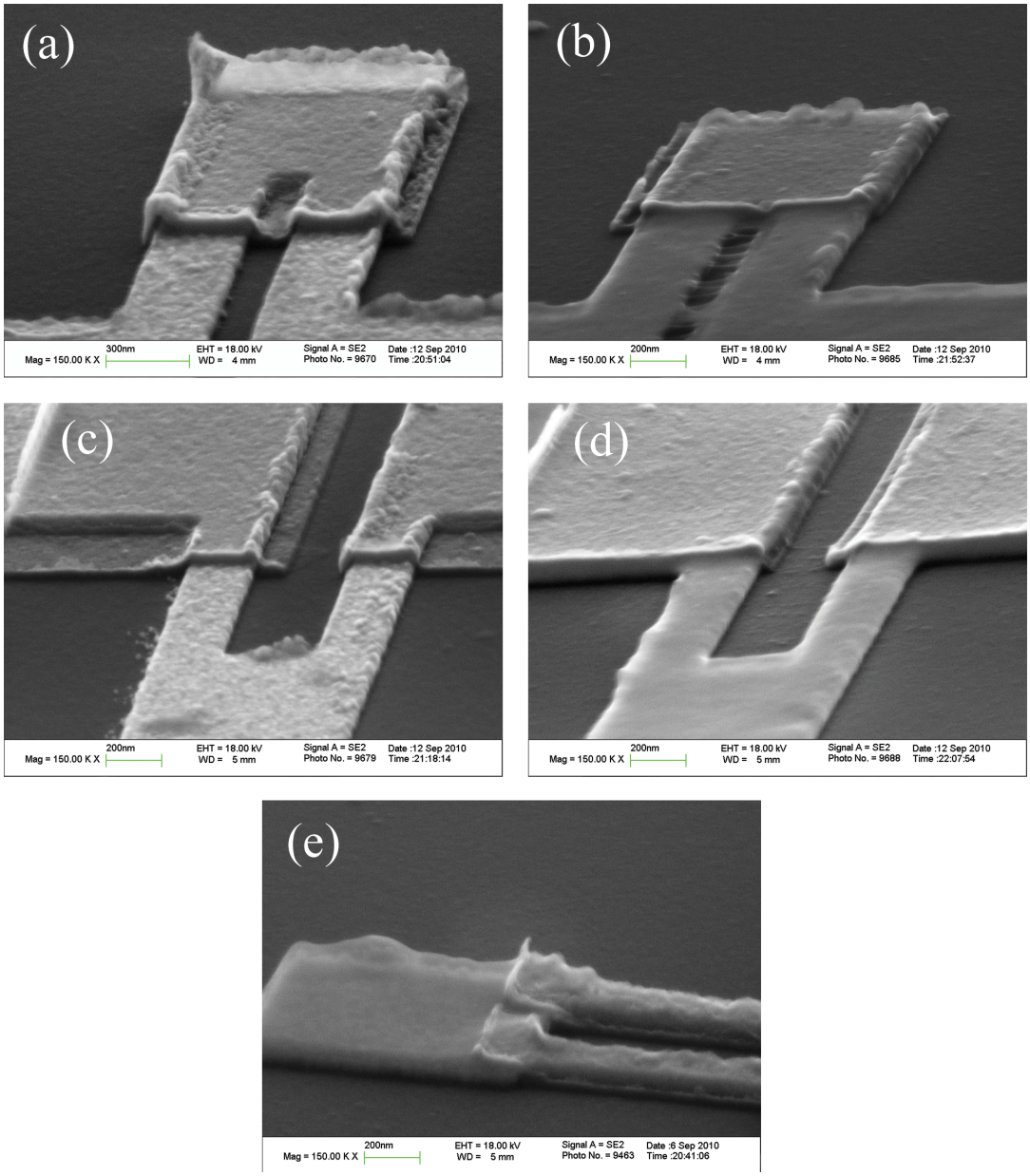

Figure 4.6: SEM images of unsuspended chromium-masked nanocantilevers before and after selectively coating the exposed gold with SI-PMMA: Cr-tip before (a) after (b) polymerization, Cr-base before (c) and after (d) polymerization, and Cr-legs after (e) polymerization, where the smooth translucent PMMA film is visible on the exposed gold, while the chromium-masked legs remain bare.

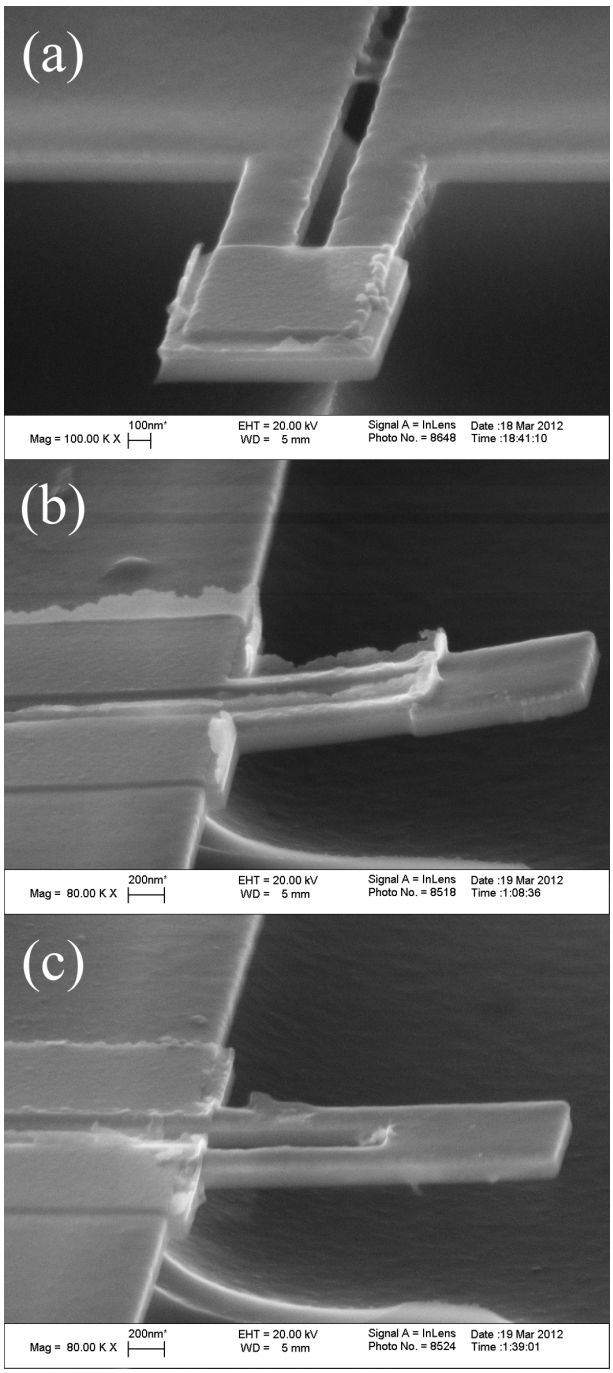

Figure 4.7: SEM images of chromium-masked nanocantilevers with localized films of SI-PBMA on the exposed gold regions: Cr-tip (a), Cr-legs (b), and Cr-base (c).

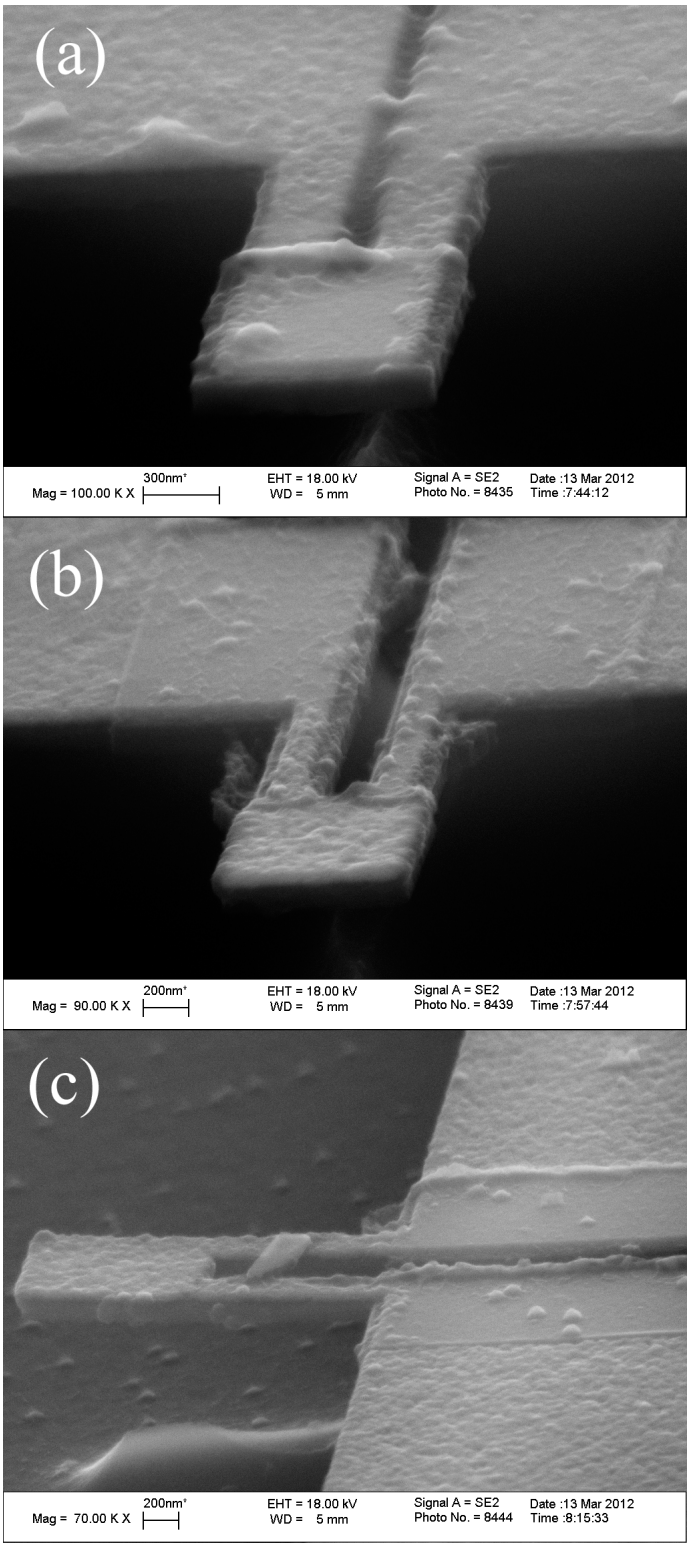

Figure 4.8: SEM images of chromium-masked nanocantilevers with poorly localized films of SI-PMA on the exposed gold regions: Cr-tip (a), Cr-legs (b), and Cr-base (c).

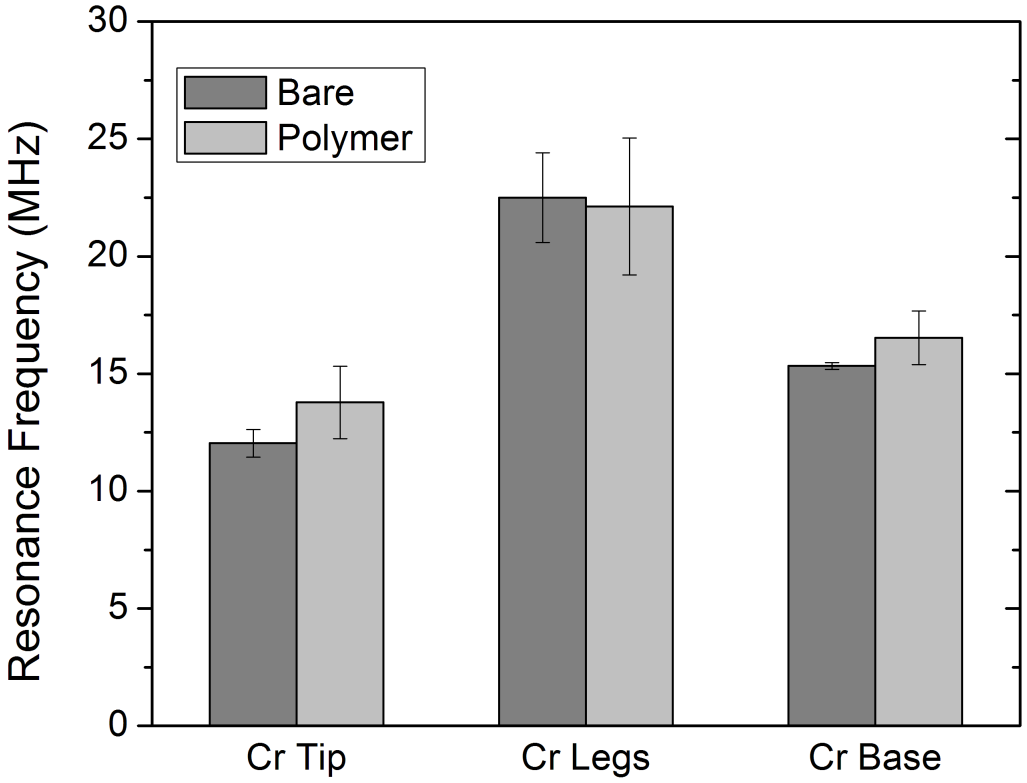

Figure 4.9: Average change in resonance frequency upon coating chromium-masked cantilevers with SI-ATRP grown polymer films.

strongly than the Cr-legs and the Cr-base sensors. Of the Cr-masked nanocantilevers with an SI-PBMA, the responses of the Cr-legs sensor were weaker than the Cr-tip and Cr-base sensors. The linearity of sensor response for chromium-masked SI-PMMA and SI-PBMA coated nanocantilevers are shown in Figures 4.13 and 4.14, respectively.

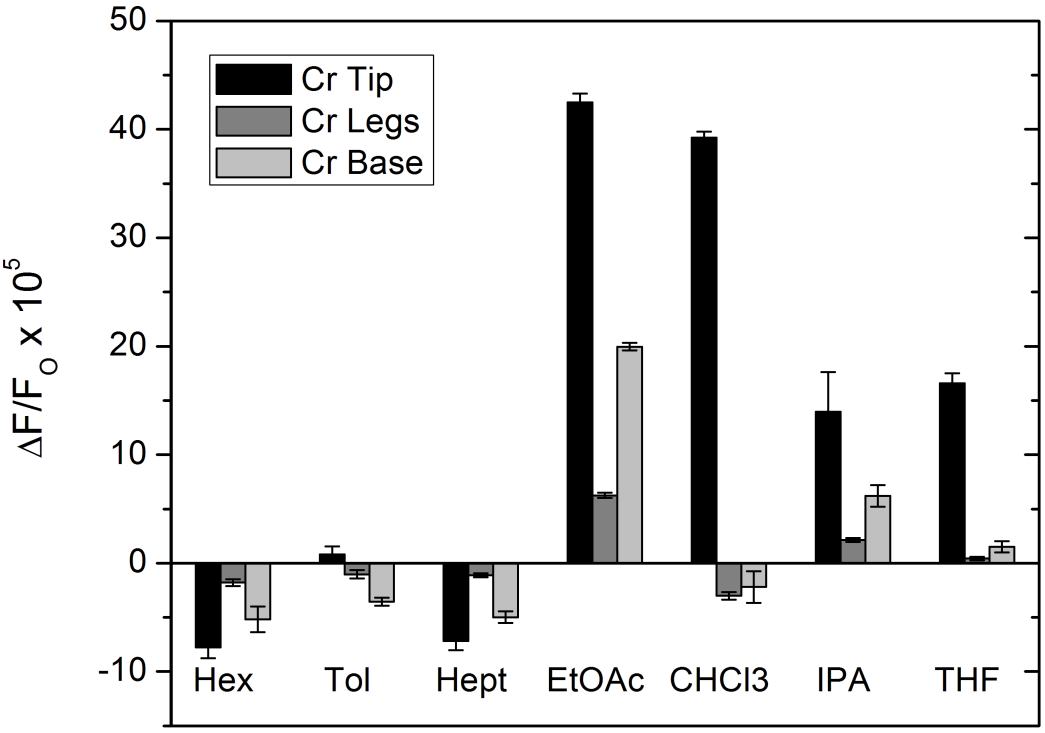

Figure 4.10: Responses of chromium-masked nanocantilevers coated with localized films of glassy SI-PMMA to a series of chemical vapors presented at 0.02 P/P°. Cr-tip nanocantilevers showed the greatest responses and Cr-legs nanocantilevers showed the smallest responses, indicating that mass-loading does not dominate the response.

Table 4.3: Relative frequency shifts of chromium-masked nanocantilevers coated with localized SI-PMMA films exposed to vapors at 0.02 P/P°.

Responses of Nanocantilevers ($\Delta f/f_0$ **x** 10^5)			
Vapor	**Cr-Tip**	**Cr-Legs**	**Cr-Base**
Hexane	-7.78 $\pm$ 0.99	-1.79 $\pm$ 0.31	-5.19 $\pm$ 1.18
Toluene	0.82 $\pm$ 0.72	-1.03 $\pm$ 0.39	-3.57 $\pm$ 0.37
Heptane	-7.17 $\pm$ 0.87	-1.11 $\pm$ 0.193	-4.99 $\pm$ 0.53
Ethyl acetate	42.50 $\pm$ 0.79	6.25 $\pm$ 0.25	19.96 $\pm$ 0.35
Chloroform	39.25 $\pm$ 0.54	-3.02 $\pm$ 0.36	-2.20 $\pm$ 1.47
Isopropanol	13.96 $\pm$ 3.67	2.13 $\pm$ 0.18	6.19 $\pm$ 1.00
Tetrahydrofuram	16.58 $\pm$ 0.94	0.42 $\pm$ 0.17	1.52 $\pm$ 0.52

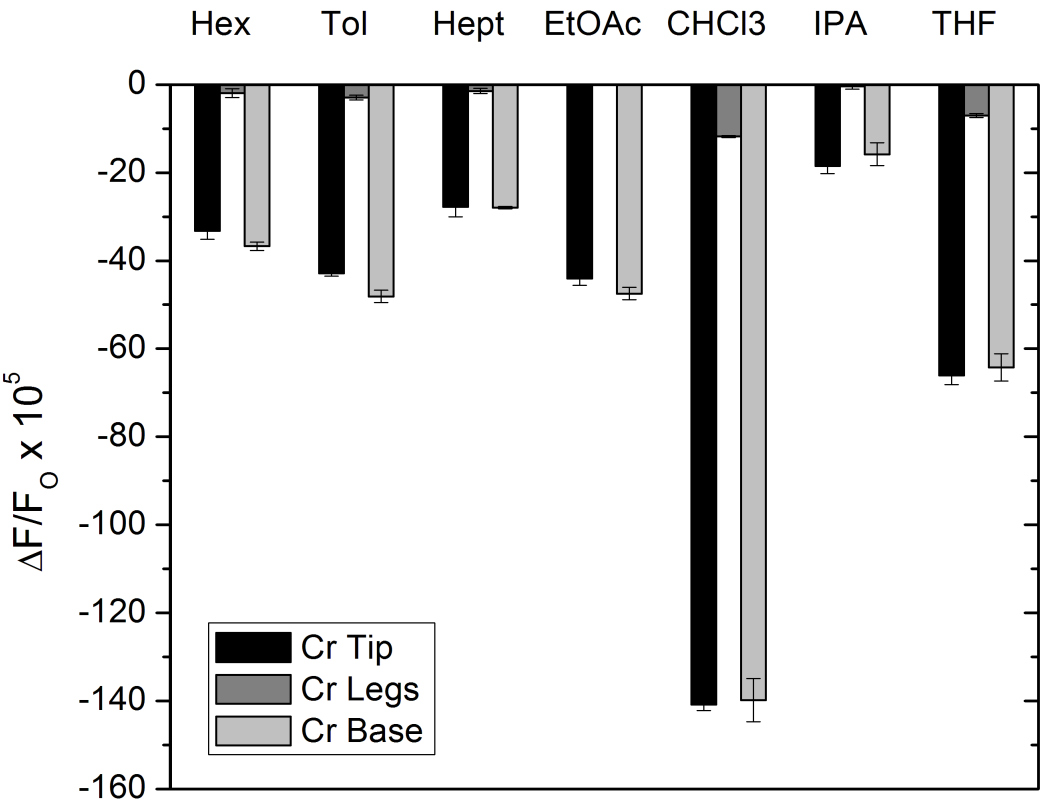

Figure 4.11: Responses of chromium-masked nanocantilevers coated with localized films of rubbery SI-PBMA to a series of chemical vapors presented at 0.02 P/P°. Cr-tip nanocantilevers exhibit much smaller responses than Cr-legs and Cr-base nanocantilevers, indicating that vapor sorption on the clamped end is essential for strong responses.

Table 4.4: Relative frequency shifts of chromium-masked nanocantilevers coated with localized SI-PBMA films exposed to vapors at 0.02 P/P°.

Responses of Nanocantilevers ($\Delta f / f_0$ ***x*** 10^5***)***			
Vapor	**Cr-Tip**	**Cr-Legs**	**Cr-Base**
Hexane	-33.24 ± 1.88	-1.93 ± 1.00	-36.72 ± 0.94
Toluene	-42.90 ± 0.58	-2.95 ± 0.51	-48.11 ± 1.38
Heptane	-27.81 ± 2.26	-1.46 ± 0.58	-27.95 ± 0.27
Ethyl acetate	-44.09 ± 1.52	0.27 ± 0.56	-47.46 ± 1.40
Chloroform	-140.80 ± 1.36	-11.80 ± 0.19	-139.87 ± 4.92
Isopropanol	-18.49 ± 1.77	-0.39 ± 0.66	-15.81 ± 2.57
Tetrahydrofuram	-66.07 ± 2.07	-7.06 ± 0.46	-64.24 ± 3.10

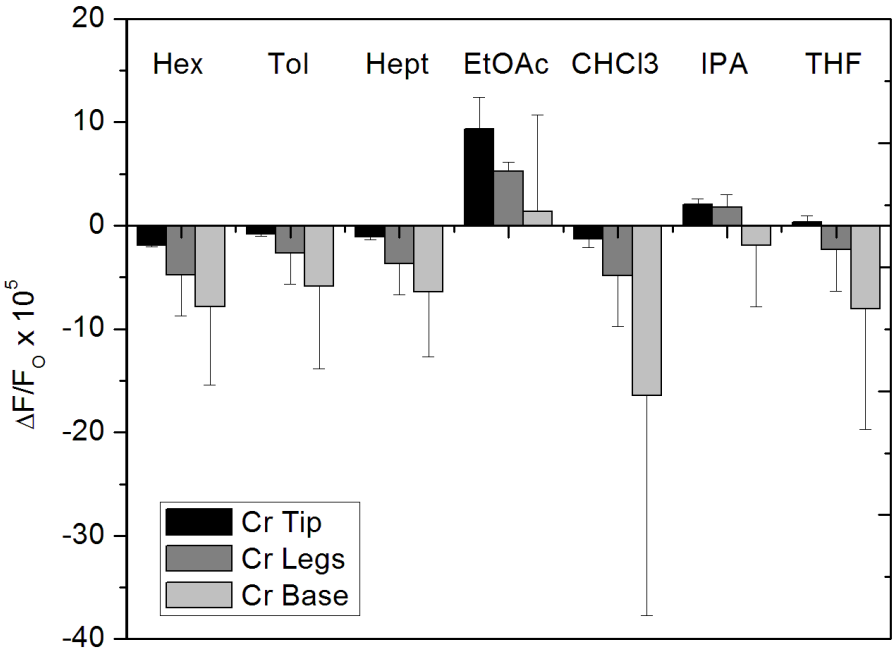

Figure 4.12: Responses of chromium-masked nanocantilevers coated with localized films of rubbery SI-PBMA to a series of chemical vapors presented at 0.02 P/P°. PMA localization was insufficient, and no discernible trend in response was observed.

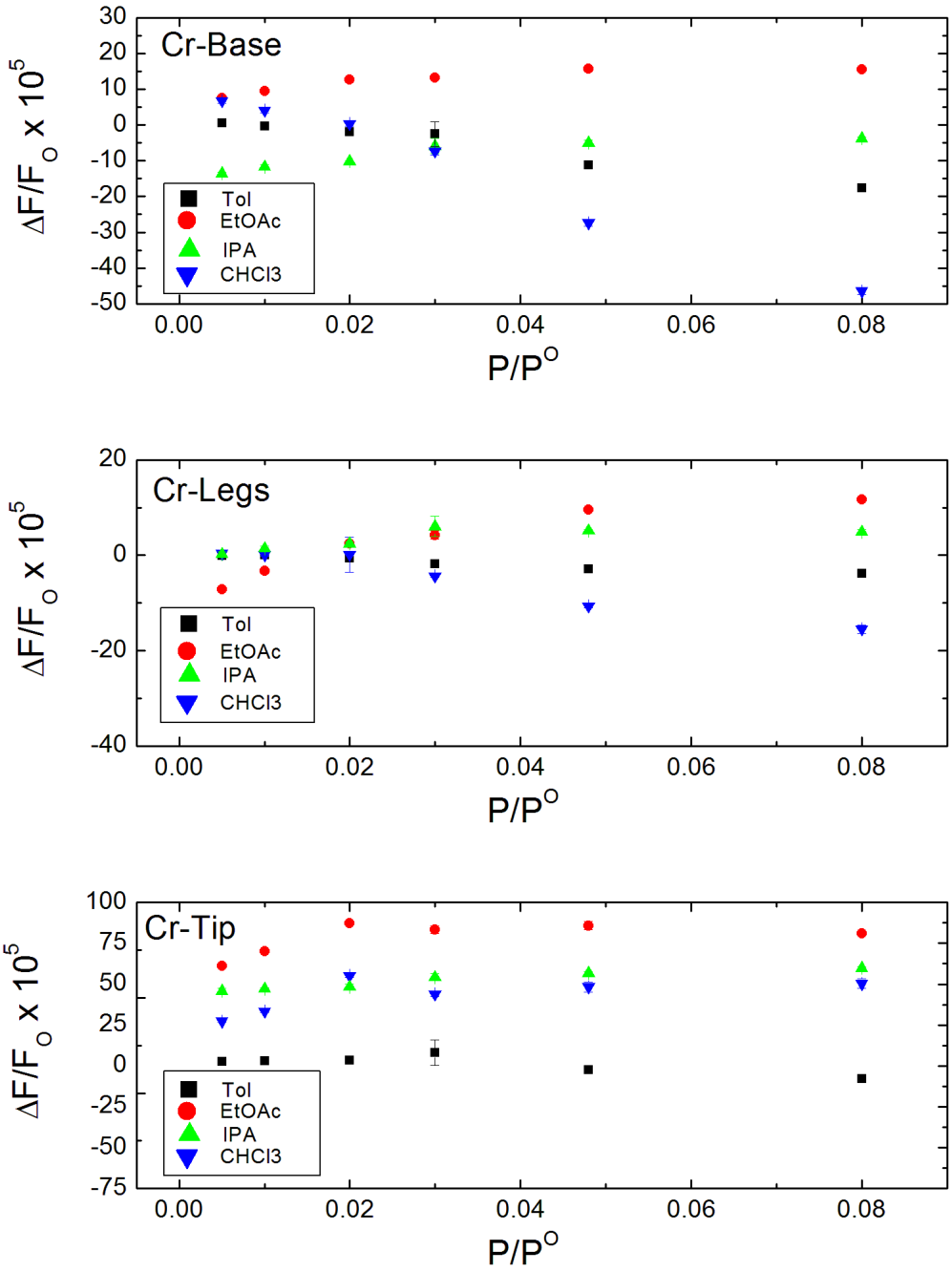

Figure 4.13: Linearity of sensor responses with respect to vapor concentration for chromium-masked nanocantilevers coated with localized SI-PMMA films.

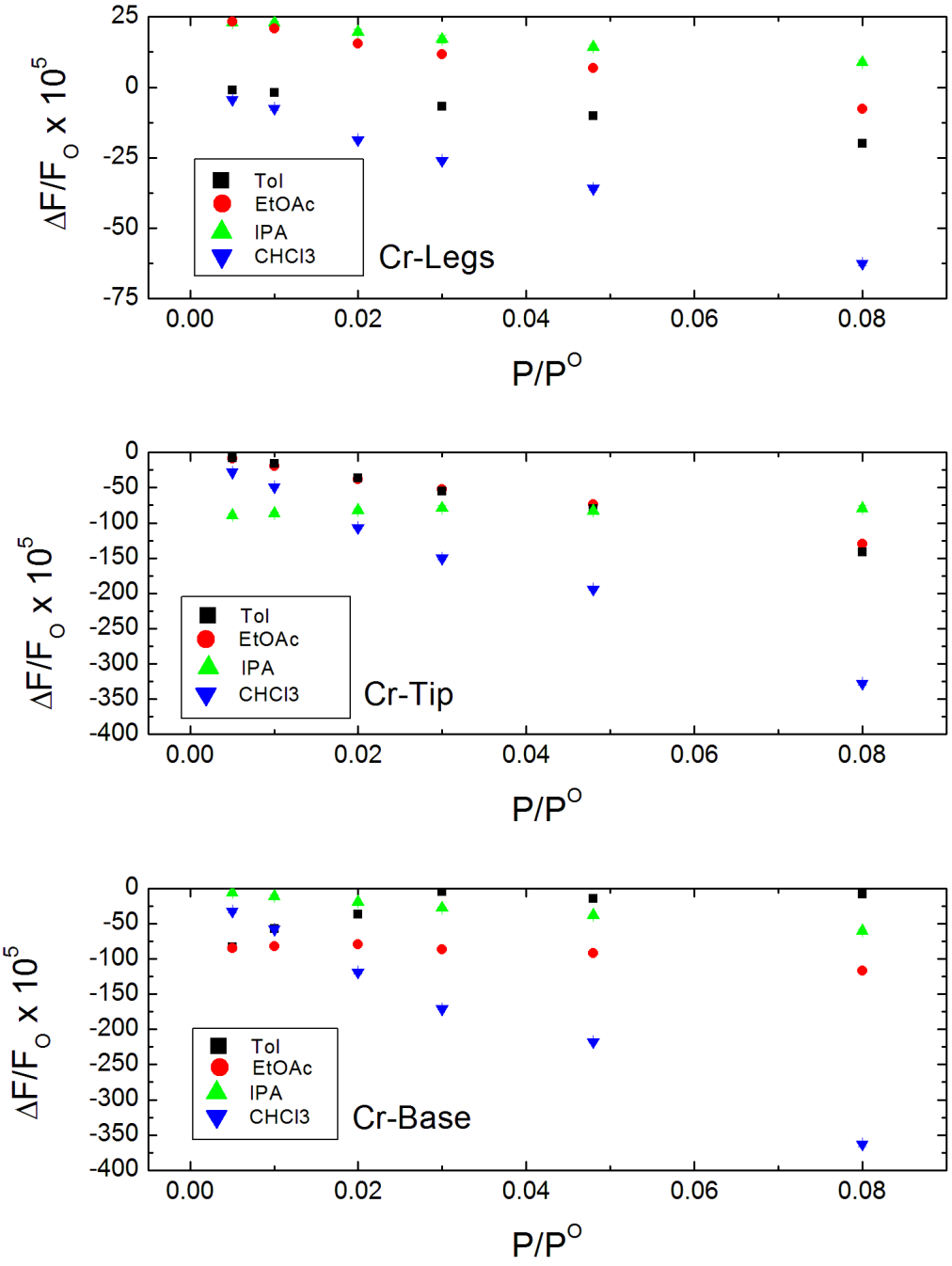

Figure 4.14: Linearity of sensor responses with respect to vapor concentration for chromium-masked nanocantilevers coated with localized SI-PBMA films.

4.4 Discussion

4.4.1 The Contribution of Stiffness to the Experimental Resonant Frequency Shifts

The calculated frequency shifts due to mass-loading were one to two orders of magnitude smaller than the frequency shifts observed during vapor exposure experiments, indicating that another mechanism must be responsible for the remainder of sensor responses. Additionally, because mass-loading decreases the resonance frequency, the positive shifts in resonance frequency observed for SI-PMMA coated sensors must be due to a different response mechanism. The resonant frequency of a nanocantilever is a function of the mass and stiffness, where the change in relative frequency can be described by,

$$\frac{\Delta f}{f_0} = \frac{\partial k}{2k} - \frac{\partial m_{eff}}{2m_{eff}} \tag{4.6}$$

where Δf is the change in frequency, f_0 is the fundamental resonance frequency, k is the spring constant, δk is the change in spring constant, m_{eff} is the NEMS effective mass, and δm_{eff} is the change in effective mass.[27] Since mass-loading cannot account for the experimentally observed frequency shifts, the vapor sorption into the polymer films must be changing the spring constant of the nanocantilever, either stiffening the sensor, as with SI- PMMA coated nanocantilevers, or softening the sensor, as with SI-PMA and SI-PBMA coated nanocantilevers. Previously, the frequency shifts of micro- and nanocantilever sensors, which could not be explained by mass loading, have been attributed to changes in sensor stiffness, as detailed in the introduction, though further study is required to develop a complete understanding of underlying causes of these changes in spring constant.

These results are a reminder that caution must be employed whenever mass-loading occurring on a micro- or nanoresonator is calculated directly from measured frequency shift. Changes in

spring constant should be taken into account when one or more continuous monolayers of vapor molecules are adsorbed on the sensor surface (as occurs with the bare nanocantilevers), or when the nanocantilever is coated with a continuous polymer film.[49]

4.4.2 Effect of Polymer Glass Transition Temperature on Sensor Behavior

The glass transition temperature (T_g) of a polymer denotes the temperature at which the material undergoes a phase change from a glassy state to a rubbery state. Below the T_g, the polymer is in a glassy state in which the polymer chains are locked into a single configuration, unable to easily move past each other, leading to a stiff material with a slow diffusion constant. Conversely, the rubbery state is characterized by significantly increased chain mobility, a softer bulk material, and an increased diffusion coefficient for vapor molecules. The polymers PMMA and PMA were chosen for this comparison study because of they represented chemically similar, but physically different sorptive materials, with PMMA being glassy and PMA being rubbery at $30\,^{\circ}\mathrm{C}$. The only chemical difference between PMA and PMMA is that PMMA has a single extra methyl group per monomer, which prevents the PMMA polymer chains from easily slipping past each other and is responsible for PMMA's greater T_g. A second rubbery polymer, PBMA, was included in these experiments because it was determined that PMA was a poor candidate for localized polymerization procedure. PBMA has a greater affinity toward non-polar analytes than PMMA or PMA due to the n-butyl group in each monomeric unit of the polymer.

When chemical vapors absorb into the polymer films, changes occur in film properties such as thickness and Young's modulus, both of which are affected by polymer chain orientation. Comparing the responses of the SI-ATRP PMMA and SI-ATRP PMA coated nanocantilevers to chemical vapors, the effect of the penetrant vapor molecules on sensor response is dependent on whether the polymer brush is glassy or rubbery. For a glassy polymer, the configuration of the chains in the

polymer brush is locked, so a small number of penetrant molecules may cause the film to stiffen like a swollen gel. In contrast, the individual chains of the rubbery polymers are able to slide past each other, allowing the chains to accommodate the penetrant molecules, which may be plasticizing the film. Given the high Young's modulus of silicon nitride of ($\sim$110 GPa) versus those of the polymers (measured by atomic force microscopy (AFM) nanoindentation as 8 GPa for a 150 nm dry PMMA brush[50] and 50-60 MPa for 50 nm dry PMA brush[45]), changes in polymer film stiffness due to vapor absorption were initially not expected to impact the stiffness of the cantilever. Further work, such as nanoindentation of polymer brush films during exposure to chemical vapors, is required to elucidate any changes occurring in Young's modulus.

While nanocantilevers coated with rubbery S-PMA and SI-PBMA films had lower Q values than cantilevers coated with dropcast PMMA and SI-PMMA films, this reduction in Q did not negatively impact the sensor responses to chemical vapors at the concentrations tested. For applications requiring trace detection, the choice of polymer film thickness must be balanced to maximize vapor capture while retaining a sufficient Q to measure small shifts in resonance frequency in order to optimize the minimum detectable level (MDL).

Nanocantilevers coated with rubbery polymer films of SI-PMA and SI-PBMA responded quickly to chemical vapors because the diffusion of vapor molecules in rubbery polymers is Fickian, as the relative mobility of the penetrant molecules is slower than the polymer chain mobility.[51] Unlike rubbery polymers, glassy polymers such as PMMA are known to exhibit non-Fickian diffusion characterized by a delayed relaxation of the polymer chains (two stage sorption), which can greatly increase the time required for the film to reach a new equilibrium state.[52,53,54,55] Due to the slow chain relaxation, glassy polymers can also exhibit history effects, such that the order of chemical vapor exposures can impact the shape and magnitude of an individual response. Given that sensor response magnitude of cantilevers coated with glassy and rubbery polymer films is similar, rubbery

polymer films are preferred due to their faster response time.

4.4.3 Localization of Polymer Films on Nanocantilever Sensors

This work demonstrates a method for highly selective deposition of localized polymer films on nanostructures post-fabrication, protecting the polymer from potentially damaging processing steps such as plasma etches. High quality polymer films are essential for vapor detection, especially for the discrimination between vapors where an array of sensors coated with a variety of chemically distinct polymer films is employed,[56] and also to study the response mechanisms behind the observed frequency shifts. The localization of the polymer film directs the absorption of chemical vapors to the sensor, or the most sensitive part of the sensor, rather than allowing a portion of the vapor molecules to be lost by absorption on non-sensitive areas, which would be detrimental for a trace detection application. This bottom up technique is amenable to wafer-scale production and adaptation to other surface initiated polymerization techniques.[29] While PMMA and PBMA were successfully localized to the gold regions of the nanocantilever, the PMA brush grew on the chromium mask as well. It is believed the failure of the chromium passivation was due to desorption of the n-hexylphosphonic acid SAM during the 48 hr, $50\,^{\circ}\mathrm{C}$ PMA polymerization reaction. Chromium was chosen for the masking layer because of its adherence to gold and its resistance to the plasma etch used to release the nanocantilevers from the substrate. A number of passivation SAMs were tested including multiple silanes, carboxylic acids, and phosphonic acids, with n-hexyl phosphonic acid exhibiting superior performance compared to all other SAMs tested. Phosphonic acid SAMs have been studied previously on titania[57] and alumina,[58] and it has also been shown that alkane thiols and alkane carboxylic acid SAMs can be formed simultaneously on adjacent gold and alumina surfaces.[59] By first protecting the chromium regions with the n-hexyl phosphonic acid SAM, subsequent exposure to BiBOEDS resulted in the initiator self assembling only on the bare

gold surface.

The responses of nanocantilevers coated with localized polymer films indicate that vapor sorption on the legs and base of the sensors is the primary source of the observed frequency shifts. For chromium masked nanocantilevers coated with SI-ATRP PMMA, the Cr-tip sensors responded more strongly to chemical vapors than the Cr-legs or Cr-base sensors. Additionally, of the chromium masked nanocantilevers coated with SI-ATRP PBMA, the Cr-legs sensors produced weak responses to chemical vapors compared to the Cr-tip and Cr-base sensors. Modeling of the shape of the nanocantilever's fundamental resonance mode showed that mass-loading from vapor absorption on the sensor's legs had only a weak effect on resonant frequency; a hundred times smaller than mass loading on the tip. Conversely, changes in sensor stiffness have the greatest effect on resonant frequency if they occur near the clamped end of the nanocantilever where the majority of the bending occurs.

4.5 Conclusions

Resonant nanocantilevers have a number of desirable qualities necessary for incorporation into highly miniaturized chemical vapor detection systems, including their small size, extreme sensitivity, and adaptability to various chemical targets. There has been a need for a method to deposit thick, uniform polymer films on nanocantilevers to both enhance vapor sorption and to develop a thorough understanding of the mechanisms behind the observed sensor responses. The challenge of depositing high-quality polymer films was overcome using SI-ATRP, and was demonstrated by growing approximately 100 nm thick films of PMMA, PMA, and PBMA on nanocantilevers. Nanocantilevers were exposed to a series of seven non-polar and polar chemical vapors to test their response speed and magnitude. While nanocantilevers coated with the glassy SI-PMMA film exhibited positive shifts in resonant frequency upon exposure to polar vapors, sensors coated with the rubbery

SI-PMA and SI-PBMA films exhibited negative shifts in resonance frequency for both non-polar and polar vapors. The responses of nanocantilevers coated with all SI-ATRP grown polymer films were one to two orders of magnitude larger than expected by mass loading alone, and were attributed to the stiffening or softening of the polymer films. Nanocantilevers coated with SI-PMA and SI-PBMA responded to all vapors within 50 s, but nanocantilevers coated with SI-PMMA required up to 2600 s to respond to polar vapors. Additionally, the bottom-up nature of SI-ATRP enabled the localization of polymer films to chosen sections of each nanocantilever by using a chromium mask, passivated with a n-hexylphosphonic acid SAM, which restricted the self assembly of the BiBOEDS polymerization initiator to the uncovered gold surface. Nanocantilevers were fabricated with three different mask geometries, Cr-tip, Cr-legs, and Cr-base, to determine what area of the sensor was the most sensitive to vapor sorption. Localization of the polymer film was achieved for SI-PMMA and SI-PBMA, but not for SI-PMA due to the elevated temperature and long polymerization time required to grow a sufficiently thick film. Cr-legs nanocantilevers with both SI-PMMA and SI-PBMA films exhibited reduced responses to chemical vapors compared to Cr-tip and Cr-base nanocantilevers. The sensor responded maximally when vapor sorption occurred on the legs and base of the sensors, providing further evidence that changes in nanocantilever spring constant dominate the observed responses. These results show that for resonant nanocantilevers coated with thick, continuous polymer films, both vapor sorption and bending at the clamped end must be maximized to enhance sensitivity. Additionally, localized polymer coating could be applied in trace detect situations where mass loading and stiffening would compete to impede sensitivity. By coating nanocantilever chemical vapor sensors with rubbery polymer brush films, the sensors respond rapidly and strongly to changes in stiffness, making it a competitive technology for incorporation into highly-miniaturized detections systems. Furthermore, this work can be applied to all resonant NEMS sensors, enabling localization of target binding to specific areas on the resonator, enabling

quantitative mass-loading calculation from frequency shifts, and maximizing resonator sensitivity by preventing the activation of competing response mechanisms.

Bibliography

[1] P. R. Lewis, R. P. Manginell, D. R. Adkins, R. J. Kottenstette, D. R. Wheeler, S. S. Sokolowski, D. E. Trudell, J. E. Byrnes, M. Okandan, J. M. Bauer, R. G. Manley, and G. C. Frye-Mason. Recent advancements in the gas-phase MicroChemLab. *IEEE Sensors Journal*, 6(3):784–795, 2006.

[2] F. Rock, N. Barsan, and U. Weimar. Electronic nose: Current status and future trends. *Chemical Reviews*, 108(2):705–725, 2008.

[3] E. Covington, F. I. Bohrer, C. Xu, E. T. Zellers, and C. Kurdak. Densely integrated array of chemiresistor vapor sensors with electron-beam patterned monolayer-protected gold nanoparticle interface films. *Lab on a Chip*, 10(22):3058–3060, 2010.

[4] C. J. Lu, W. H. Steinecker, W. C. Tian, M. C. Oborny, J. M. Nichols, M. Agah, J. A. Potkay, H. K. L. Chan, J. Driscoll, R. D. Sacks, K. D. Wise, S. W. Pang, and E. T. Zellers. First-generation hybrid MEMS gas chromatograph. *Lab on a Chip*, 5(10):1123–1131, 2005.

[5] K. J. Albert, N. S. Lewis, C. L. Schauer, G. A. Sotzing, S. E. Stitzel, T. P. Vaid, and D. R. Walt. Cross-reactive chemical sensor arrays. *Chemical Reviews*, 100(7):2595–2626, 2000.

[6] F. J. Ibañez, U. Gowrishetty, M. M. Crain, K. M. Walsh, and F. P. Zamborini. Chemiresistive vapor sensing with microscale films of gold monolayer protected clusters. *Analytical Chemistry*, 78(3):753–761, 2006.

[7] R. S. Jian, R. X. Huang, and C. J. Lu. A micro GC detector array based on chemiresistors employing various surface functionalized monolayer-protected gold nanoparticles. *Talanta*, 88:160–167, 2012.

[8] E. S. Snow, F. K. Perkins, E. J. Houser, S. C. Badescu, and T. L. Reinecke. Chemical detection with a single-walled carbon nanotube capacitor. *Science*, 307(5717):1942–1945, 2005.

[9] J. A. Robinson, E. S. Snow, and F. K. Perkins. Improved chemical detection using single-walled carbon nanotube network capacitors. *Sensors and Actuators A-Physical*, 135(2):309–314, 2007.

[10] J. W. Grate. Acoustic wave microsensor arrays for vapor sensing. *Chemical Reviews*, 100(7):2627–2647, 2000.

[11] Jay W. Grate, Susan L. Rose-Pehrsson, David L. Venezky, Mark Klusty, and Hank Wohltjen. Smart sensor system for trace organophosphorus and organosulfur vapor detection employing a temperature-controlled array of surface acoustic wave sensors, automated sample preconcentration, and pattern recognition. *Analytical Chemistry*, 65(14):1868–1881, 1993.

[12] L. Wang, D. Fine, and A. Dodabalapur. Nanoscale chemical sensor based on organic thin-film transistors. *Applied Physics Letters*, 85(26):6386–6388, 2004.

[13] P. C. Chen, F. N. Ishikawa, H. K. Chang, K. Ryu, and C. Zhou. A nanoelectronic nose: a hybrid nanowire/carbon nanotube sensor array with integrated micromachined hotplates for sensitive gas discrimination. *Nanotechnology*, 20(12):8, 2009.

[14] L. A. Pinnaduwage, H. F. Ji, and T. Thundat. Moore's law in homeland defense: An integrated sensor platform based on silicon microcantilevers. *IEEE Sensors Journal*, 5(4):774–785, 2005.

[15] N. V. Lavrik, M. J. Sepaniak, and P. G. Datskos. Cantilever transducers as a platform for chemical and biological sensors. *Review of Scientific Instruments*, 75(7):2229–2253, 2004.

[16] H. P. Lang, M. K. Baller, R. Berger, Ch Gerber, J. K. Gimzewski, F. M. Battiston, P. Fornaro, J. P. Ramseyer, E. Meyer, and H. J. Gntherodt. An artificial nose based on a micromechanical cantilever array. *Analytica Chimica Acta*, 393(1-3):59–65, 1999.

[17] Peter J. Chapman, Frank Vogt, Pampa Dutta, Panos G. Datskos, Gerald L. Devault, and Michael J. Sepaniak. Facile hyphenation of gas chromatography and a microcantilever array sensor for enhanced selectivity. *Analytical Chemistry*, 79(1):364–370, 2006.

[18] R. Datar, S. Kim, S. Jeon, P. Hesketh, S. Manalis, A. Boisen, and T. Thundat. Cantilever sensors: Nanomechanical tools for diagnostics. *MRS Bulletin*, 34(6):449–454, 2009.

[19] Y. T. Yang, C. Callegari, X. L. Feng, K. L. Ekinci, and M. L. Roukes. Zeptogram-scale nanomechanical mass sensing. *Nano Letters*, 6(4):583–586, 2006.

[20] H. Y. Chiu, P. Hung, H. W. C. Postma, and M. Bockrath. Atomic-scale mass sensing using carbon nanotube resonators. *Nano Letters*, 8(12):4342–4346, 2008.

[21] K. Jensen, K. Kim, and A. Zettl. An atomic-resolution nanomechanical mass sensor. *Nature Nanotechnology*, 3(9):533–537, 2008.

[22] M. Li, H. X. Tang, and M. L. Roukes. Ultra-sensitive NEMS-based cantilevers for sensing, scanned probe and very high-frequency applications. *Nature Nanotechnology*, 2(2):114–120, 2007.

[23] K. Eom, H. S. Park, D. S. Yoon, and T. Kwon. Nanomechanical resonators and their applications in biological/chemical detection: Nanomechanics principles. *Physics Reports-Review Section of Physics Letters*, 503(4-5):115–163, 2011.

[24] J. Tamayo, D. Ramos, J. Mertens, and M. Calleja. Effect of the adsorbate stiffness on the resonance response of microcantilever sensors. *Applied Physics Letters*, 89(22):3, 2006.

[25] D. Ramos, J. Tamayo, J. Mertens, M. Calleja, and A. Zaballos. Origin of the response of nanomechanical resonators to bacteria adsorption. *Journal of Applied Physics*, 100(10):3, 2006.

[26] Dongkyu Lee, Seonghwan Kim, Namchul Jung, Thomas Thundat, and Sangmin Jeon. Effects of gold patterning on the bending profile and frequency response of a microcantilever. *Journal of Applied Physics*, 106(2):024310, 2009.

[27] T. Thundat, G. Y. Chen, R. J. Warmack, D. P. Allison, and E. A. Wachter. Vapor detection using resonating microcantilevers. *Analytical Chemistry*, 67(3):519–521, 1995.

[28] M. Li, E. B. Myers, H. X. Tang, S. J. Aldridge, H. C. McCaig, J. J. Whiting, R. J. Simonson, N. S. Lewis, and M. L. Roukes. Nanoelectromechanical resonator arrays for ultrafast, gas-phase chromatographic chemical analysis. *Nano Letters*, 10(10):3899–3903, 2010.

[29] R. Barbey, L. Lavanant, D. Paripovic, N. Schuwer, C. Sugnaux, S. Tugulu, and H. A. Klok. Polymer brushes via surface-initiated controlled radical polymerization: Synthesis, characterization, properties, and applications. *Chemical Reviews*, 109(11):5437–5527, 2009.

[30] G. G. Bumbu, M. Wolkenhauer, G. Kircher, J. S. Gutmann, and R. Berger. Micromechanical cantilever technique: A tool for investigating the swelling of polymer brushes. *Langmuir*, 23(4):2203–2207, 2007.

[31] N. I. Abu-Lail, M. Kaholek, B. LaMattina, R. L. Clark, and S. Zauscher. Micro-cantilevers with end-grafted stimulus-responsive polymer brushes for actuation and sensing. *Sensors and Actuators B-Chemical*, 114(1):371–378, 2006.

[32] C. Bradley, N. Jalili, S. K. Nett, L. Q. Chu, R. Forch, J. S. Gutmann, and R. Berger. Response characteristics of thermoresponsive polymers using nanomechanical cantilever sensors. *Macromolecular Chemistry and Physics*, 210(16):1339–1345, 2009.

[33] T. Chen, D. P. Chang, T. Liu, R. Desikan, R. Datar, T. Thundat, R. Berger, and S. Zauscher. Glucose-responsive polymer brushes for microcantilever sensing. *Journal of Materials Chemistry*, 20(17):3391–3395, 2010.

[34] G. G. Bumbu, G. Kircher, M. Wolkenhauer, R. Berger, and J. S. Gutmann. Synthesis and characterization of polymer brushes on micromechanical cantilevers. *Macromolecular Chemistry and Physics*, 205(13):1713–1720, 2004.

[35] Y. T. Yang, K. L. Ekinci, X. M. H. Huang, L. M. Schiavone, M. L. Roukes, C. A. Zorman, and M. Mehregany. Monocrystalline silicon carbide nanoelectromechanical systems. *Applied Physics Letters*, 78(2):162–164, 2001.

[36] I. Bargatin, E. B. Myers, J. Arlett, B. Gudlewski, and M. L. Roukes. Sensitive detection of nanomechanical motion using piezoresistive signal downmixing. *Applied Physics Letters*, 86(13):3, 2005.

[37] I. Bargatin, I. Kozinsky, and M. L. Roukes. Efficient electrothermal actuation of multiple modes of high-frequency nanoelectromechanical resonators. *Applied Physics Letters*, 90(9):3, 2007.

[38] D. M. Jones and W. T. S. Huck. Controlled surface-initiated polymerizations in aqueous media. *Advanced Materials*, 13(16):1256–1259, 2001.

[39] K. Matyjaszewski, P. J. Miller, N. Shukla, B. Immaraporn, A. Gelman, B. B. Luokala, T. M. Siclovan, G. Kickelbick, T. Vallant, H. Hoffmann, and T. Pakula. Polymers at interfaces: Us-

ing atom transfer radical polymerization in the controlled growth of homopolymers and block copolymers from silicon surfaces in the absence of untethered sacrificial initiator. *Macromolecules*, 32(26):8716–8724, 1999.

[40] C. Xu, T. Wu, C. M. Drain, J. D. Batteas, M. J. Fasolka, and K. L. Beers. Effect of block length on solvent response of block copolymer brushes: Combinatorial study with block copolymer brush gradients. *Macromolecules*, 39(9):3359–3364, 2006.

[41] E. J. Severin, B. J. Doleman, and N. S. Lewis. An investigation of the concentration dependence and response to analyte mixtures of carbon black/insulating organic polymer composite vapor detectors. *Analytical Chemistry*, 72(4):658–668, 2000.

[42] S. M. Briglin, M. S. Freund, P. Tokumaru, and N. S. Lewis. Exploitation of spatiotemporal information and geometric optimization of signal/noise performance using arrays of carbon black-polymer composite vapor detectors. *Sensors and Actuators B-Chemical*, 82(1):54–74, 2002.

[43] M. S. Hanay, S. Kelber, A. K. Naik, D. Chi, S. Hentz, E. C. Bullard, E. Colinet, L. Duraffourg, and M. L. Roukes. Single-protein nanomechanical mass spectrometry in real time. *Nat Nano*, 7(9):602–608, 2012.

[44] S. Timoshenko, D.H. Young, and W. Weaver. *Vibration Problems in Engineering*. Wiley, New York, 4 edition, 1974.

[45] M. Lemieux, S. Minko, D. Usov, M. Stamm, and V. V. Tsukruk. Direct measurement of thermoelastic properties of glassy and rubbery polymer brush nanolayers grown by "grafting-from" approach. *Langmuir*, 19(15):6126–6134, 2003.

[46] V. Koutsos, E. W. van der Vegte, and G. Hadziioannou. Direct view of structural regimes

of end-grafted polymer monolayers: A scanning force microscopy study. *Macromolecules*, 32(4):1233–1236, 1999.

[47] Scientific Polymer Products, Inc.

[48] S. Saha, M. L. Bruening, and G. L. Baker. Facile synthesis of thick films of poly(methyl methacrylate), poly(styrene), and poly(vinyl pyridine) from Au surfaces. *Acs Applied Materials & Interfaces*, 3(8):3042–3048, 2011.

[49] T. Liu, S. Pihan, M. Roth, M. Retsch, U. Jonas, J. S. Gutmann, K. Koynov, H. J. Butt, and R. Berger. Frequency response of polymer films made from a precursor colloidal mono layer on a nanomechanical cantilever. *Macromolecules*, 45(2):862–871, 2012.

[50] Davide Tranchida, Elena Sperotto, Antoine Chateauminois, and Holger Schonherr. Entropic effects on the mechanical behavior of dry polymer brushes during nanoindentation by atomic force microscopy. *Macromolecules*, 44(2):368–374, 2011.

[51] R. M. Felder, G. S. Huvard, and R. A. Fava. 17. Permeation, Diffusion, and Sorption of Gases and Vapors. In *Methods in Experimental Physics*, volume Volume 16, Part C, pages 315–377. Academic Press, 1980.

[52] A. R. Berens and H. B. Hopfenberg. Diffusion of organic vapors at low concentrations in glassy PVC, polystyrene, and PMMA. *Journal of Membrane Science*, 10(2-3):283–303, 1982.

[53] M. Sanopoulou and J. H. Petropoulos. Systematic analysis and model interpretation of micromolecular non-fickian sorption kinetics in polymer films. *Macromolecules*, 34(5):1400–1410, 2001.

[54] Maria-Chiara Ferrari, Enrico Piccinini, Marco Giacinti Baschetti, Ferruccio Doghieri, and Giulio C. Sarti. Solvent-induced stresses during sorption in glassy polycarbonate: Experi-

mental analysis and model simulation for a novel bending cantilever apparatus. *Industrial & Engineering Chemistry Research*, 47(4):1071–1080, 2008.

[55] Maria Grazia De Angelis and Giulio C. Sarti. Solubility of gases and liquids in glassy polymers. *Annual Review of Chemical and Biomolecular Engineering*, 2(1):97–120, 2011.

[56] N. S. Lewis. Comparisons between mammalian and artificial olfaction based on arrays of carbon black-polymer composite vapor detectors. *Accounts of Chemical Research*, 37(9):663–672, 2004.

[57] Ellen S. Gawalt, Michael J. Avaltroni, Norbert Koch, and Jeffrey Schwartz. Self-assembly and bonding of alkanephosphonic acids on the native oxide surface of titanium. *Langmuir*, 17(19):5736–5738, 2001.

[58] Laura B. Goetting, Tao Deng, and George M. Whitesides. Microcontact printing of alkanephosphonic acids on aluminum: Pattern transfer by wet chemical etching. *Langmuir*, 15(4):1182–1191, 1999.

[59] P. E. Laibinis, J. J. Hickman, M. S. Wrighton, and G. M. Whitesides. Orthogonal self-assembled monolayers: Alkanethiols on gold and alkane carboxylic-acids on alumina. *Science*, 245(4920):845–847, 1989.

Chapter 5

Concluding Remarks

This thesis presented three projects aimed at developing resonant nanocantilevers into chemical vapors sensors than could be incorporated into highly-miniaturized chemical detection systems. It was shown that an array of five nanocantilevers, functionalized with thin, dropcast polymer films, could function as an electronic nose that was capable of discriminating between chemical vapors as well as an array of macroscale chemiresistive sensors. This work revealed that, with the current level of baseline noise, nanocantilevers would not become a competitive technology without employing a better surface functionalization. The sensitivity of nanocantilevers to chemical vapors was improved by using surface initiated polymerization to grow thick, uniform polymer brush films. The uniformity and sensor-to-sensor reproducibility of the polymer brush films enabled further study of the mechanisms governing the responses of the nanocantilever sensors. Polymer films were localized to either the clamped-end or free-end of the nanocantilevers using a chromium-masking and passivation scheme. Both the location of the polymer film and its glass transition temperature greatly affected sensor response behavior. It was found that the observed frequency shifts of the polymer-coated nanocantilever that occurred upon exposure to chemical vapors were primarily due to changes in stiffness, rather than mass-loading, as had been expected at the outset of this work.

While the use of surface initiated polymerization has greatly improved the performance of nanocantilever sensors, the thickness of the polymer films grown on a given sensor should be chosen

based on the needs of a particular application in terms of sensitivity and response time. A thicker polymer film will absorb a larger number of vapor molecules, inducing a larger frequency shift, but could also reduce the resonance quality factor (Q), increasing the minimum detectable shift in resonance frequency, effectively reducing the sensitivity. The reduction of Q can be significant for thick, rubbery polymer films, which are preferred over glassy polymers because of the rate of vapor diffusion through rubbery films is much greater than for glassy polymer films. Furthermore, by increasing the thickness of the polymer films, the time required for absorption and desorption increases, which is of concern when nanocantilevers are used for high-speed applications such as back-end detectors for a micro-GC column.

The study of resonant nanocantilever sensors will continue to be an active area of research. There are a number of specific challenges that must be overcome to see nanocantilevers implemented in chemical vapor detection systems. Firstly there is a need to achieve a thorough theoretical understanding of the underlying mechanisms governing nanocantilever stiffness change. Secondly, methods for the actuation and readout of large nanocantilever arrays that can be incorporated into a highly miniaturized vapor detection system must be developed. Thirdly, techniques for the coating of a large array of closely packed nanocantilevers with a variety of polymer films must be devised in order to create a truly nanoscale electronic nose. To be successful in the long-term, any synthetic strategy must be amenable to wafer-scale production and require only minimal processing times. All of these challenges offer the opportunity for furthering scientific understanding while learning how to integrate resonant nanocantilevers into highly-miniaturized chemical vapor detection systems that have the potential for greatly improving public health and safety.